The Pennsylvania State University

The Graduate School

Department of Civil and Environmental Engineering

LENGTH LIMITATIONS OF PRESTRESSED CONCRETE GIRDER INTEGRAL ABUTMENT BRIDGES

A Thesis in

Civil Engineering

by

Keisha T. Baptiste

Submitted in Partial Fulfillment
of the Requirements
for the Degree of

Master of Science

December 2009

The thesis of Keisha T. Baptiste was reviewed and approved* by the following:

Jeffery A. Laman
Associate Professor of Civil Engineering
Thesis Advisor

Andrew Scanlon
Professor of Civil Engineering

Angelica Palomino
Assistant Professor of Civil Engineering

Peggy A. Johnson
Professor of Civil Engineering
Head of the Department of Civil and Environmental Engineering

*Signatures are on file in the Graduate School.

ABSTRACT

The construction of integral or jointless bridges in North America has become increasingly popular because of the many advantages over conventional, jointed bridges. However, conservative limits have been set on the maximum length of integral abutment bridges (IABs) because no analysis or design guidelines for IABs exist. Additionally, the behavior and potential problems associated with IABs at increased lengths are largely unknown. This study developed 3D numerical models in ANSYS that simulate IAB behavior to study the critical bridge response, establish a practical IAB maximum length, and identify potential distress in IABs at extreme lengths.

Key components to IAB behavior included in the numerical models are soil-pile interaction, abutment-pile interaction and construction joint detail. The loads on the numerical models were ambient temperature, AASHTO temperature gradient, time-dependant loads, and backfill pressure. A parametric study was performed with an initial bridge length of 1000′ (305 m) considering the effects of: (1) abutment height; (2) soil stiffness; (3) construction joint flexibility; and (4) pile orientation on IAB response.

Results of the parametric study showed weak axis oriented piles developed higher pile stress than strong axis oriented piles and abutment height had the greatest effect on IAB critical response. Taller abutments, moderate construction joint stiffness, low soil stiffness and strong axis pile orientation are best suited for IABs at extreme lengths because these conditions yield comparatively lower pile stress, moment and concrete stress at the abutment-pile connection. Based on analysis results, IABs at extreme lengths develop high stress in the piles, deck, the abutment at the construction joint and the

backwall-girder connection, limiting the length of IABs. A practical maximum length of 1500′ (457 m) was established based on IAB limiting factors. For IAB lengths beyond 1500′ (457 m), cracking will most likely develop at the backwall-deck connection, the abutment at the construction joint and at the abutment-pile connection. High stress, approaching yield, is also likely to develop in steel H-piles in IABs at extreme lengths.

TABLE OF CONTENTS

LIST OF FIGURES

LIST OF TABLES

ACKNOWLEDGEMENTS

I would like to express my sincere appreciation to my thesis advisor Dr. J.A. Laman for his deep insight, guidance and motivation during this project, without you this project would not have been possible. I would like to thank Dr. Andrew Scanlon and Dr. Angelica Palomino for serving on my committee and for their valuable contributions to this project.

A special thanks also goes to Dr. Woo Seok Kim for your time, patience and recommendations to my many modeling difficulties. Thanks to Professor Ivi Smid, Abdul Aziz and the staff at the Information Technology Services (ITS) at Pennsylvania State University for all your assistance with the numerical modeling.

I cannot end without thanking my family and friends, on whose constant encouragement and love I have relied throughout my time here at Penn State, I would not have made it without you.

Chapter 1

INTRODUCTION

1.1 Background

For many years transportation agencies have endured considerable problems associated with the use of expansion joints in conventional jointed bridges. These expansion joints and bearings are used to accommodate the expansion and contraction of the superstructure due to thermally induced loads and time dependent effects such as creep and shrinkage.

Over time, expansion joints tend to leak and are largely responsible for the deterioration of bridge bearings and supporting structure from de-icing chemicals. Debris also tends to become lodged in expansion joints restricting intended movement. Retaining hardware for joints can also become loosened by snowplows and repeated vehicular impact posing a potential risk to motorists. Support bearings designed in conjunction with expansion joints are typically a significant initial investment and are costly to install, maintain and replace. Most bearings eventually rupture, split, or fail as a result of corrosion or loss of lubrication. As a result, bridge elements can become overstressed or damaged.

IABs are steadily becoming more popular among bridge owners. IABs remain in service longer with only moderate maintenance and occasional repairs required (Burke 1990). Now, at least 40 states have adopted some form of integral or semi-integral bridge design. In 2004, a survey was conducted by the Federal Highway Administration (FHWA) and the Constructed Facilities Center (CFC) at West Virginia University

(WVU), to determine the usage and design of Integral Abutment and Jointless Bridges (IAJB) in the United States. The IAJB 2004 survey was distributed to all 50 States' Department of Transportation (DOT), DC DOT, Puerto Rico Highway and Transportation Authority, and the Federal Lands Highway Division. Thirty-nine of fifty-three (74%) agencies responded and reported that there are approximately 13,000 integral abutment bridges in-service, of which there are more than 9,000 fully integral abutment bridges (Maruri et.al., 2005). Based on the information received from the survey conducted by the FHWA and by Kunin and Alampalli (2000), Table 1.1 summarizes the design criteria for full integral bridges.

Table 1.1 Range of Design Criteria for Prestressed Concrete IABs (Maruri et.al., 2005)

Parameter	**Range**
Maximum Span	60 – 160 ft (18-49 m)
Total Length	150 - 1175 ft (46-358 m)
Maximum Skew*	45º
Maximum Curvature	0-10º

*Measured from a line perpendicular to the bridge axis.

The design and analysis of IABs are more difficult than that of conventional jointed bridges due to (1) difference in boundary conditions, (2) uncertainties of loads and material properties, and (3) nonlinearities in the factors affecting the bridge behavior (Kim 2009). These factors include:

- annual and diurnal temperature fluctuations;
- creep and shrinkage; and

- non-linear soil-structure interaction

Because of complex IAB behavior, short and long-term response is more difficult to predict and consequently, a relatively conservative approach to design and analysis has been adopted by state Department of Transportations (DOTs).

Presently, the *American Association of State Highway and Transportation Officials Load and Resistance Design Manual,* AASHTO LRFD (2008), has no analysis or design guidelines for IABs and no recommendations on the maximum length of IABs. Therefore, length limits in most states are based on performance of in-service IABs. There is a need for further research into the behavior of IABs at extreme lengths and the development of design standards that address the problems encountered in the design and detailing of these bridges.

Tennessee has the longest set limit of 800 ft (244 m) for prestressed concrete girder IABs. However, Tennessee also holds the record for the longest IAB constructed, which has a length of 1,175 ft (358 m). States such as Colorado and Oregon also built IABs greater than 1000 ft (305 m) with lengths 1,112.9 ft (339m) and 1,100.7 ft (336m) respectively.

The present study identifies stress development at critical locations and examines potential distress at these locations. This will be done through the development of numerical models using previously established modeling methodologies to investigate the behavior of IABs at extreme bridge lengths, i.e. beyond 1000 ft (305 m). The use of numerical models has been proven to predict, with high accuracy, the response of IABs. As a result, the modeling techniques developed in previous research studies can be used

to investigate the behavior and identify potential areas of distress in IABs at increased lengths.

1.2 Problem Statement

IABs are typically comprised of single or multiple-spans built without expansion joints. The end girders are cast integrally with the back-wall and usually have a continuous deck from one abutment to the other. The response from both primary and secondary loads must be accommodated by other means because there are no expansion joints.

Primary loads are applied directly to the bridge structure and are typically accounted for in the initial design; these include, dead, live, snow and wind loads. Additional secondary loads resulting from the bridge response to external or internal changes over time: (1) temperature-induced expansion/contraction, (2) differential settlement, (3) thermal gradients and (4) creep and shrinkage (Hassiotis and Roman 2005), are not usually accounted for in the initial design. These secondary loads can result in stresses comparable to those caused by gravity loads. For example, the Pennsylvania Department of Transportation (PennDOT) specifies that these superimposed forces (creep, shrinkage and thermal gradient) should be considered for concrete structures exceeding 600 ft (244 m).

Daily and seasonal temperature changes impose cyclic displacements on the bridge superstructure and ultimately on the abutments, backfill and steel H-piles. These displacements are a function of temperature fluctuations, material properties and structure length. Therefore, as IABs increase in length they are subjected to a larger response. The

increased bridge response can cause serious damage if not properly accounted for. These IABs may experience:

- distress at the abutment-pile location;
- increased moment and stress in piles;
- distress at the backwall-abutment connection; and
- increased concrete stresses at connections such as: girder-backwall , deck-abutment, etc

The maximum permitted IAB length varies from state to state and is usually limited by the maximum thermal movement allowed and empirical data collected from in-service IABs. Because conservative limits have been set on the maximum length of IABs, behavior and potential problems at increased lengths are still unknown. A thorough understanding of IAB behavior at longer lengths and practical limits on the length of the structure are imperative to quality long term performance of the structure. Some issues of concern are:

- the range over which empirical data can be extended before additional analysis is required;
- orientation of the steel H-piles;
- effect of larger bridge response on the backwall-abutment connection;
- geometric, material and geotechnical properties affecting IAB behavior; and
- need for additional/alternate design of bridge components.

1.3 Scope of Research

Field data collected over a seven (7) year period from instrumented bridges along the I-99 extension in central Pennsylvania have been used in previous studies to calibrate numerical models and refine modeling techniques to predict the behavior of IABs. The numerical model methodologies were used to develop models to:

- compare predicted and measured response of IABs;
- evaluate the superstructure stresses;
- simulate hysteresis behavior; and
- develop load and resistance factors for IAB design.

These studies have:

- validated the use of numerical modeling for use in predicting both the short-term and long-term behavior of IABs;
- shown a close correlation between the predicted response of both 2D and 3D models;
- developed methods to accurately simulate loads and bridge component behavior and;
- identified key factors affecting bridge behavior.

This study investigates IAB behavior at extreme lengths using numerical models developed using modeling techniques established in previous studies. Each bridge model used in this study has four prestressed, BT-72 girders spaced at 12′-0″ (3.7 m) that support a 9″ (229 mm) thick, cast-in-place, concrete deck. A typical IAB cross-section is shown in Figure 1.1. The bridge models are symmetric about the longitudinal and

transverse axes and do not include skew end supports. Half of the IAB is modeled with equally spaced pier supports, as shown in Figure 1.2. An abutment height of 9′-0″ (2.7 m) was used in the initial model and altered in the parametric study, shown in Figure 1.3. The abutments are supported by 8 steel HP12x74 (HP310x110) piles embedded 2′-0″ (0.61 m) into the abutment and supported by a single layer of soil, above the water table, and driven to bedrock. The typical backfill material, an open graded sub-base (OGS) coarse aggregate, used by the Pennsylvania Department of Transportation was adopted in this study.

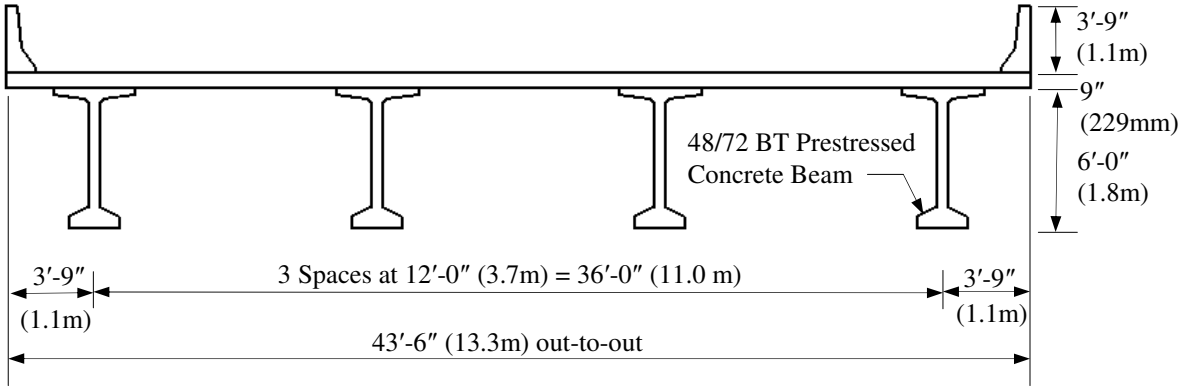

Figure 1.1 Typical Cross Section of IAB

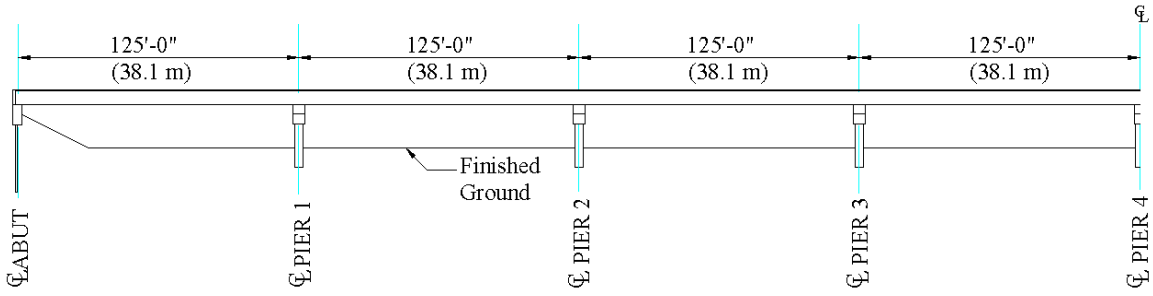

Figure 1.2 Typical Elevation of Bridge Considered in Numerical Model

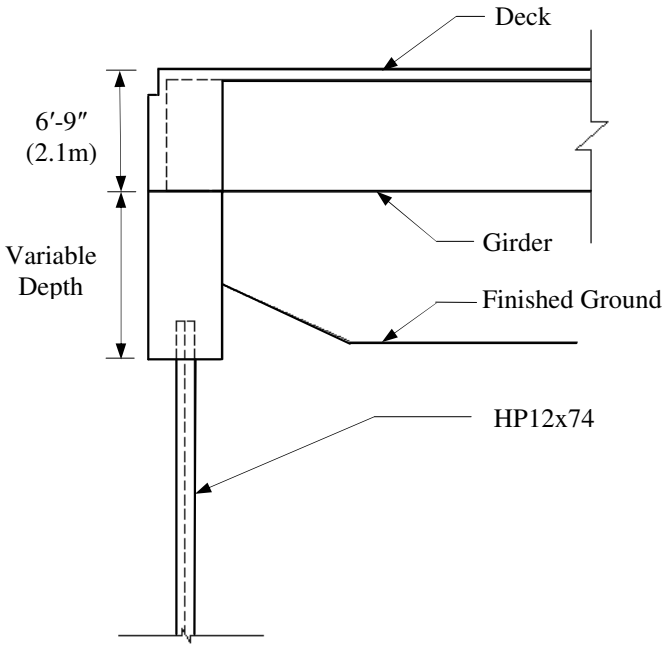

Figure 1.3 Section of Integral Abutment

This study utilizes the commercially available software ANSYS, to develop 3D numerical models. The loads used in the applied to the numerical model are:

(1) temperature range using Procedure A for moderate climates recommended by AASHTO LRFD (2008);

(2) temperature gradient using Zone 3 positive and negative temperature values recommended by AASHTO LRFD (2008);

(3) time dependant effects, creep and shrinkage coefficients recommended by AASHTO LRFD (2008); and

(4) backfill pressure on abutment using open graded sub-base (OGS) coarse aggregate; and

(5) soil pressure on piles using defined soil properties from soil reports of monitored bridges.

IAB structures experience two types of non-linearity: (1) geometric; and (2) material. These nonlinearities are a result of concrete cracking, non-linear soil response, and non-linear behavior at the abutment construction joint. The IAB response of the models in this study is expected to be non-linear due to these factors. For the purpose of this study, the non-linear soil response and abutment connections were considered while the material properties were considered to be linearly elastic-perfectly plastic.

This study investigated the effects on: (1) pile head displacement; (2) maximum pile stress; (3) maximum pile moment; (4) concrete stress at abutment-pile location; and (5) girder bottom stresses. In addition to bridge response, this study also investigates potential distress and failures at the following locations:

- girder-backwall contact;
- girder bearings;
- construction joint; and
- abutment-deck connection.

A parametric study was performed varying four bridge parameters. Three different abutment heights were investigated with heights 4′-0″ (1.2 m), 9′-0″ (2.7 m) and 12′-0″. The pile orientation was varied between strong and weak axis bending and stiff clay, medium clay and sand were used for the soil types. The influence of the construction joint stiffness was also investigated in this study. The connections considered were (1) pinned, (2) PennDOT Standard #5 U shaped bars @ 9″ spacing (#25 mm bars @ 229 mm); and (3) rigid connection. Both expansion and contraction cases were considered in this study.

The material and soil properties used in the bridge models were adopted from field data collected from monitored bridges in Pennsylvania (Laman *et al.* 2006). The bridge model responses were examined and compared to AASHTO LRFD (2008) limits. Ultimately, the maximum length of IABs is established based on the configuration that yields forces and stresses within the established AASHTO limits.

1.4 Objective and Tasks

The overall objective of this study is to establish length limits for IABs when subjected to thermal and time dependant loads. Additionally, this study provides design recommendations for longer IABs. The tasks to be completed toward the objective are:

1. develop numerical models of an IA bridge using previously developed modeling techniques and applied loads; and
2. perform a parametric study varying the geometric and material properties.

The numerical model developed in this study identifies critical locations of high stresses and provides a better understanding of bridge behavior under thermal and time-dependant loads. Initially, a 1,000 ft (305 m) IAB, is modeled and is used in identifying the high stress locations on the bridge superstructure and substructure. The initial bridge length is selected based on length limits of in-service IABs. A parametric study is performed to establish the contribution of specific bridge parameters to the development of stresses at critical bridge locations. The bridge configuration that experiences comparably lower stresses is used to establish a practical maximum length. From these tasks, the objectives of this study are:

1. identify the primary limiting factor for IAB length;
2. establish a practical IAB length limit; and
3. suggest alternate construction and/or details.

Chapter 2

LITERATURE REVIEW

2.1 Introduction

IABs are becoming the bridge of choice over conventional jointed bridges in many states because of the numerous problems associated with the use of deck joints and girder bearings. In general, IABs are designed without the use of expansion joints on the bridge deck. The deck, girders and abutment are usually cast integrally, forming a rigid frame structure. This allows stiffness and flexibility to be distributed along the entire structure. The advantages of considering bridges built without the use of expansion joints include:

- reduced cost and maintenance;
- increased stability and durability;
- faster construction;
- improved seismic performance; and
- improved ride quality.

IABs generally perform well in-service despite the absence of a standardized guide for design and a thorough understanding of bridge behavior. Integral bridges, when properly designed, perform more effectively, remain in service longer and often only require moderate maintenance and occasional repairs (Burke 1990).

IAB design eliminates the problems associated with expansion/contraction joints; they are however, plagued with problems similar to traditional jointed bridges. Both IAB

and jointed bridges currently use the same construction practices. As a result, early age, transverse cracking of IAB bridge decks have been observed in many cases. These cracks are of some concern but do not have significant bearing on the structural integrity of the bridge. More severe cracking has been observed at the ends of approach slabs due to settlement and the forces from bridge expansion and contraction.

Currently, Tennessee dominates in the construction of long IABs and has over 30 years experience in IA and jointless bridge design. The Tennessee Department of Transportation (TDOT) limits the length of IA steel bridges to 500 ft (160 m) and concrete bridges to 800 ft (240 m) based on limits placed on the maximum allowable horizontal displacement. However, Tennessee's longest steel and prestressed concrete IABs in-service are 575 ft (175 m) and 1,175 ft (360 m) respectively, the prestressed concrete IAB being the longest, fully integral abutment bridge reported in the United States (Burdette, 2005). This bridge is located on State Route 50 over Happy Hollow Creek in Hickman County, Tennessee.

It is TDOT's policy to design all bridges continuous and jointless whenever possible. TDOT is steadily gaining the confidence to build longer bridges because of the excellent performance of in-service bridges. The Kingsport Bridge, a 2,700 ft (850 m) bridge, also constructed by TDOT, has a continuous deck with finger-type joints at the abutments only. These joints, however, were later replaced with modular expansion joints because of leakage under the finger joints. The bridge structure consists of: (1) four prestressed, precast concrete box girders; (2) prestressed, precast subdecking; and (3) cast-in-place concrete deck, continuous over 29 spans (Burdette *et al.* 2003). Shortly after the bridge opening in 1981, significant cracking was observed at the diaphragm of one of

the piers and minor cracking at the diaphragm of girders where the piers were slightly skewed. However, bridge inspection reports show that little has changed in the bridge condition 20 years after its initial opening (Burdette *et al.*, 2003).

Guidelines for design and detailing of IABs are limited and are heavily influenced by past and local experience. There are many uncertainties surrounding the design and in-service behavior of integral bridges at any length. AASHTO LRFD (2008) states, "*….Maximum span lengths, design considerations, should comply with the recommendations outlined in FHWA Technical Advisory T 5140.13 (1980), except where substantial local experience indicates otherwise."* The FHWA advisory has now been withdrawn therefore allowing local experience to take precedence. The design of IABs, as a result, is based on very conservative design methods involving maximum length, horizontal alignment, skew angle and vertical grade.

This chapter discusses some of the previous research on length limits of IABs. It also examines the primary issues associated with IAB behavior and factors influencing the behavior of specific bridge components. Consequently, the behavior and response of bridge components can aide in predicting overall IAB behavior at increased lengths. Research has developed and refined numerical models that contribute to understanding and predicting IAB response. This chapter also discusses these modeling techniques that form an essential part of the numerical modeling used in this study.

2.2 Length Limits

IABs continue to perform well with minimal problems and have reduced construction and maintenance costs. This has propelled research into the behavior and

viability of IABs at longer lengths to capitalize on the many advantages. The maximum horizontal displacement accommodated by the abutment and piles usually determines the acceptable length of the superstructure (Hassiotis, 2005). Arockiasamy (2005) suggested that the maximum length of IABs depends on factors such as:

- seasonal temperature variations;
- soil properties; and
- pile flexibility.

Standardized design procedures for IABs can be established when there is a thorough understanding of all IAB loads and its effect on the structure. These design procedures can be extended to include bridge structures at increased lengths, minimizing any potential structural problems. Research in determining allowable lengths for integral abutment bridges has suggested limiting parameters to include:

- low cycle fatigue effects on piles;
- maximum horizontal displacement; and
- secondary forces and stresses.

Fatigue Effects

Increased length and temperature loads on IABs directly influences the cyclic displacement experienced. As IABs increase in length, the magnitude of the cyclic displacements may cause steel piles to experience deformations beyond their elastic limit. This may result in ultimate strength failure or reduction in strength due to low-cycle fatigue effects. Additionally, abutments may develop large shear forces and bending moments exceeding ultimate capacity (Dicleli and Albhaisi, 2003).

Dicleli and Albhaisi (2003) conducted a study to determine the maximum length of IABs based on the displacement capacity of H-piles driven in sand and the shear and flexural capacity of the abutment. Low-cycle fatigue models were used to determine the maximum number of cyclic deformation steel H-pile could withstand. Static pushover analyses were then performed on bridge models that included non-linear soil-pile behavior. Based on results from the pushover analysis, Dicleli and Albhaisi (2003) developed two equations to estimate the maximum length of a proposed integral bridge. The maximum length is based on the smaller value of Equation 2.1 and 2.2 using:

1. low-cycle fatigue pile performance:

$$L_{\max 1} = \frac{2\Delta_{Dn}}{\gamma_T \alpha_T \Delta T_n} \tag{2.1}$$

where, $L_{max1}$is maximum length of integral abutment bridge, Δ_{Dn} is the displacement at one end of the bridge based on low-cycle fatigue failure of the piles, α_T is the coefficient of thermal expansion for the deck material, ΔT_n is the negative design temperature range and γ_T is the load factor for thermal effects.

2. abutment flexural capacity:

$$L_{\max 2} = \frac{2\Delta_{Dp}}{\gamma_T \alpha_T \Delta T_p} \tag{2.2}$$

where, L_{max1} is maximum length of integral abutment bridge, Δ_{Dp} is the displacement at one end of the bridge based on abutment's flexural capacity, ΔT_p is the positive design temperature range, and γ_T is the load factor for thermal effects.

Using the AASHTO LRFD (1998) specified maximum and minimum design temperatures for concrete structures of 10°F to 81°F (-12°C to 27°C) for moderate

climates, and 0°F to 81°F (-18°C to 27°C) for cold climates, the results of Equations (2.1) and (2.2) recommended maximum lengths for concrete structures should be 490 ft to 870 ft (149 m - 265 m) in cold climates and 590 ft to 1050 ft (180 m to 320 m) in moderate climates based on pile and abutment flexural capacity.

Arsoy (2002) investigated the damage to three different pile types under thermally induced, cyclic lateral displacements, to determine the pile type best suited for use in IABs. The tests were performed on steel H-piles, pipe piles and prestressed concrete piles. Table 2.1 presents the pile types and material properties used in the study and Table 2.2 summarize the tests performed on the steel H-piles.

Table 2.1 Properties of Piles Used in Experiments, (Arsoy 2002)

Pile Type	Strength ksi (MPa)	Area in^2 (m^2)	Area moment of Inertia, I in^4 (m^4)	Young's modulus, E, ksi (MPa)	Specifications
H-pile	54.0 (372)	12.4 (8.0E-3)	71.7 (3.0 E-5)	29,000 (200,100)	A572- Grade 50
Pipe pile	45.0 (310.5)	21.2 (1.4 E-2)	484 (2.0 E-4)	29,000 (200,100)	Grade 3 steel 14″ (356 mm) ø outer dia. ½″ (12.7 mm) ø thick.
Prestressed concrete	5.0 (34.5)	144 (9.3 E-2)	1,728 (7.2 E-4)	4,000 (27,600)	Five ½″ (12.7 mm) ø, 270 ksi (1863 MPa) low-lax strands

Table 2.2 Description of Test Performed on H-piles (Arsoy, 20002)

Designation	Description
HP-AA	Application of 75 major cycles on the H-pile. Maximum target stress: ± 17 ksi (117.3 MPa).
HP-BB	Simulation of 75-year temperature variations by 75 large cycles and 27,375 smaller cycles following HP-AA. Maximum target stress: ± 17 ksi (117.3 MPa).
HP-CC	Application of 75 major cycles on H-pile following test HP-BB. Maximum target stress: ± 17 ksi (117.3 MPa).
HP-DD	Attempting to fail the H-pile by using the maximum displacement stroke of the hydraulic actuator.

Table 2.3 Summary Test Results on Steel H-piles obtained from (Arsoy, 2000).

Test Series	Maximum displacement in (mm)	Bending Strain , με	Vertical load kips (kN)	Strain imposed by vertical load (με)
HP-AA	0.5 (12.7)	580	38 (169)	87
HP-BB	0.5 (12.7)	580	38(169)	87
HP-CC	0.5 (12.7)	580	38(169)	87
HP-DD	0.85 (12.7)	1140	38(169)	87

Test HP-AA of Table 2.3 showed no sign of distress with strains measured at 580 με plus an additional 87 με. There was a decrease in lateral load capacity for HP-BB showing the influence of the smaller daily cycles. No lateral load reduction was observed in HP-CC test confirming the influence of smaller daily cycles on load bearing capacity of piles. For the static load test in series HP-DD, the results showed no reduction in linear load displacement response.

The H-piles withstood a maximum of 1140 με plus an additional 87 με. These strains correspond to a stress of approximately 36 ksi (248 MPa), which is well below the

54 ksi (373 MPa) yield strength of the HP10x42 pile used in the study. From the results obtained, Arsoy (2002) concluded that H piles, oriented about the weak axis, are best suited for use in IABs. These piles and orientation are able to withstand cyclic displacement cycles with no sign of distress and damage as long as the total stress induced in the pile does not exceed the yield strength of the steel. The pipe piles, however, had high flexural stiffness compared to H-piles with weak axis bending, which developed large shear forces in the abutment for a given displacement (Arsoy *et al*. 2002). Prestressed concrete piles experienced significant damage under thermal induced cyclic loading (Oesterle *et al*. 1998).

Maximum Horizontal Displacement

Some states restrict the maximum length of IABs based on local DOT limits on the total horizontal displacement allowed. The equation of thermal expansion, Equation (2.3) is used to predict bridge expansion:

$$\Delta L = L\,\alpha\,(T_{max} - T_{min}) \tag{2.3}$$

where, ΔL is the thermal movement, L is the length of the bridge, α is the coefficient of thermal expansion, and T_{max} and T_{min} are the maximum and minimum design temperatures respectively. The design criteria used by TDOT allows 1″ (25.4 mm) horizontal pile displacement in each direction (expansion and contraction). For two abutments moving in 2 directions this corresponds to a total bridge movement of 4″ (101.6 mm). Tennessee has an extreme temperature range of 28ºF to 92ºF (-2.2°C to 33.3°C) and concrete bridges are designed using a temperature range of 25ºF to 95ºF (-4ºC to 35ºC). Using Equation 2.3 and design temperature range for concrete bridges results in a total

horizontal displacement of 0.5 in (13 mm) per 100 ft (31 m) for free expansion. This results in a limit of 800′-0″ (243.8 m) for concrete IABs (Burdette 2002).

Tennessee's 1,175ft (358 m) IAB would have a predicted free expansion horizontal displacement of approximately 6″ (152.4 mm), clearly exceeding the TDOT recommended limit of 4″ (101.6 mm). Table 2.4 shows the properties of this IAB.

Table 2.4 TDOT's Longest Concrete IAB (Concrete Structures Magazine, 2000).

Properties	Bridge
Bridge Length ft (m)	1,175 (358)
No. of Spans	9
Span Length	127 to 138 (38.7 to 42.1)
Bridge width, ft (m)	45 (13.7)
Slab thickness, in (mm)	8 11/42 (210)
Girder type	Prestressed bulb-T beams
Girder height, in (mm)	72 (1,828.8)
No. of girders	6
Curvature (deg)	4.75

The piers were designed to withstand both axial dead and live loads and large lateral displacements from thermally induced loads. The pier columns were designed to deflect as a result of the induce moment and the restraining forces at the top of the pier. TDOT also recommends (Concrete Structures Magazine, 2000):

- the entire deck and diaphragms be placed in one operation to prevent cracking of the diaphragm at supports;
- casting the deck in the mid-span area of adjacent spans before placing the interior diaphragm concrete;

- casting deck under positive bending moment in the end spans concurrently with abutment back wall and wing walls to achieve a jointless deck at the integral abutments; and
- construction joints at least 10 ft. (3 m) and not more than 15 ft (4.6 m) from the interior support.

Secondary forces and stresses

As IABs become longer there is an increased cyclic displacement causing stresses to increase at critical locations. Paul (2003) developed 2D and 3D Finite Element (FE) models of a monitored bridge to investigate superstructure stresses in IABs. The models were calibrated using field data collected from bridges located outside Port Maltilda, along the I-99 in Pennsylvania, establishing modeling techniques to give the closest correlation with field data. These techniques were then extended to develop 2-D models of 5 bridges of varying lengths to study the superstructure forces and stresses. Table 2.5 presents the varied bridge parameters used in Paul (2003) study.

Table 2.5 Varied Bridge Parameters, (Paul, 2003).

Bridge Length, ft (m)	Number of Spans	Abutment Height, ft (m)	Pile Orientation
152′ (46.3m)	1 & 2		
344′ (104.8)	3 & 4	4′, 9′ and 14′	
600′ (182.9m)	4 & 5	(1.2, 2.7, 4.3)	Strong and Weak
800′ (243.8m)	5 & 6		
1000′ (304.8m)	6, 7 & 8		

Paul (2003) concluded that thermally induced superstructure forces were significantly higher for longer length bridges. Bridge length has a larger influence on moment, axial

and shear stresses than abutment height. The results of this study were summarized comparing: (1) superstructure moments, axial and shear forces; (2) bridge axial stress and top and bottom girder axial stress; and (3) top of abutment translation and rotation. Table 2.6 and Table 2.7 present some of the data obtained.

Abutment Height

The magnitudes of moment, axial and shear stresses in the superstructure generally increase when abutment height increases. Translation and rotation of the abutment decrease as abutment height is increased, indicating abutment height limits the displacement of the abutment, as shown in Table 2.6. A taller abutment is more difficult to move, thus developing larger superstructure stresses. Therefore, when conditions allow, it is more practical to construct a shorter abutment to reduce superstructure stresses.

Table 2.6 Superstructure Response to Change in Abutment Height (Paul, 2003)

Abutment Height ft (m)	Superstructure			Bridge			Abutment	
	Moment kip-ft (N-m)	Axial kip (N)	Shear kip (N)	Axial Stress ksi (MPa)	Bot. Stress ksi (MPa)	Top Slab Stress ksi (MPa)	Translation in (mm)	Rotation deg
4 (1.2)	-16394.9 (-2.2 E7)	-2501.0 (-1.1 E7)	126.3 (5.6 E5)	-0.264 (-1.8)	-0.967 (-6.7)	0.583 (4.0)	-2.301 (-58.4)	0.024
9 (2.7)	-20182.6 (-2.7 E7)	-3198.0 (-1.4 E7)	155.3 (6.9 E5)	-0.337 (-2.3)	-0.190 (-1.3)	0.717 (4.9)	-2.142 (-54.4)	0.0215
14 (4.3)	-24154.8 (-3.3 E7)	-3930.9 (-1.7 E7)	185.9 (8.3 E5)	-0.415 (-2.9)	-1.425 (-9.8)	0.859 (5.9)	-1.974 (-50.1)	0.0165

Bridge Length

The values of moment, axial and shear stresses in the superstructure generally increase when bridge length is increased. A general increase the bridge behavior was also observed by the increase in axial stress, the bottom superstructure bending stress and top slab stress. Translation and rotation of the abutment also increased as the bridge length increased, shown in Table 2.7. This indicates that the overall bridge response is increased with an increase in bridge length because the thermal loads act on a much larger superstructure.

Table 2.7 Superstructure Response to Change in Bridge Length (Paul, 2003)

Bridge Length ft (m)	Superstructure			Bridge			Abutment	
	Moment kip-ft (N-m)	Axial kip (N)	Shear kip (N)	Axial Stress ksi (MPa)	Bot. Stress ksi (MPa)	Top Slab Stress ksi (MPa)	Top Translation in (mm)	Rotation (deg)
152 (46.3)	8345.4 (1.1 E7)	-1561.7 (-6.9 E6)	0.0 (0.0)	-0.174 (-1.20)	-0.598 (-4.13)	0.354 (2.44)	-0.205 (-5.21)	0.0025
344 (104.9)	12239.9 (1.7 E7)	-2385.1 (-1.1 E7)	130.4 (5.8 E5)	-0.292 (-2.01)	-1.328 (-9.16)	0.766 (5.29)	-0.625 (-15.9)	0.0079
600 (182.9)	14696.4 (2.0 E7)	-2424.4 (1.1 E7)	127.2 (5.7 E5)	-0.269 (-1.85)	-1.053 (-7.27)	0.623 (4.30)	-1.291 (-32.8)	0.0143
800 (243.8)	16222.6 (2.2 E7)	-2470.3 (1.1 E7)	128.3 (5.7 E5)	-0.261 (-1.80)	-0.957 (6.60)	0.577 (3.98)	-1.808 (-45.9)	0.0195
1000 (304.8)	20182.6 (2.7 E7)	3198.0 (1.4 E7)	155.3 (6.9 E5)	-0.337 (-0.233)	-1.190 (8.21)	0.717 (4.95)	-2.142 (-54.4)	0.0215

Generally, moment, axial force and shear force obtained for weak-axis bending of piles are smaller than for strong-axis, which shows the significance of pile orientation in

forces and stresses developing in the superstructure. However, pile orientation has the least effect when compared to the change in other bridge (Paul, 2003). When moment, shear force and axial force obtained for expansion were compared to bridge contraction magnitudes, the magnitudes for bridge contraction were generally lower than that of bridge expansion. Paul (2003) determined that:

- maximum thermally-induced bending stresses occur over the abutment;
- an increase in abutment height induces larger stresses for bridge expansion but smaller stresses for contraction; and
- there is a general increase in the thermally induced superstructure moment, axial and shear forces with increase in bridge length.

The trends observed by Paul (2003) contributed to the decision to include some of the parameters investigated in the parametric study and properties of the initial bridge modeled in this study. This information also provides some insight into the effect of increased bridge length on IAB behavior. For the purposes of this study, an abutment height of 9 ft (2.7 m) is used in the initial model and altered in the parametric study. It is anticipated that abutment height and pile orientation will influence the overall bridge behavior.

2.3 Bridge Components

2.3.1 Superstructure

The superstructure of IABs is composed of the deck, girders, parapets and cross-frames and typically has the same design as conventional bridges. The superstructure is

normally cast monolithically with the abutment, forming a connection that is capable of transferring moments, shear and axial forces. The superstructure is most exposed to solar radiation, wind currents, and precipitation (Fennema, 2003) and is responsible for the overall expansion and contraction of the bridge due to thermal changes. Superstructure temperature, however, is most influenced by the ambient temperature. As integral bridges become longer, there is an increase in deck surface area exposed to thermal loads. Consequently, with an increase in deck length, an increase in forces and stresses is expected.

In 1996, engineers inspected a total of 84 bridges in New York, 30 with steel superstructures and 54 with prestressed concrete superstructures (Alampalli and Yannotti, 1998). A condition rating scale was used to categorize the bridge condition based on visible conditions of deck, approach slabs, abutment etc. The bridge ratings indicate that integral bridges have performed very well and appear to function as originally designed. IABs also showed superior performance when condition ratings for both integral and conventional jointed bridges were compared. However bridge skew and span length significantly influenced deck and approach slab condition rating- a greater skew angle and bridge length resulted in lower condition ratings (Alampalli and Yannotti, 1998).

Mourad and Tabsh (1999) studied transverse and longitudinal stresses in the deck slab of IABs due to truck loads. The study investigated positive and negative moment regions for an IAB using a finite element analysis. The results were compared to the stress distribution in the concrete deck of a simply supported bridge. Mourad and Tabsh (1999) considered two composite, steel girder IABs, loaded with HS20-44 trucks. Table 2.8 compares magnitudes obtained from the finite element analysis with AASHTO LRFD

(1996) proposed method. Mourad and Tabsh (1999) concluded that positive and negative bending moments in the deck were lower than those in simply supported bridges (Mourad 1999). It was also observed that stresses from the finite element analysis were less than the stresses obtained using the AASHTO LRFD method.

Table 2.8 Maximum Transverse Stresses in Deck Slabs, Mourad & Tabsh (1999)

Structure (1)	AASHTO Method ksi (MPa) (2)	Finite Element Analysis ksi (MPa) (3)	Simply Supported (MPa) (4)
Bridge 1	0.416 (2.87)	0.254 (1.75)	0.303 (2.09)
Bridge 2	0.286 (1.97)	0.174 (1.20)	0.207 (1.43)

2.3.2 Girder to back-wall connection

Precast concrete girders are connected to each other at end diaphragms using two vertical rows of transverse reinforcement passing through the web of the girders. PennDOT, uses 4 # 8 bars spaced at 9″ (#25 mm bars @ 229 mm) in each row, shown in Figure 2.1. This reinforcement ensures full transmission of all translation and live load rotation of the superstructure to the backwall (Hassiotis and Roman, 2005).

An increase in temperature causes superstructure expansion and the girders are pushed against the backwall. This may cause high stresses to develop at the girder back-wall connection. When there is a decrease in temperature, the superstructure contracts and the girders are pulled away from the back-wall. The movement of the girders is resisted primarily by the transverse reinforcement provided. As bridge lengths increase, the longitudinal displacement also increases. This study investigates how much distress occurs at this girder back-wall connection, the shear stress in the transverse reinforcement

and the shear stress in the girder at the transverse threading location when there is an increase in thermally induced displacement.

2.3.3 Backwall – Approach Slab

All states use reinforcing bars to connect the approach slab to the abutment. In states such a Pennsylvania, Massachusetts, New Jersey, New York, and Virginia diagonal bars, as shown in Figure 2.1, while other states use straight bars (Hassiotis and Roman 2005). These bars transmit the lateral displacement and rotation of the backwall to the approach slab.

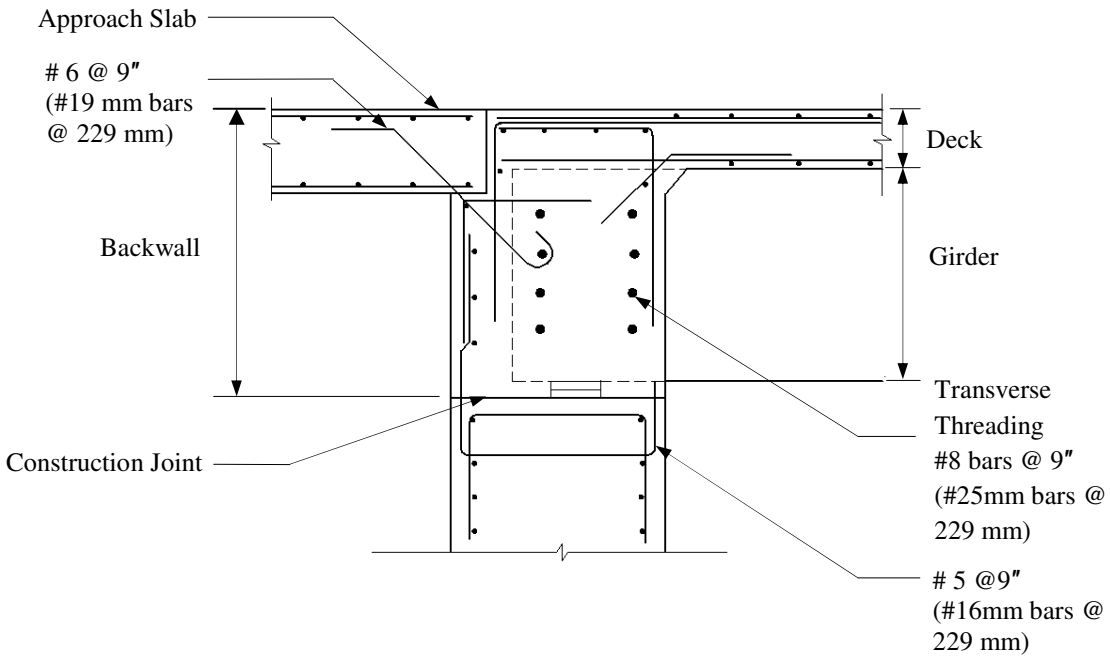

Figure 2.1 Backwall- Approach Slab Connection

Figure 2.2 shows a typical section detail of an approach slab used by PennDOT. The end of the approach slab rests on a sleeper slab with a 4″ (101.6 mm) Neoprene strip seal expansion joint separating the approach slab and the concrete pavement. PennDOT

uses two sheets of 4 MIL (0.1 mm) polyethylene sheeting between the approach and the sleeper slab. The sheets act as a bond breaker and create a sliding surface for the lateral movement from the abutment. The approach slab is designed as a simply supported structure and the lateral movement of the approach slab is resisted primarily by the friction between the approach slab and the sleeper slab, as well as the resistance from the compression of the expansion joint. This resistance is significantly less than the backfill and soil resistance from the soil-structure interaction and can be ignored in numerical modeling.

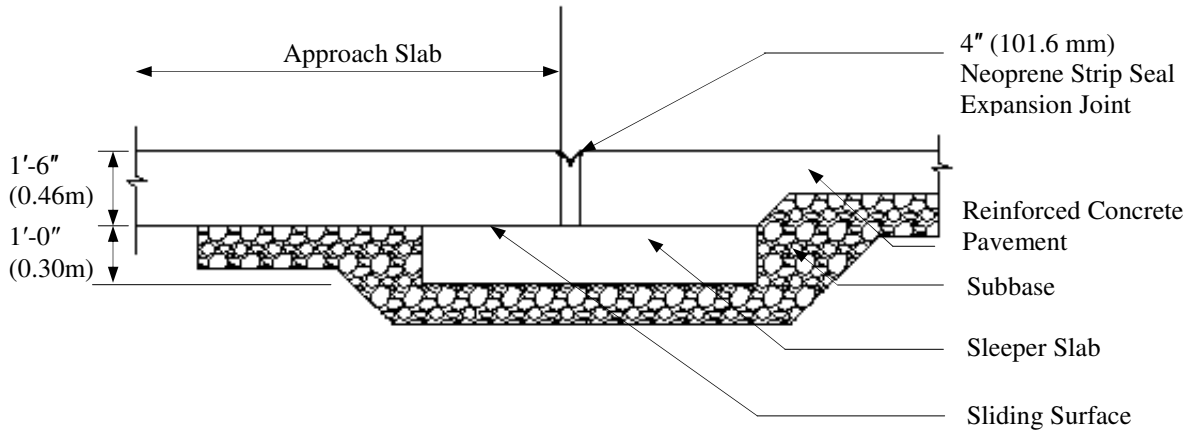

Figure 2.2 Approach Slab Adjacent to Roadway

2.3.4 Abutment

The abutments of IABs are designed to accommodate the cyclic displacements of the superstructure and transfer these forces to piles and supporting soil. Stub type abutments are usually most desirable for IABs in which the abutment is supported by a single row of piles (Arockiasamy *et al,* 2004). These abutment types provide the flexibility needed to accommodate superstructure expansion and contraction. Expansion of the superstructure induces a lateral translation and rotation of the abutment. The

resistance of the supporting backfill material induces a compressive axial force on the abutment. Abutments are, therefore, designed very conservatively to prevent cracking and to transfer large forces.

In 1985, however, the FHWA examined 580 abutments in 314 bridges in the United States and Canada and concluded that over 75 percent of the abutments experienced significantly larger vertical movement than what the designer intended (Mistry, 2005). This was in part due to the girders or beams acting as struts when the abutments move inwards preventing further horizontal movement.

2.3.4.1 Back-wall abutment connection

A cold-joint (construction joint) is used to connect the back-wall to the abutment. State DOTs such as NYDOT, NJDOT, MHD, IDOT and PennDOT use a connection consisting of U-shaped reinforcing bars fixed at the top of the abutment and extend into the back-wall. Figure 2.1 shows a typical PennDOT detail of the transverse threading used. State DOTs utilizing this type of connection typically use #5 reinforcing bars with spacing between 6″ (152 mm) and 12″ (305 mm). PennDOT uses #5 bars spaced at 9″ (ø16mm at 229 mm) and this detail was also used in this study.

Other state DOTs such as NYDOT and NJDOT use a 1 ½″ (38.1 mm) diameter dowel to connect the back-wall to the abutment, as shown in Figure 2.3. Field monitoring (Laman *et al.* 2006) observed significant rotation and translation in response to thermal movements of the superstructure as opposed to a fixed connection as previously assumed. Numerical models developed in previous studies, (Dicleli, 2003, 2004; Haung *et al.*, 2008; Knickerbocker, 2005; and Thippeswamy 2002) the abutment was modeled as a

continuous (rigid) structure. This connection allows no rotation between the end diaphragm and the abutment.

The construction joint significantly influences the abutment response, consequently influencing the allowable maximum length of an IAB. The different construction joint reinforcing used in different states was considered in this study. This study investigated effects of the construction joint flexibility on IABs at extreme lengths and the distress at this location. This study investigates the three backwall- abutment connection conditions (1) perfectly hinged; (2) PennDOT Standard; and (3) perfectly rigid.

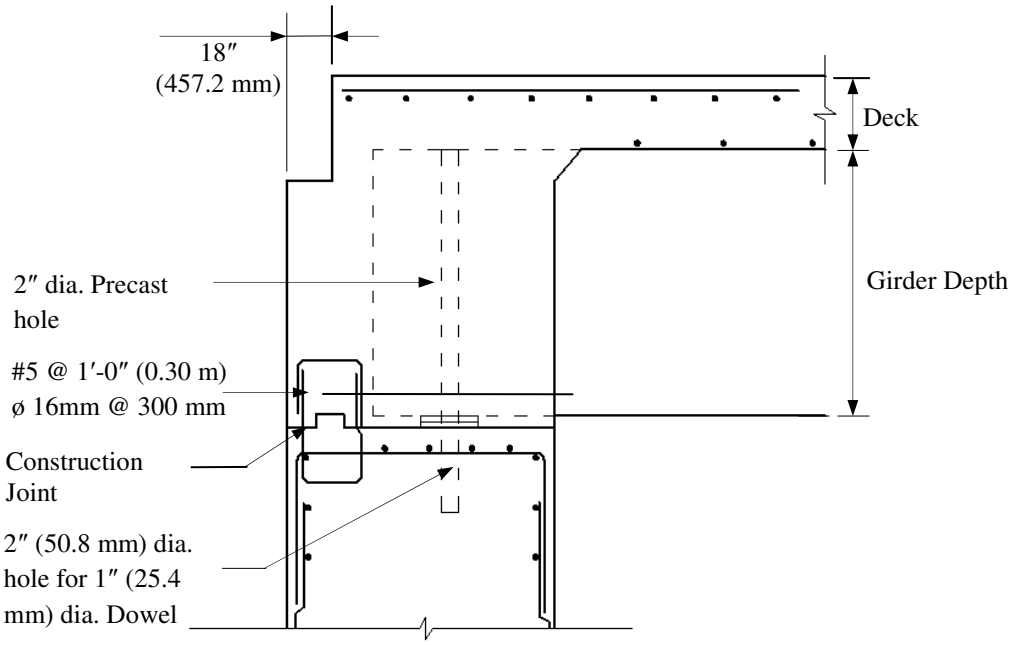

Figure 2.3 Typical Detail of NYSDOT Standard Abutment-Backwall Connection

2.3.5 Piles

Most integral abutments are of the stub-type, supported by a single row of flexible piles. Steel H-piles are most commonly used because of their flexibility and ability to withstand large displacements. IAB piles, used in northern states, are subjected to one dominant cyclic displacement per year due to seasonal temperature changes as well as smaller daily cyclic displacements. Lateral loads from the bridge superstructure are transferred to the piles and supporting soil. The resistance to lateral loads depends on soil and pile stiffness. If the soil surrounding the piles is relatively stiff, it resists the lateral movement and the pile-abutment connection will tend to develop high stresses.

Pile orientation plays an important role in the ability of steel H-piles to deflect when subjected to lateral loads. Most state DOTs require weak axis orientation for H-piles, however, this orientation has the potential for yield and low-cycle fatigue (Dunker and Liu, 2007). State DOTs such as Caltrans, IDT, IDOT and TDOT specify strong axis orientation for H-piles. Strong axis orientation is sometimes used to avoid the possibility of local buckling (Huckabee et al., 2005) and is less flexible that weak axis orientation.

AISC 13th Edition LRFD Code Commentary F for Design of Flexural Members, states that compact sections develop fully plastic stress distributions, assuming a linear elastic behavior up to full plastic; non-compact sections can experience inelastic flange local buckling where the flange buckles prior to forming a fully plastic section; and slender sections experience elastic flange local buckling prior to reaching yield. Since most H-piles are non-compact, there is a possibility of flange local buckling when these piles are used. However Vesić (1977) states that “Experience shows that buckling of

fully embedded piles is extremely rare, even in soft soils, as long as they are capable of supporting a pile in friction."

One of the most important design considerations is the ability of the foundation piles to withstand both the vertical load and bridge longitudinal displacements. This plays an important role in the determination of maximum lengths of IABs. For IABs to be built longer, the stresses in the pile should be minimized despite the increase in the cyclic expansion and contraction. For longer integral bridges piling stresses may approach or equal the yield stress of the piles (Burke, 1993) Some design options to decrease stress in the piles are (1) use of more laterally flexible piles; (2) use of pre-bored holes or sleeves for piles; (3) details to create a hinge at the top of piles; (4) use of detailing at the top of the pile to cause slippage; and (5) use of compressible material directly behind the abutment (Duncker and Liu, 2007). These options decrease the resistance to pile movement, causing the piles to develop less stress.

This present study investigates the distress in the concrete at the abutment-pile location and examines the maximum stress and moments along the pile. The parametric study ignores gravity loads and only considers stress in the pile due to thermally induced lateral loads. This study uses 8 steel HP 12x74 (HP310x110) steel piles, 30′- 0″ (9.1 m) long; with yield strength of 50 ksi (345 MPa). The number of piles and the pile type will remain constant for this study. The piles were embedded 2′-0″ (0.61 m) into the abutment to ensure a fixed boundary condition and supported by a single layer of soil and assumed to be driven down to bedrock.

2.4 Soil-Structure Interaction

The non-linear behavior of the soil-structure interaction is one of the most complex aspects in the design of IABs. Soil structure interaction includes: (1) abutment-backfill; and (2) soil-pile interaction. There are many methods used to predict the response of laterally loaded piles. The most common methods are: (1) brom's method; (2) elastic method; and (3) *p-y* curve methods. The use of *p-y* curves is the most widely used method of evaluating soil-pile interaction of laterally loaded piles. A non-linear relationship is considered between the soil pressure *(p)* and the pile displacement *(y)*. Traditional *p-y* curve models developed in 1970's by Reese and Matlock uses non-linear springs (Winkler springs) to represent the soil response at discrete locations. These curves were established through the use of field tests using uniform soil and adjusted using empirical parameters to extrapolate beyond the soils specific field test conditions (Ashour, 2000).

Fennema (2003) investigated the use of *p-y* curves in developing multi-linear soil springs to simulate soil-pile interaction in IAB numerical models. Linear soil springs were developed using Petroleum Institute COMP624P and *p-y* curves were generated using the method found in the FHWA handbook, *Behavior of Piles and Pile Groups under Lateral Load* (Reese, 1985). Fennema (2003) compared numerical pile models utilizing both linear and multi-linear soil springs; with soil springs developed using COMP624P. Fennema (2003) validated the use of multi-linear soil springs developed from *p-y* curves for use in numerical models to predict soil-pile interaction.

2.4.1 Abutment-backfill interaction

During expansion of the superstructure the movement of the back-wall and abutment is resisted by the back-fill behind the abutment and piles. It has been demonstrated that maximum abutment displacement is significantly less than free expansion of superstructure used for the current design estimation (Kim 2009). The soil imposes a compressive force on the backwall and abutment, resisting its displacement. This significantly increases the passive pressure on the structure. This behavior depends on: (1) the magnitude of the horizontal displacements and (2) the properties of the supporting soil. However, Kim (2009) determined that a change in backfill stiffness does not significantly affect IAB response.

The abutment-backfill interaction is simulated in numerical analysis using a nonlinear, force-displacement relationship. This present study uses a Winkler spring model, based on classical Rankine's lateral earth pressure theory, assuming a linear variation between active and passive pressures (Kim 2009). The backfill material used in this study is an OGS coarse aggregate used by PennDOT.

2.4.2 Soil-pile interaction

The lateral movement of IAB piles is significantly influenced by the soil stiffness around the piles. The stiffness of the supporting soil depends on the soil type. Arockiasamy *et al*. (2004) investigated the effects of: (1) sand with different degrees of compaction; (2) depth of predrilled holes; (3) piles without predrilled holes; (4) height of water table; (5) varying soil types; and (6) pile orientation, on pile horizontal displacement, moment and axial force. Arockiasamy *et al*. (2004) demonstrated that:

- An increase in shear and axial force was observed as the soil stiffness increased. These forces were generally higher for piles embedded in single layered soils than for piles in different soil layers;
- An increase in horizontal displacement was observed with a reduction of soil stiffness;
- Maximum shear and horizontal displacement varied significantly when the pile orientation was changed; and
- Piles without predrilled holes experienced higher stresses and depended on the soil type and predrilled holes do not significantly contribute to stress.

Laterally loaded pile behavior along the entire length of the pile is defined by a family of *p-y,* force *(p)* – lateral displacement *(y),* curves used to simulate soil-structure interaction. This present study uses *p-y* curves to simulate the hysteretic soil-structure interactions in the numerical models. The FE models in this present study use *p-y* curves based on the properties of piles embedded in a uniform layer of soil, above the water table and driven to bedrock.

2.5 Thermal Effects

Overall IAB behavior is significantly influenced by the thermal loads on the structure. Superstructure expansion and contraction is a result of the change in bridge temperature due to thermal effects. The effects influencing bridge temperature depends on:

- ambient air temperature;

- solar radiation;
- precipitation; and
- wind velocity.

Thermal properties of the structure materials also significantly affect bridge response to thermal effects. These include: (1) coefficient of thermal expansion; (2) thermal conductivity; and (3) temperature gradients. These properties control the flow of heat through the structure, and are important in determining the effective bridge temperature. Emerson (1977) found that the longitudinal movement of the bridge was mainly influenced by the mean or effective bridge temperature. Bridge temperature is determined based on: (1) ambient air temperature; and (2) temperature gradient through the depth of the structure.

2.5.1 Ambient Temperature

Ambient air temperature is the most influential component of thermal loading on IABs. It therefore has the most influence on overall IAB behavior. Lawver (2000) investigated the response of an IAB in Minnesota and found that environmental loads and solar radiation caused a larger bridge response than live loads.

AASHTO LRFD (2008) suggests a design temperature range of 10 ºF to 80ºF (-12.2ºC to 26.7ºC) for moderate climates and -17.8ºC to 26.7ºC (0ºF to 80ºF) for cold climates. A moderate climate is designated to states where the number of freezing days per year (i.e. average temperature below 32ºF (0ºC)) are less than 14. A cold climate is designated to states where the number of freezing days per year is greater than 14.

Data obtained from the weather station at one of the four monitored bridges in Pennsylvania, bridge 203, as well as information obtained from the National Climate Data Center, were used in studies by Pugasap *et al*. (2006) and Kim (2008) to represent the temperature loading on IABs. The temperature loading was defined using a sinusoidal function that best fit the data obtained from a weather station from shown in Figure 2.4.

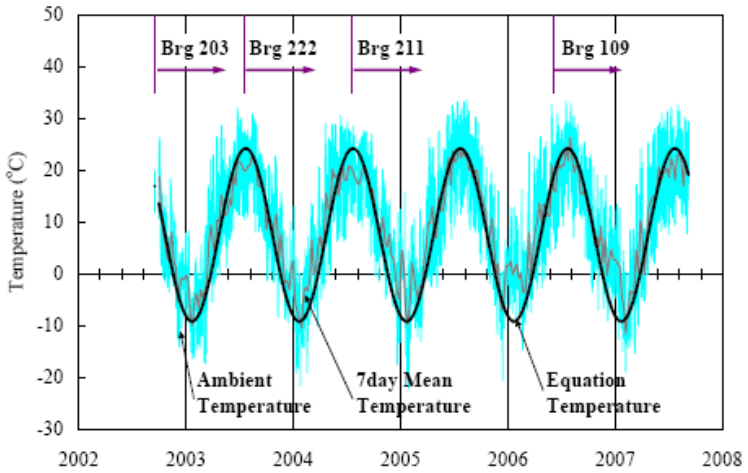

Figure 2.4 Temperature variations on monitored bridges (Kim, 2008)

This temperature loading was represented by the function:

$$T(t) = T_m + A \sin(\omega t + \phi) \tag{2.4}$$

where T_m is the mean temperature, A is the amplitude of temperature fluctuations, ω is frequency, t is analysis time (days) and ϕ *p*hase lag (radians).

AASHTO LRFD (2008) recommends a design temperature range of 10 ºF to 80 ºF (-12.2ºC to 26.7ºC). An example procedure from *AASHTO Guide Specifications: Thermal effects in Concrete Bridge Superstructures* uses a temperature of 30ºF rise for expansion and a 40ºF fall for contraction. PennDOT specifies that the backwall and deck pour must be done when the ambient temperature is between 40ºF and 85ºF (-1.1 °C and

29.4 °C). Therefore, an extreme temperature of +30ºC rise and -40ºC fall is used in this study assuming the effective bridge temperature at which the bridge was restrained was approximately 50ºC (10 ºC). This study utilizes an extreme design temperature static analysis, to determine the maximum forces and stresses that occur in bridge components.

2.5.2 Temperature Gradient

Temperature gradient occurs from unequal temperature through the depth of the bridge superstructure. A study conducted by Girton *et al*. (1990), showed that the highest bridge temperature 120 ºF (49 ºC) occurred on the deck upper surface for the Boone River Bridge, and the lowest bridge temperature of -16ºF (27 ºC) was uniform throughout the superstructure depth. This unequal heating is a result of the large deck surface area exposed to the solar radiation.

The girder temperature is affected by heat conduction from the deck and an increase in ambient air temperature. However, the girders may also experience some cooling from the wind. This results in an unequal heat distribution through the depth of the superstructure and ultimately unequal expansion of the top and bottom. This can cause differential strains due to bending of the bridge girders and additional stresses in the superstructure.

AASHTO LRFD (2008) provides a multi-linear temperature gradient to determine both top and bottom, positive and negative temperatures. These values correspond to concrete deck with asphalt overlay and Zone 3 taken from the Solar Radiation Zones for the United States specified by AASHTO LRFD (2008). Figure 2.5 shows the standard values recommended by AASHTO LRFD (2008) that is used in this study. The multi-linear temperature gradient is converted to an equivalent linear temperature variation

because a multi-linear gradient cannot be modeled using ANSYS. An equivalent linear temperature gradient is developed and added to the ambient temperature load.

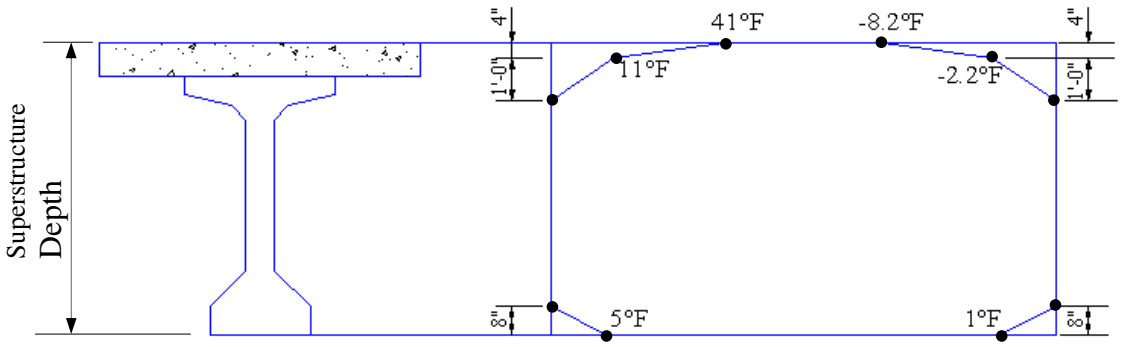

Figure 2.5 Temperature Gradients for Numerical Model

2.6 Time dependant effects

Time dependant effects include concrete creep, shrinkage and prestressing steel relaxation. These factors induce additional strain in the bridge structure. Creep is defined as the permanent deformation of a body under sustained stresses. Creep causes increase deflections in the structure, reduces prestress in concrete bridge components and a redistribution of forces in a redundant structure. Creep of concrete depends on three factors:

- Concrete temperature;
- Applied stress magnitude and duration; and
- Concrete age at the time of the applied stress.

Shrinkage in concrete is a result of continued drying of concrete which causes a decrease in size. At first, as concrete cures, the evaporated moisture does not cause a significant change in volume; however, with continued drying the concrete tends to

shrink significantly. Shrinkage can cause warping of concrete components, such as slabs, which induces additional forces and stresses at certain locations and some deflections in non-symmetric components. PennDOT specifies that superimposed forces (creep, shrinkage and thermal gradient) should only be considered if the structure exceeds 600-ft for concrete structures.

Design recommendations from: American Concrete Institute Committee 209 (ACI 209), CEB-FIP MC 90, and Model B3 can be used to calculate the creep coefficients, aging coefficients and shrinkage strains. A preliminary investigation conducted by Pugasap (2006), was performed to cross-verify and select the best suited method for determining these coefficients. The data from bridge 222 was used to calculate the creep coefficients using the different design methods.

Pugasap (2006) determined that the values for creep coefficients, aging coefficients and shrinkage strains all showed a similar trend and the results using the different design recommendations showed an insignificant difference. As a result, the ACI 209 recommendation was chosen because of its ease of use.

In the present study, the age-adjusted effective modulus method based on ACI Committee 209 is used to calculate the strains and corresponding stresses using, creep coefficient $\varphi(t, t_o)$ and shrinkage coefficient, $\varepsilon (t, t_o)$ recommended by AASHTO LRFD (2008). The concrete strains obtained using this method were then converted to an equivalent temperature load and applied to the numerical model.

2.7 Coefficient of Thermal Expansion

AASHTO LRFD (2008) recommends a thermal coefficient of 6.0×10^{-6} in/in/ºF (10.8×10^{-6} mm/mm/ ºC) for concrete structures. This value, however, does not account for variation in local material properties (Ndon 1995). Research has shown that the coefficient of thermal expansion of concrete depends on materials used in the mix. Emanuel and Hulsey (1977) stated that besides stress, the coefficient of thermal expansion for concrete depends on:

- the richness of the mix;
- kind of cement;
- type of aggregate;
- water-cement ratio;
- age; and
- temperature fluctuations.

Girton *et al*. (1989) collected core samples from the abutments of the Boone River and Maple River Bridges in Iowa to determine the coefficient of thermal expansion for each bridge. Based on the results, values of 4.5×10^{-6} in/in/ºF (2.5×10^{-6} mm/mm/ºC) for the Boone River Bridge, a prestressed girder IAB, and a value of 5.0×10^{-6} in/in/ºF (2.8×10^{-6} mm/mm/ºC) for the Maple River Bridge, a steel girder bridge were measured. In comparison, the value recommended by AASHTO LRFD (2008) is significantly higher than those measured. Ndon (1995) also conducted similar studies on the same bridges in Iowa. The results from field, laboratory data and the use of an empirical formula developed by Emmanuel and Hulsey (1977) were used to estimate the coefficient

of thermal expansion for the two aggregate types, limestone and gravel. The empirical formula used is:

$$\alpha_c = f_T (f_M f_A \beta_P \alpha_S + \beta_{FA} \alpha_{FA} + \beta_{CA} \alpha_{FA}) \quad (2.5)$$

where α_c is the thermal coefficient of expansion,

f_T is the correction factor for temperature alterations (1.0 for controlled environment, 0.86 for outside exposure);

f_M is the moisture correction factor;

f_A is the age correction factor;

β_P is the proportion by volume of paste,

α_s is the thermal coefficient of expansion of saturated hardened neat cement paste [11 ppm/ºC (6 ppm/ºF)];

β_{FA} is the proportion by volume of fine aggregate;

α_{FA} is the thermal coefficient of expansion of fine aggregate; and

β_{CA} is the proportion by volume of coarse aggregate, and α_{FA} is the thermal coefficient of expansion of fine aggregate.

The results are summarized in the table below:

Table 2.9 Coefficient of Thermal Expansion from Field, Lab and Empirical Data

Concrete	Field coefficient [10^{-6} /ºF (10^{-6} /ºC)]	Lab coefficient [10^{-6} /ºF (10^{-6} /ºC)]	Empirical values [10^{-6} /ºF (10^{-6} /ºC)]
Limestone aggregate	4.0 (7.2)	4.5 (8.1)	4.7 (8.5)
Gravel aggregate	4.7 (8.5)	5.2 (9.4)	5.3 (9.5)

The values obtained range from 4.0 to 5.3x10^{-6} in/in/ºF (2.2 to 2.9x10^{-6} in/in/ºC), these show a close agreement with each other and also corroborate the results obtained by Girton *et al*. (1989). For the purpose of this study, the value of the coefficient of thermal expansion was taken 6.0x10^{-6}in/in/ºF (10.8x10^{-6} mm/mm/ ºC) as recommended by AASHTO LRFD (2008). Despite evidence that shows this value to be a slight overestimate, this present study seeks to determine the maximum length thus using the higher limit of this value is justified.

2.8 Modeling Methodologies

The use numerical models have been successful in predicting the behavior of IABs. Approximately 7 years of field data from 4 monitored IABs, located along the Interstate 99 in Central Pennsylvania was collected and used in studies. The bridge properties monitored bridges are shown in Table 2.10.

Table 2.10 Monitored Integral Abutment Bridges.

Structure No.	Total Length ft (m)	No. of Spans	Spans ft (m)
109	420 (128.0)	4	88-122-122-88 (26.8-37.2-37.2-26.8)
203	172 (52.4)	3	44-88-37 (14.3-26.8-11.3)
211	114 (34.7)	1	114 (34.7)
222	62 (18.9)	1	62 (18.9)

The data collected from these bridges were used to analyze, calibrate and refine techniques used in IAB modeling. The following studies have developed modeling methodologies used in the development of IAB models.

- Fennema (2003) "Predicted and Measured Response of an Integral Abutment Bridge";
- Paul (2003) "Thermally Induced Superstructure Stresses in Prestressed Girder Integral Abutment Bridges";
- Pugasap (2006) "Hysteresis Model Based Prediction of Integral Abutment Bridge Behavior"; and
- Kim (2008) "Load and Resistance Factor Design for Integral Abutment Bridges".

In these studies it was determined that:

- The soil-structure interaction could be accurately modeled through the use of multi-linear springs from p-y curves;

- Creep and shrinkage should be considered in IAB modeling;
- Backfill pressure should be included in the numerical model; and
- The abutment back-wall connection can be modeled using a moment-curvature relationship as opposed to a fixed or pinned connection as previously assumed.

Chapter 3

NUMERICAL MODELING

3.1 Introduction

IABs are highly indeterminate structures with non-linear, soil-structure interaction, making them more difficult to analyze than conventional jointed bridges. Designers have subsequently simplified IAB analysis and design because of uncertainties in IAB behavior and modeling difficulties. Fenema (2003), Paul (2003), Pugasap (2006) and Kim (2008) have developed and refined modeling techniques used in developing numerical models that show a close correlation between the predicted and measured response of IABs.

Previous studies on IAB behavior utilized 2D numerical models that allowed many parameters to be investigated. However, 2-D IAB models are unable to identify potential distress at specific locations of bridge components. The present study developed 3-D models using modeling techniques that were validated with field data from four (4) monitored IABs in Pennsylvania to predict IAB response under thermal and time dependant loads. Finite element models for the present study are generated using the general purpose software package ANSYS. ANSYS was chosen because it is capable of modeling the required nonlinear soil-structure interaction behavior, the elastic perfectly plastic pile behavior, and complex geometry of structural concrete components. To better identify potential distressed locations, the geometry of 3-D models generated in this study is modeled in great detail, specifically at the backwall-girder connection.

Kim (2008) and Pugasap (2006) used over 7 years of field data to calibrate and refine IAB modeling techniques. The modeling techniques developed by Kim (2008) and Pugasap (2006) predict, with a significant degree of accuracy, the behavior and long term effects of various loads on IABs. Modeling techniques by Kim (2008) are used in this present study to develop numerical models for use in a parametric study.

This chapter presents in detail the modeling techniques used to generate numerical models for the parametric study that investigates the critical response of IABs at extreme lengths. The parametric study will investigate the pile head displacement, pile moments, and stresses at several locations. The bridge configuration that results in lowest response is determined from the parametric study and is used to establish practical length limits of IABs. Using this bridge configuration, the length is increased and the stresses, moments and displacements at specific bridge locations checked against limiting values. Force and stress limits are those set by AASHTO LRFD (2008) Bridge Design Specifications, 4th Edition, 2007 with 2008 interims and the PCI Bridge Design Manual (2005).

3.2 Bridge Geometry

A symmetrical, 1000′-0″ (305 m) IAB with no skew was selected for the initial numerical model and parametric study. The bridge cross section design used in this study is modeled after structure 203, a PennDOT bridge located in Port Matilda, PA (refer to Table 2.10). Bridge 203 was chosen because it is typical of IAB construction in Pennsylvania.

The bridge superstructure is typical slab-on-girder, with a 9″ (229 mm) reinforced concrete deck that is assumed fully composite with 4 AASHTO-PCI, BT-72 prestressed concrete girders. Figure 3.1, shows the detailed bridge cross-section.

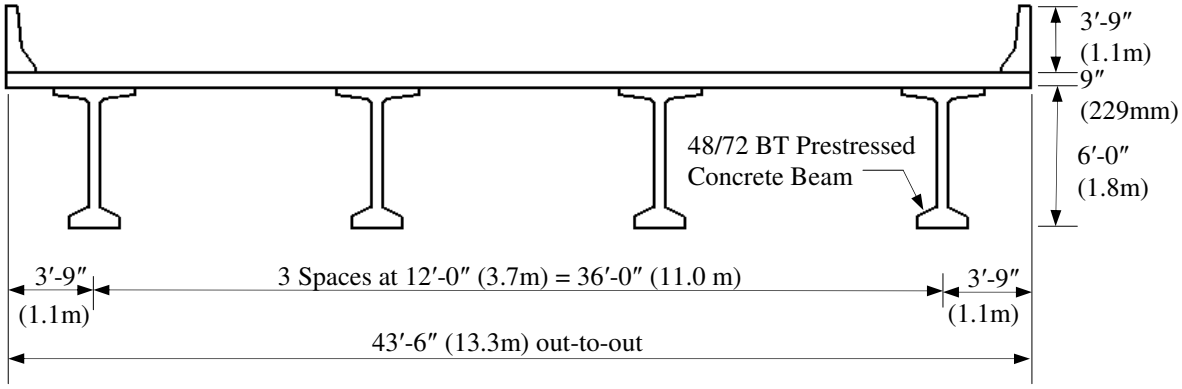

Figure 3.1 Superstructure Cross-Section of Study Model

The girders of the study model are supported by 7 identical, hammerhead piers and elastomeric bearings, as shown in Figure 3.2. All spans are equal length and considered continuous for all live loads and simply supported for dead loads. An abutment thickness of 4′-0″ (1.2 m) and a width of 43′-6″ (13.3 m) are used in this study. The abutment is supported by eight HP12x74 (HP310x110) piles driven in a single layer of soil to bedrock as shown in Figure 3.3.

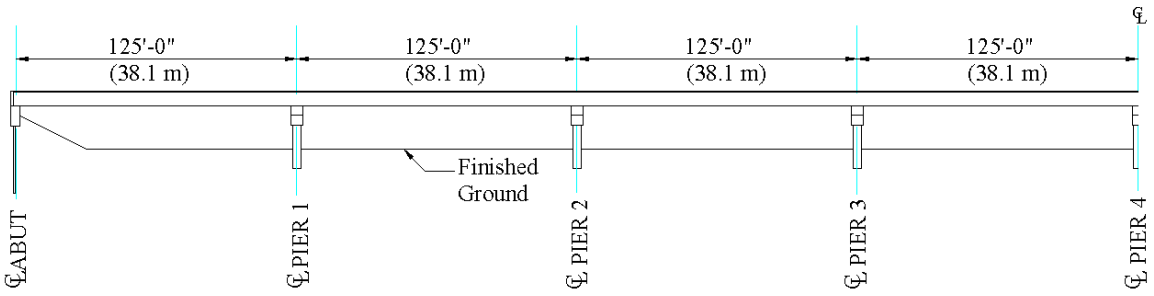

Figure 3.2 Elevation of Study Model

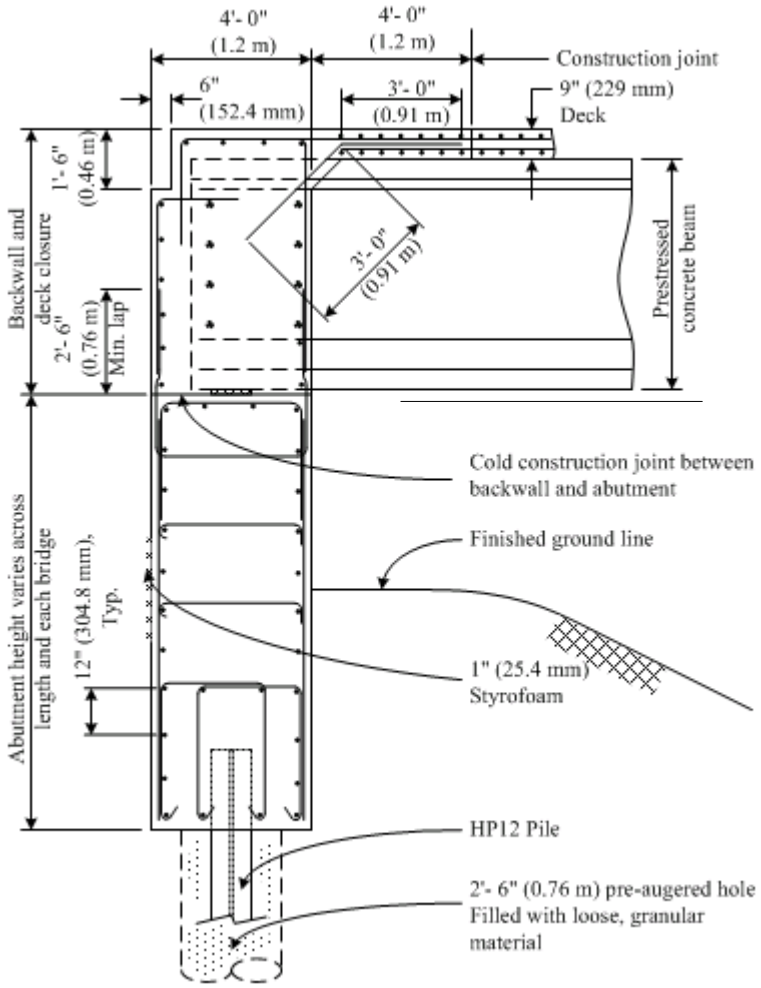

Figure 3.3 Abutment Section of Study Model

Taking advantage of the bridge symmetry, half of the bridge is modeled in both the longitudinal and transverse directions. The frictional forces generated from the approach slab are negligible compared to the effect of the loads acting on the structure (Dicleli *et al*. 2003). Presently, no studies provide evidence that parapets and wingwalls have a significant effect on IAB behavior. Therefore, approach slabs, parapets, and wingwalls are not considered in the numerical models for this study.

3.3 Study Model

Eight-node SOLID45 elements are used to model the backwall, abutment and girders closest to the abutment. A surface to surface contact pair is created between the backwall and solid girders using CONTACT175 and TARGET170 elements. The contact surface allows for stress in compression only, with no penetration of the two components, while permitting separation of the components in tension. The transverse threading connecting the girders are modeled using BEAM4 elements rigidly connected to the girders and ends of the backwall.

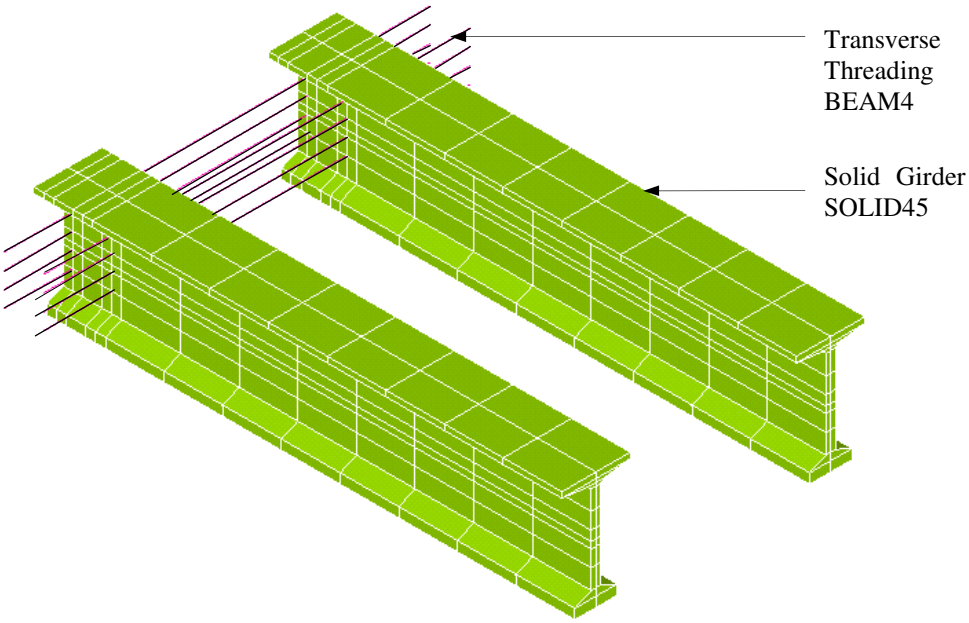

Figure 3.4 Solid Girder and Transverse Threading

At the abutment the elastomeric bearings are modeled using SOLID45 elements that are connected to the abutment and girders through shared ANSYS keypoints. Bearings at the pier locations are modeled as 3″ (76.2 mm) long BEAM4 elements connected to the pier hammerhead and girders using rigid links. The girders adjacent to the abutment are modeled using solid elements for approximately 10% of the total bridge

length. Girders throughout the rest of the bridge length are modeled using BEAM4 elements because a detailed analysis of the stresses in the girders in this location is not required for this study.

The connection between the solid and beam elements utilizes a Beam-Solid Assembly defined by a rigid constraint. The beam-solid connection is used to couple the motion of 2 nodes, were one node is defined as the pilot node from the target surface (beam) and the other from the contact surface (solid). The pilot node governs the motion of the target surface transferring forces/ moments or rotation/ translations for the entire target surface. A pilot node is defined at node (I) of the beam element and solid nodes are defined as the contact nodes, shown in Figure 3.5.

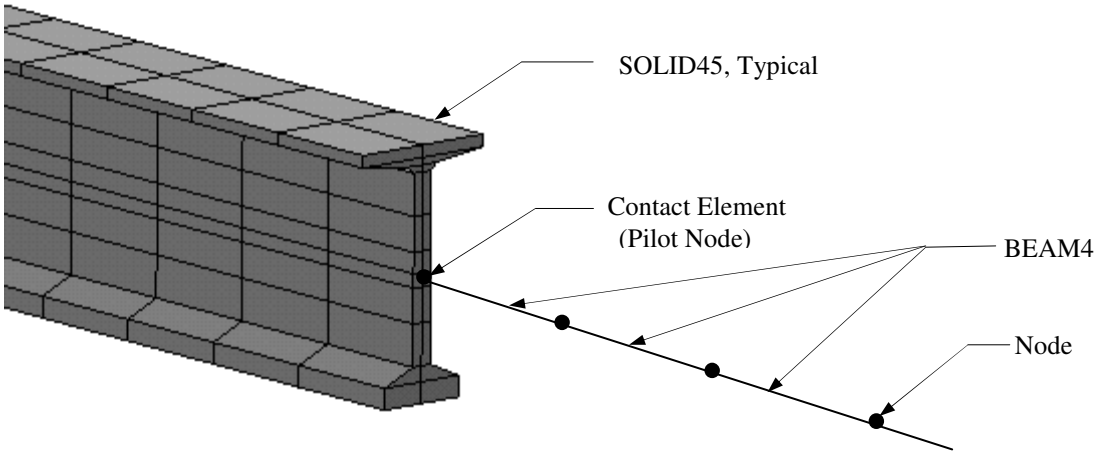

Figure 3.5 Solid to Beam Contact

The 9″ (229 mm) reinforced concrete deck is modeled using linear-elastic SHELL63 elements having both bending and membrane capabilities with six degrees of freedom at each node as shown in Figure 3.6.

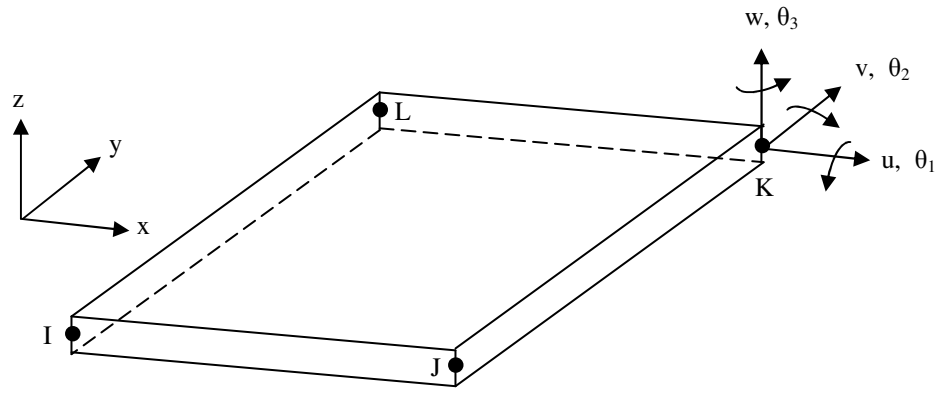

Figure 3.6 SHELL63 Elastic Shell at Deck

The deck is connected rigidly to the backwall at the deck elastic neutral axis (ENA). To simulate full composite behavior, multi-point constraint (MPC184) rigid link elements (Figure 3.7) connect the top of the girder (SOLID45) and deck ENA. Where BEAM4 elements are used to model the girders, rigid links connect the ENA of the deck and girders at 10′-0″ (3.0 m) intervals as shown in Figure 3.8. The deck mesh varies from 1′ to 10′ (0.3 m to 3.0 m) with a finer mesh at the abutment where a more detailed analysis result is needed.

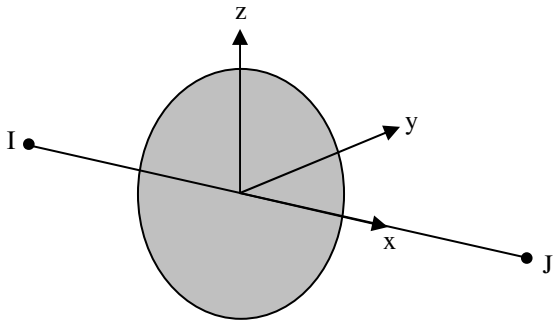

Figure 3.7 MPC184 Rigid Link/Beam

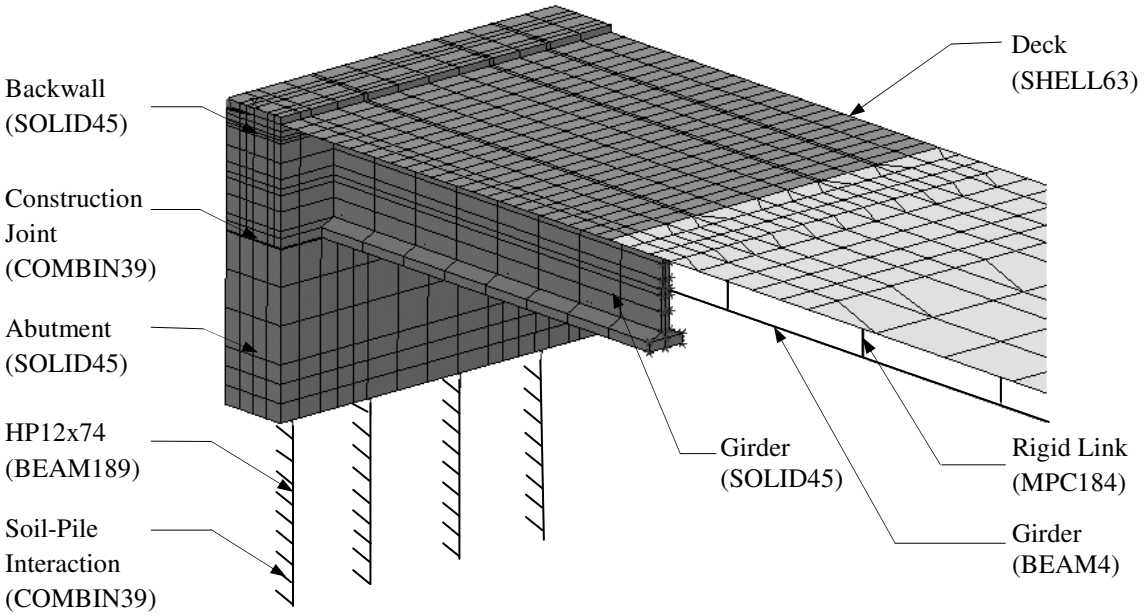

Figure 3.8 Cross-Section of Model Superstructure

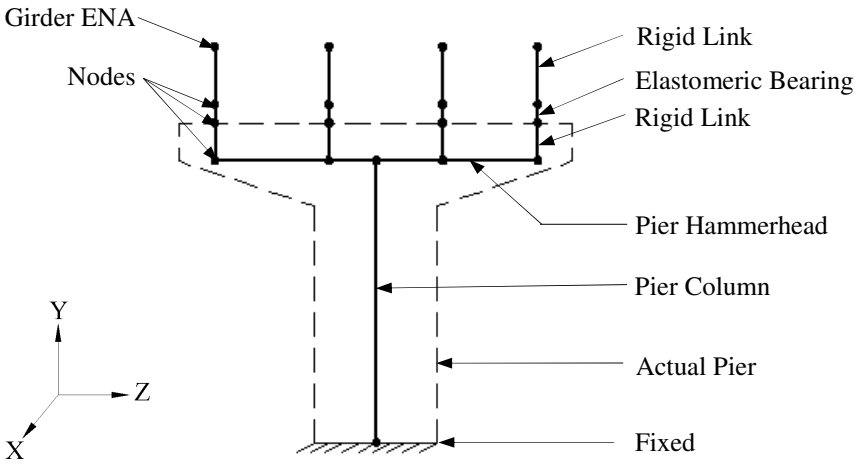

Figure 3.9 Cross-Section of Pier Model

3.4 Material Properties

3.4.1 Bridge Components

The material properties used in this study were adopted from bridge monitoring reports by Laman *et al*. (2006) from monitored IABs along the I-99 in Pennsylvania (Table 2.10). Concrete components were modeled using homogeneous, isotropic elements and are assumed linear-elastic. The non-linear behavior of the steel pile were assumed to be elastic perfectly plastic. The material properties used in this study are shown in Table 3.1.

Table 3.1 Material Properties of Study Model

Bridge Component	Strength f'_c, ksi (MPa)	Young's Modulus, E, ksi (MPa)	Poisson's Ratio	Thermal Expansion Coefficient, in/in/ ºF (mm/mm/ ºC)
Deck and Backwall	4.0 (27.6)	3644 (25,124)	0.2	6.0E-6 (11E-6)
Girder	8.0 (55.2)	5154 (35,536)	0.2	6.0E-6 (11E-6)
Piers and Abutment	3.0 (20.7)	3156 (21,760)	0.2	6.0E-6 (11E-6)
Steel H-Piles	50 (345)	29000 (200,000)	0.3	6.5E-6 (12E-6)
Transverse Threading (#8 bars)	60 (345)	29000 (200,000)	0.3	6.5E-6 (12E-6)

3.4.2 Bearings

Bearings are orthotropic materials having different stiffness properties in orthogonal directions. Steel reinforced bearings are typically used on IABs and are designed to permit relatively large shear and withstand high compressive loads.

In the present study, elastomeric bearings are modeled using 3D solid elements at the abutment and 3″ (76.2 mm) beam elements at the pier supports. To model the behavior of the 3D bearing, three Young's moduli E_X, E_Y and E_Z were required. Three separate Poisson's ratios were also required, ν_{XY}, ν_{YZ} and ν_{XZ} and the in-plane shear modulus G_{XZ}.

AASHTO LRFD (2008) allows two design methods for elastomeric bearings: Method A, applicable to plain, steel reinforced and fiber glass reinforced elastomeric bearings and Method B, applicable to steel reinforced elastomeric bearings. Method B uses AASHTO LRFD (2008) equations, (3.1) and (3.2), with a nominal hardness of 50 on the shore scale to determine the Young's Modulus of the bearing material.

$$E_C = 6GS^2 \tag{3.1}$$

where E_c is the effective compressive modulus of elasticity (ksi), G is the shear modulus of the elastomer and S is the shape factor of the thickest layer of an elastomeric bearing. The shape factor is calculated using Equation 3.2.

$$S = \frac{LW}{2h_{ri}(L+W)} \tag{3.2}$$

where L is the length (in), of the rectangular bearing in the span direction, W is the width (in) of the bearing in the transverse direction and h_{ri} is the thickness of the ith layer in the

elastomeric bearing as shown Figure 3.10. Table 3.2 summarizes the properties of the elastomeric bearings used in this study.

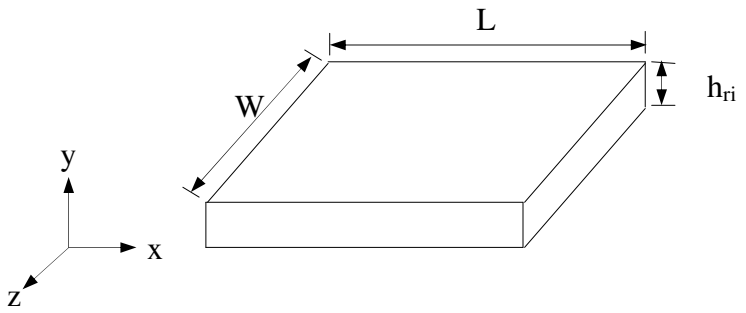

Figure 3.10 Elastomeric Bearing

Table 3.2 Material Properties of Elastomeric Bearing.

Bridge Component	Young's Modulus ksi, (MPa)			Poisson's Ratio			Shear Modulus, G, ksi (MPa)
	EX	EY	EZ	νXY	νYZ	νXZ	GXZ
Elastomeric Bearings	1795 (12,386)			0.49			0.1 (0.69)

3.5 Loads

3.5.1 Ambient Temperature Load

This study utilizes the AASHTO LRFD (2008) recommended design temperature range of 10ºF to 80ºF (-2.2ºC to 26.7ºC) for concrete structures in moderate climates. A reference temperature of 50ºF (10 ºC) was assumed, i.e. the temperature at which the backwall and deck were cast. The assumed reference temperature translates to a temperature rise (expansion) of + 30 degree and -40 degree fall (contraction).

3.5.2 Temperature Gradient

The superstructure thermal gradient contributes significantly to superstructure stresses in IABs and is included in this study by using AASHTO LRFD (2008) multi-linear temperature gradients for the mid-Atlantic area. Because the multi-linear temperature gradients cannot be modeled in ANSYS, an equivalent, linear, temperature gradient was determined based on equivalent axial and bending strains recommended by AASHTO LRFD (2008), shown in Figure 3.11.

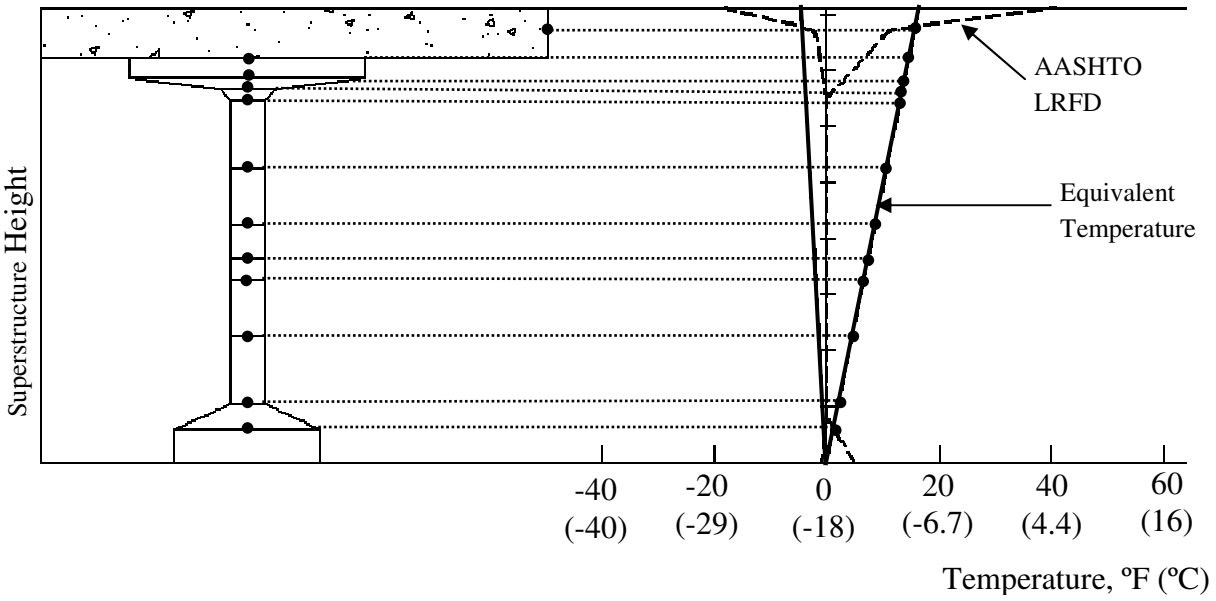

Figure 3.11 Temperature Gradient for Study Model in Pennsylvania

The temperature gradient values corresponding to depth of the deck ENA is applied to the nodes of the deck. Temperature values at each depth corresponding to node locations of the solid girder were determined and applied at nodes along the

superstructure depth. For the beam girder, the top and bottom temperatures were specified.

3.5.3 Time-Dependant Loads

The load effect of time-dependant loads, creep, shrinkage and prestressing steel relaxation, was determined using the age adjusted elastic modulus method (AAEM) that results in net time-dependant strains. The AAEM accounts for time-dependant effects by considering that the concrete modulus of the reinforced deck and precast girder varies with time. Strains obtained from the time-dependant effects were converted to equivalent temperatures using the equivalent temperature method based on the thermal expansion coefficient.

AASHTO LRFD (2008) age-adjusted, creep coefficient $\varphi(t, t_o)$ and aging coefficient, $\chi(t, t_o)$, for concrete were used in this study to determine equivalent time-dependant temperatures. Figure 3.12 shows the variation of temperature along the 125′ (38.1 m) span length computed using the AAEM method. Time-dependant effects were more critical for contraction models because the computed strains resulted in an equivalent negative temperature. The equivalent temperatures were determined for each depth (y) of the superstructure and added to the ambient temperature, the temperature gradient, and applied to the nodes of the solid girder. The ambient temperature, temperature gradient, and time-dependant temperatures at the top and bottom were applied to the beam elements assuming a linear distribution.

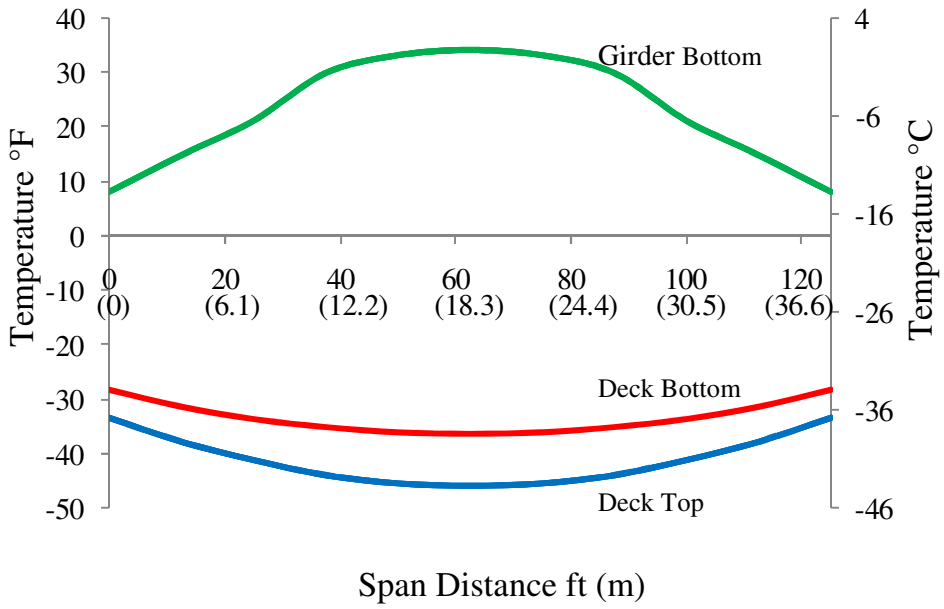

Figure 3.12 Temperature Distribution Along Span Length

3.6 Construction Joint

The standard PennDOT detail for integral abutments was modeled numerically in this study using #5 (ø16 mm) "U" shaped bars spaced at 9″ (229 mm) (Figure 3.13).

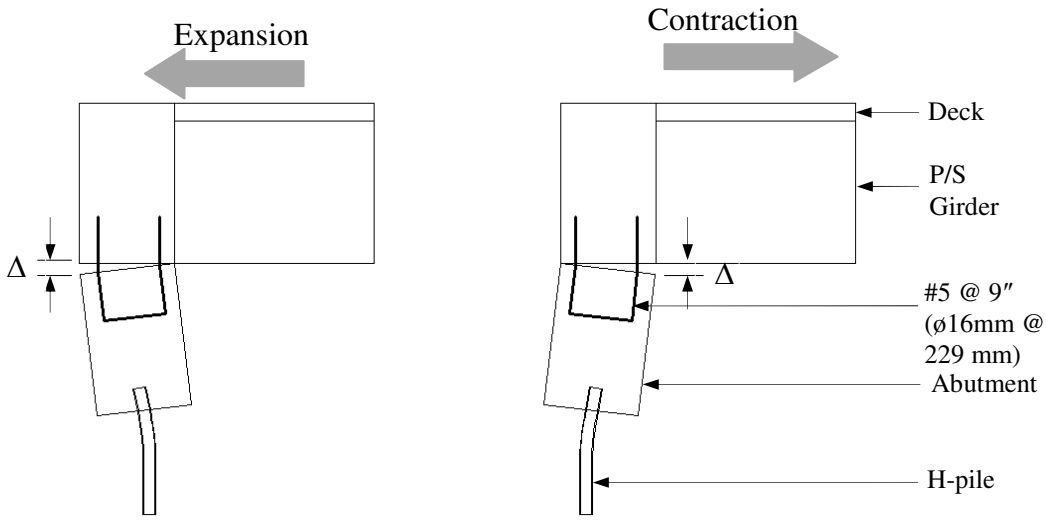

Figure 3.13 Construction Joint Model

ANSYS COMBIN39, a non-linear unidirectional element with generalized force-deflection capabilities, is used to connect the backwall to the abutment. The elastic perfectly plastic property of COMBIN39 is based on the force-displacement curve of the joint reinforcement, shown in Figure 3.14. This force-displacement curve was derived from the typical stress-strain curve of reinforcing steel based on the area and spacing of the rebar.

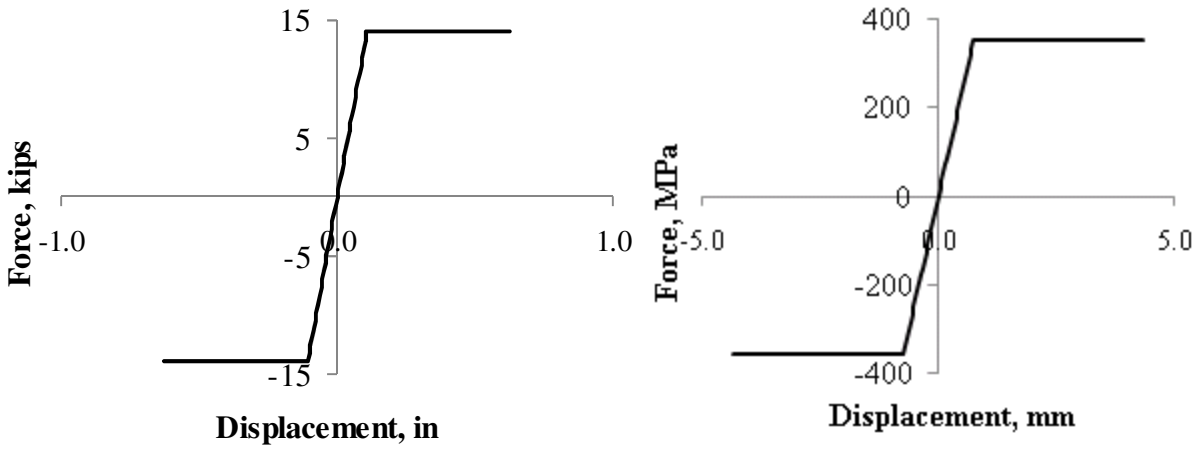

Figure 3.14 Force-Displacement Curve Construction Joint Rebar

3.7 Soil- Pile Interaction

The soil-pile interaction along the depth of the pile is defined by *p-y* curves, a nonlinear load *(p)* – lateral displacement *(y)*. This study utilizes LPILE, a special purpose program for analyzing piles under lateral loading, to generate a family of p-y curves specific to each soil type considered in this study. The *p-y* curves for the soil are generated using LPILE at 12″ (0.304 m) increments along the pile depth. The *p-y* curves are represented in the numerical model using non-linear COMBIN39 springs.

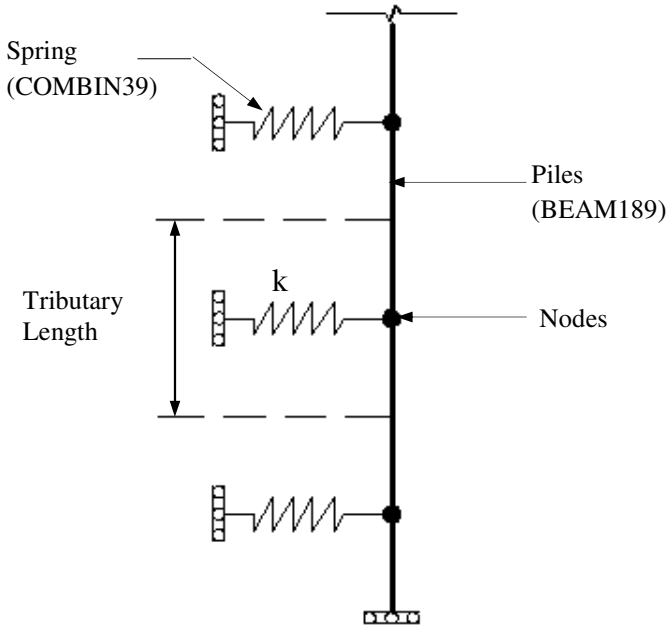

Figure 3.15 Pile Model

The soil properties used in this study were adopted from geotechnical reports for Structure 211 and field monitoring data collected from bridges 109, 203, 211 and 222 (Laman *et al.* 2006). Table 3.3 presents soil properties used to generate *p-y* curves for the numerical model.

Table 3.3 Soil Properties Used in Parametric Study

Soil Type	k pci (MN/m^3)	ε_{50} in (mm)	ϕ deg	c psi (kN/m^2)	γ pci (kN/m^3)
Sand	125 (33.9)	0	33.3	0	0.042 (11.4)
Medium Clay	100 (27.2)	0.01 (0.25)	0	6.94 (47.8)	0.066 (18.0)
Stiff Clay	400 (108.6)	0.005 (0.127)	0	20 (138)	0.081 (22.0)
Bedrock	4000 (1086.8)	0.001 (0.025)	0	9000(62,053)	0.048 (13.0)

where γ is the unit weight of soil; c is the undrained shear strength; ε_{50} is the soil strain parameter; and ϕ is the internal angle of shearing resistance. A set of p-y curves represent the lateral deformation of soil under a horizontally applied pressure in a discrete vertical section of drilled shaft at any depth. Figure 3.16 shows a set of p-y curves for the soil types used in this study at 182″ (4 623 mm) below the surface.

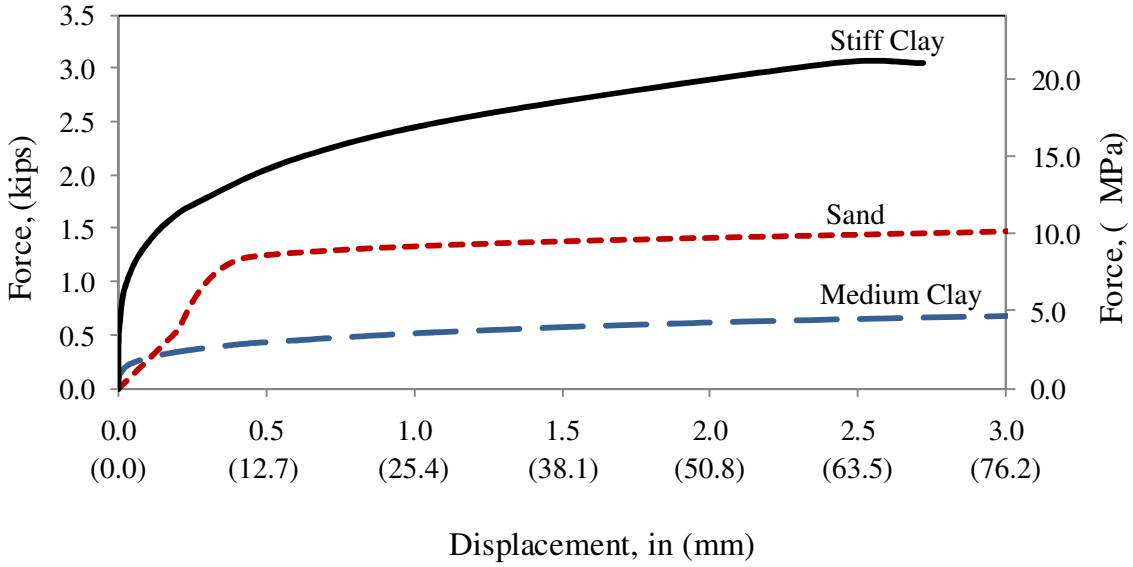

Figure 3.16 Soil Stiffness Comparison

3.8 Backfill Pressure

The backfill pressure acting on the backwall and abutment is considered in the numerical model for this study. Hydrostatic pressure is considered 1′-6″ (0.46 m) from the top of the superstructure to account for the presence of an approach slab and 2′-7″ (0.79 m) from either sides of the backwall and abutment to account for wing-walls on either side. The active and passive coefficients, K_a and K_p are determined using

Rankine's lateral earth pressure theory. The initial slope, K_h, was determined from pressures and corresponding abutment displacements obtained from field data (Laman *et.al*. 2006).

Figure 3.17 shows the modified *p-y* curve model applied to the numerical model. After backfilling, an initial at-rest lateral earth pressure, P_o is applied to the model as an external pressure. The lateral backfill pressure is assumed to vary linearly between active pressure, P_a, and passive pressure, P_p. Therefore, a reduced active pressure, P_a-P_o and reduced passive pressure, P_p-P_o, is applied to the model. The backfill pressure, *(p)* vs. displacement *(Δ)* curve at each depth is simulated in the numerical model using COMBIN39 non-linear springs. The material properties used in this study were adopted from the typical OGS material used by PennDOT for IABs and are shown in Table 3.4

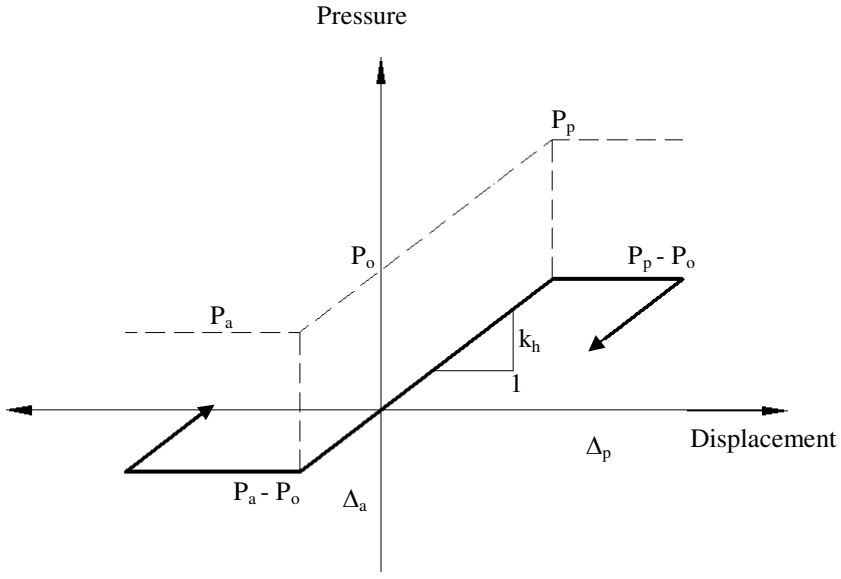

Figure 3.17 Modified Abutment-Backfill Model

Table 3.4 Backfill Properties

Soil Type	γ pci (kN/m^3)	Φ Deg	k_h pci (kN/m^3)
Backfill (PennDOT OGS)	0.069 (18.7)	34	43.8 (11,870)

where k_h is the subgrade modulus determined using field monitoring data for the backfill pressure and displacement taken from the four monitored bridges.

3.9 Parametric Study

Arockiasamy (2004), Dicleli (2003), Huang (2008), Kim (2008) and Paul (2003) have all investigated the effects of various geometric and structural properties of bridge components and geotechnical properties on IAB behavior. These studies have determined the most influential parameters for short to medium lengths. The present parametric study focuses on the critical response of IABs at extreme lengths. This study investigates the effect of: (1) abutment height; (2) soil stiffness; (3) construction joint stiffness; and (4) pile orientation, on:

- pile head displacement;
- pile moment;
- maximum stress in piles;
- concrete stress at abutment-pile location; and
- girder bottom stress

Abutment heights of 4′, 9′ and 12′ (1.2 m, 2.7 m and 3.7 m) were used in this study. These values represent the lower, intermediate and upper values of abutment heights used by PennDOT and are typical in other states. The foundation soil type was varied between stiff clay, medium clay and sand thereby representing a range of soil stiffness that influence IAB behavior differently. Two pile orientations, strong and weak axis bending are investigated to determine the effects of pile stiffness on IABs at extreme lengths. The bridge models developed for the parametric study are shown in Figure 3.18 (a), (b) and (c).

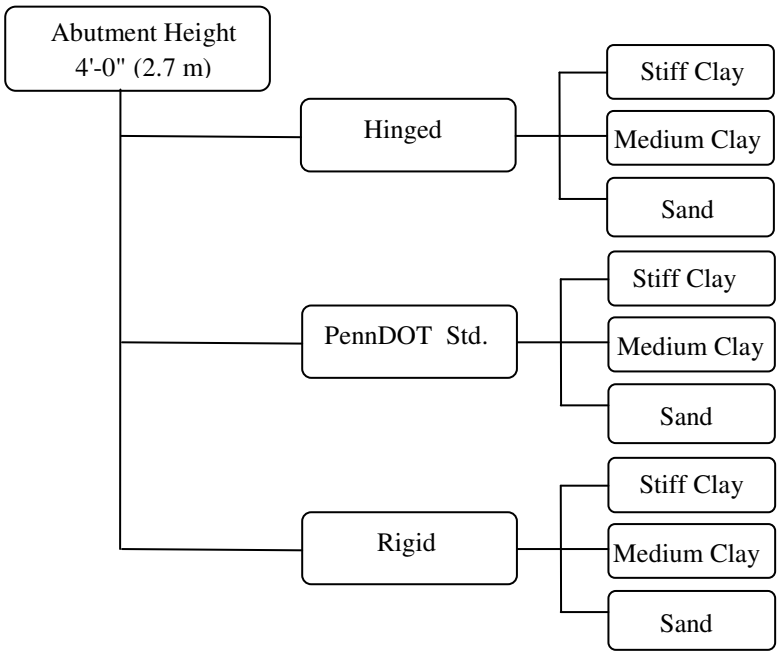

(a) Numerical Models with Abutment Height 4´-0˝

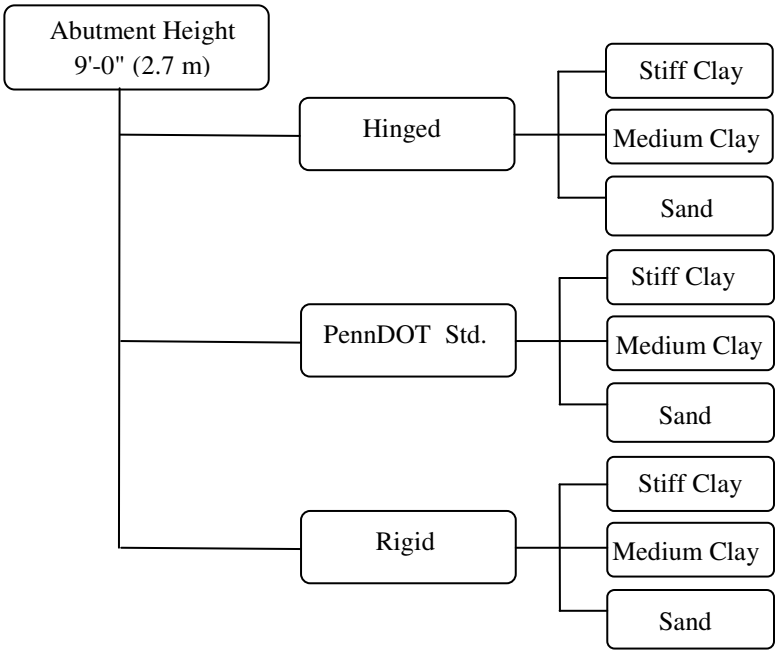

(b) Numerical models with abutment height 9′-0″ (2.7 m)

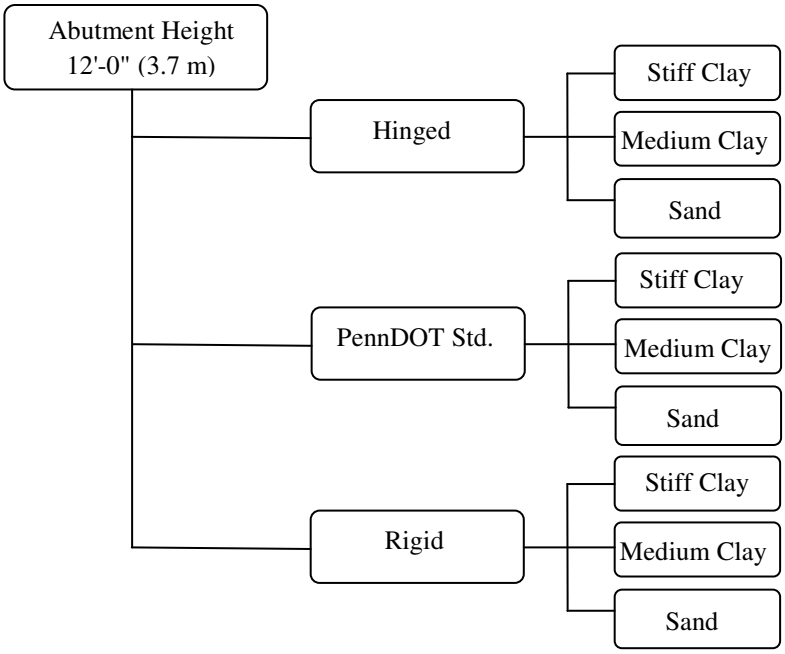

(c) Numerical models with abutment height 12′-0″ (3.7 m)

Expansion/Contraction and Strong/Weak pile orientation was considered for each model.

Figure 3.18 Models developed for Parametric Study

Chapter 4

PARAMETRIC STUDY RESULTS

4.1 Introduction

This chapter presents the results from the parametric study performed using the numerical models described in Chapter 3. The parametric study comprises 108 numerical models in which the following parameters are varied: (1) abutment height; (2) soil stiffness; (3) construction joint stiffness; and (4) pile orientation. The study considers the effect of the fore-mentioned parameters on: (1) pile head displacement; (2) pile bending stress; (3) pile bending moment; (4) concrete stress at abutment pile location; and (5) bottom girder stress, under thermal and time dependant loads only.

The results of the parametric study are presented graphically to illustrate IAB behavior trends. The pile bending stress and moments are plotted and compared to pile yield stress (F_y) and pile plastic moment (M_p). Concrete stress at the abutment-pile connection is plotted and compared to the modulus of rupture (f_r) of the abutment concrete. The modulus of rupture was calculated using:

$$f_r = 8.3 \sqrt{f'_c} \tag{4.1}$$

where f'_c is the 28 day compressive strength of concrete in psi or MPa. The girder bottom tensile stress is compared to AASHTO LRFD (2008) limit for tension stress. Other bridge components are also investigated to determine if stress values exceed failure limits set by AASHTO. Locations investigated for distress include: (1)

construction joint; (2) girder-backwall connection; (3) transverse threading; (4) elastomeric bearing; and (5) deck.

4.2 Pile Displacement

Figures 4.2 through 4.4 present the maximum pile head displacement with respect to: (1) abutment height; (2) soil stiffness; (3) construction joint stiffness; and (4) pile orientation for both expansion and contraction cases. The sign convention for pile head displacement designates negative (-) displacement for expansion cases and positive (+) displacement for contraction cases, as shown in Figure 4.1.

Abutment height has the largest effect on pile head displacement. Up to a 69% decrease in pile head displacement was observed when the abutment height is increased for expansion and up to a 54% decrease in contraction cases, as shown in Figure 4.2. Pile head displacement shows a 20% decrease when soil stiffness is increased for expansion and contraction cases, observed in Figure 4.3. Construction joint stiffness has some influence on pile head displacement as up to a 24% change is observed in Figure 4.4.

Pile orientation did have a significant effect on the bridge components investigated with differences of less than 0.2 in (5.1 mm). Additionally, the magnitudes of weak axis oriented pile displacement are larger than that of strong axis oriented values.

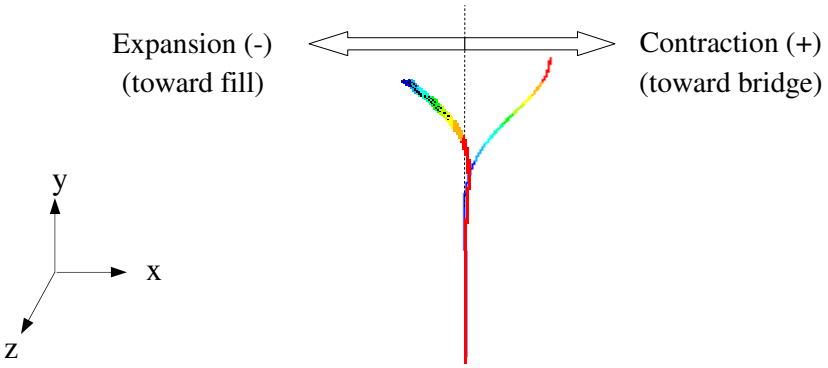

Figure 4.1 Sign Convention of Pile Displacement

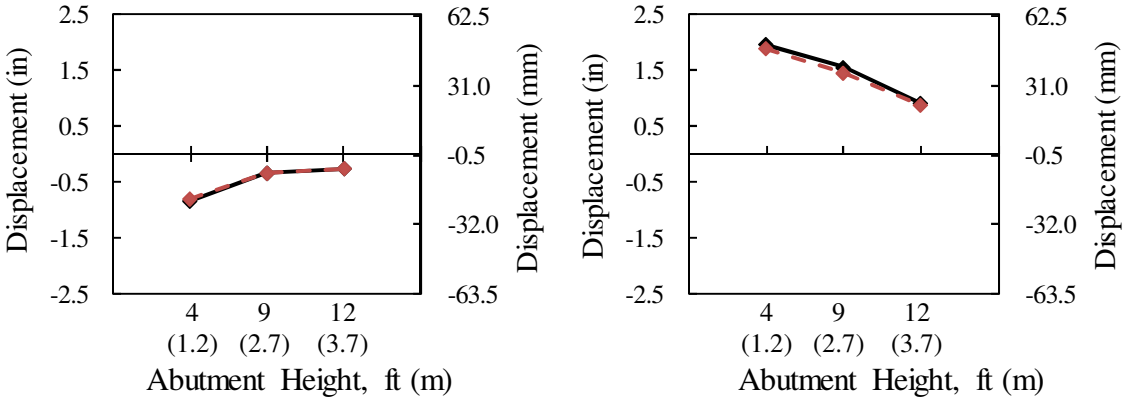

(a) Hinged and Bridge Expansion

(b) Hinged and Bridge Contraction

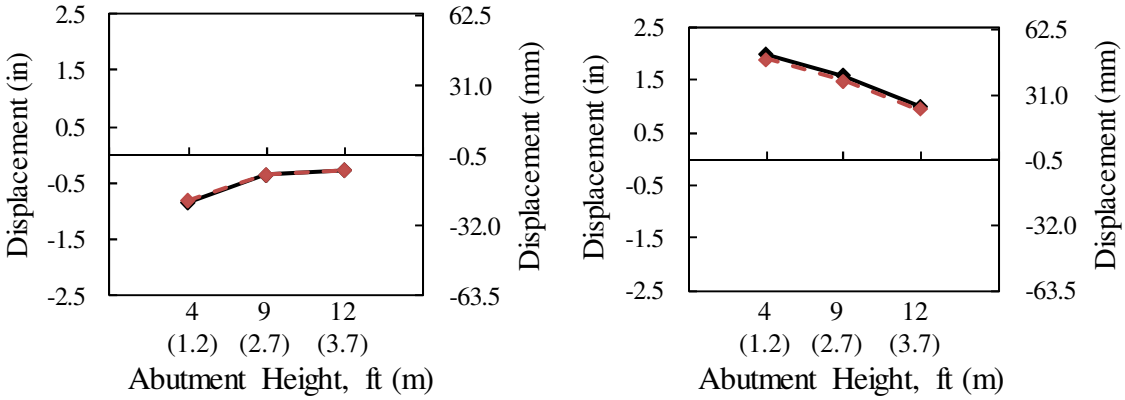

(c) PA Std. and Bridge Expansion

(d) PA Std. and Bridge Contraction

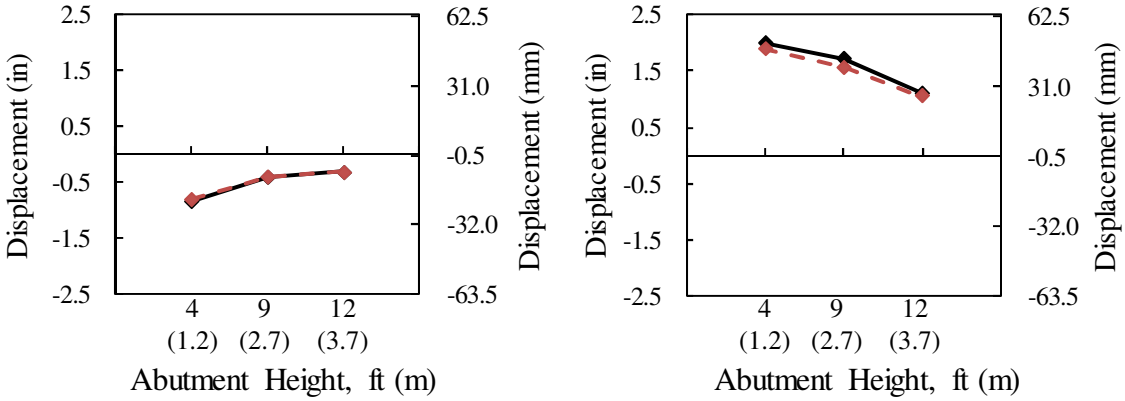

(e) Rigid and Bridge Expansion

(f) Rigid and Bridge Contraction

Soil Type: Stiff Clay

(- - ◆ - - : Strong Axis; ——◆—— : Weak Axis)

Figure 4.2 Abutment Height Influence on Pile Head Displacement

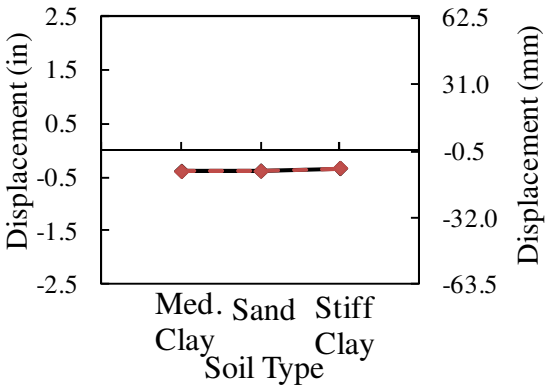

(a) Hinge and Bridge Expansion

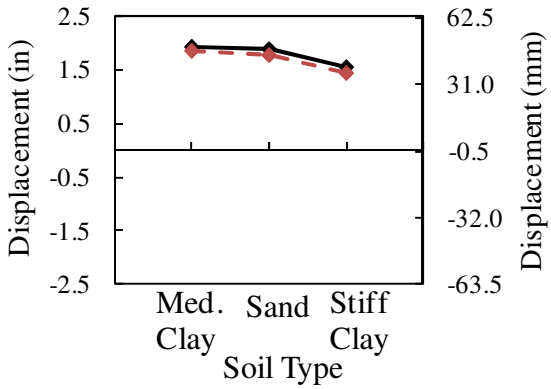

(b) Hinge and Bridge Contraction

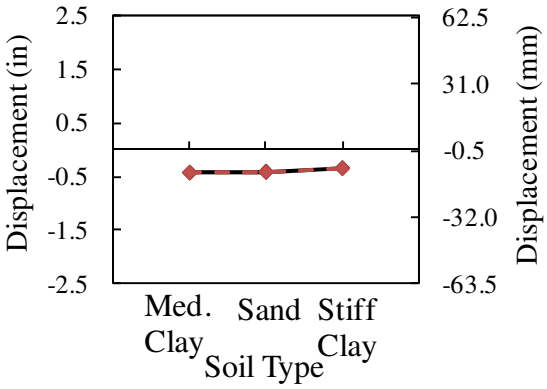

(c) PA Std. and Bridge Expansion

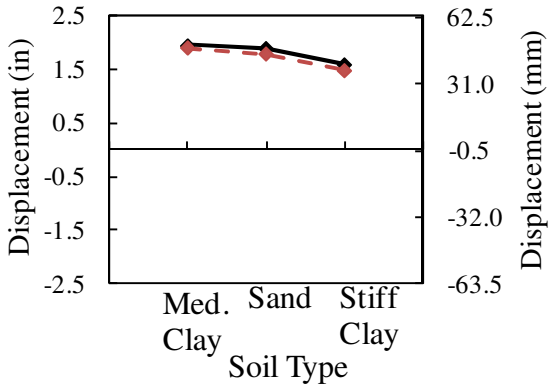

(d) PA Std. and Bridge Contraction

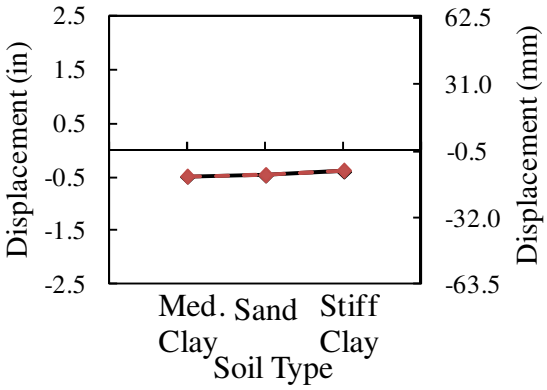

(e) Rigid and Bridge Expansion

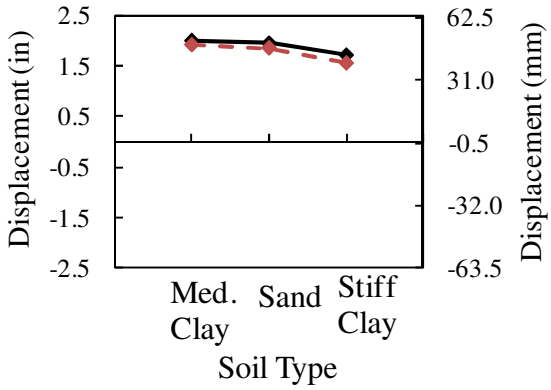

(f) Rigid and Bridge Contraction

Abutment Height: 9′-0″ (2.7 m)

(– –◆– – : Strong Axis; —◆— : Weak Axis)

Figure 4.3 Soil Type Influence on Pile Head Displacement

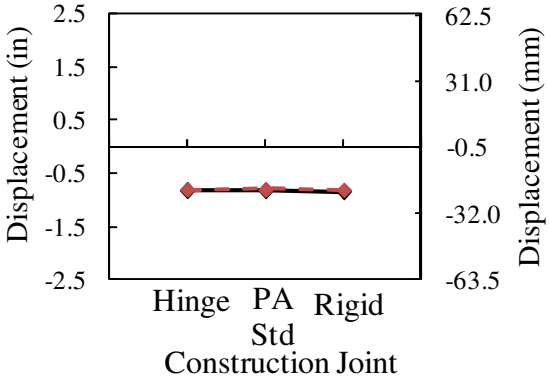

(a) H = 4 ft (1.2 m) Bridge Expansion

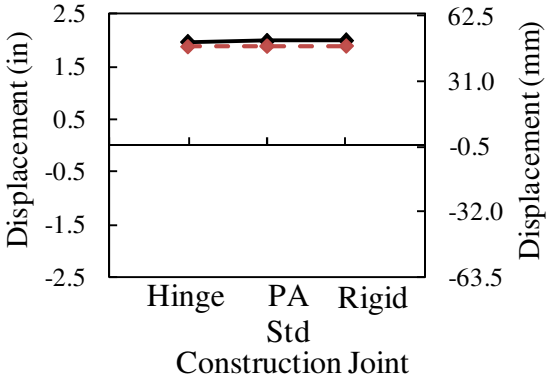

(b) H = 4 ft (1.2 m) Bridge Contraction

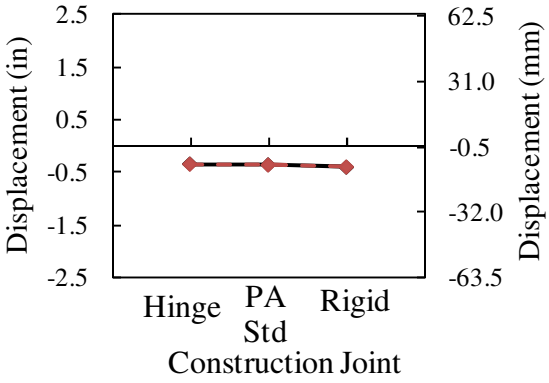

(c) H = 9 ft (2.7 m) Bridge Expansion

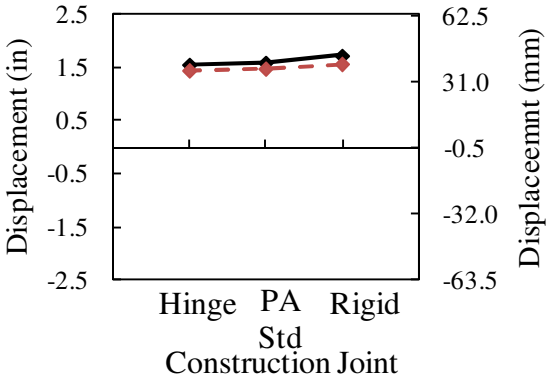

(d) H = 9 ft (2.7 m) Bridge Contraction

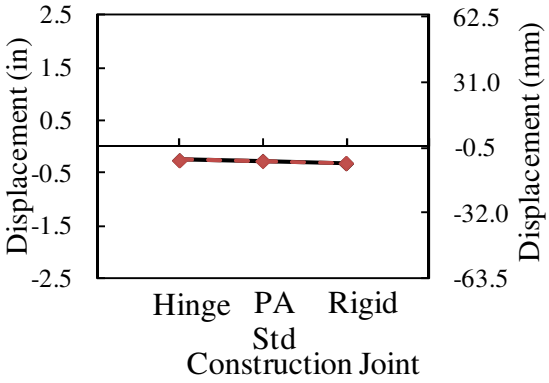

(c) H = 12 ft (3.7 m) Bridge Expansion

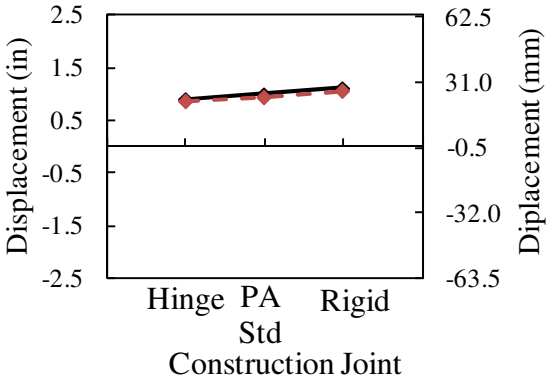

(f) H = 12 ft (3.7 m) Bridge Contraction

Soil Type: Stiff Clay

(– –◆– – : Strong Axis; —◆— : Weak Axis)

Figure 4.4 Construction Joint Influence on Pile Head Displacement

4.3 Max Stress in Piles

Figures 4.5 through 4.8 present the maximum pile bending stress with respect to: (1) abutment height; (2) soil stiffness; (3) construction joint stiffness; and (4) pile orientation for both expansion and contraction cases. The parametric study considers only the bending stress due to thermal loads - axial stress from dead loads is not included in this evaluation. The HP12x74 (HP310x110) pile used in this study has a yield stress, F_y, of 50 ksi (345 MPa). This yield stress is represented by the dotted lines in the figures.

Abutment height has a significant influence on pile maximum stress as observed in Figure 4.5. There is up to a 61% decrease in pile stress when the abutment height is increased for expansion and a 55% decrease is observed in contraction cases. The contraction cases, however, are larger than expansion cases with up to a 292% increase observed. This demonstrates that bridge contraction is a more critical state for pile bending stress and results in piles reaching yield stress in most cases.

It is observed from Figure 4.6 that an increase in pile bending stress occurs with an increase in soil stiffness. A 76% increase in stress is observed for expansion cases while only a 25% increase for contraction cases. A 33% decrease in pile bending stress in expansion cases and a 47% increase in pile bending stress for the contraction cases is observed with an increase in construction joint stiffness as shown in Figure 4.7. However, cases with abutment height equal to 4′-0" (1.2 m) does not follow a similar trend.

Overall weak axis orientation results in higher pile bending stress than strong axis orientation with contraction cases showing up to a 49% difference in pile bending stress magnitudes between strong and weak axis pile orientation.

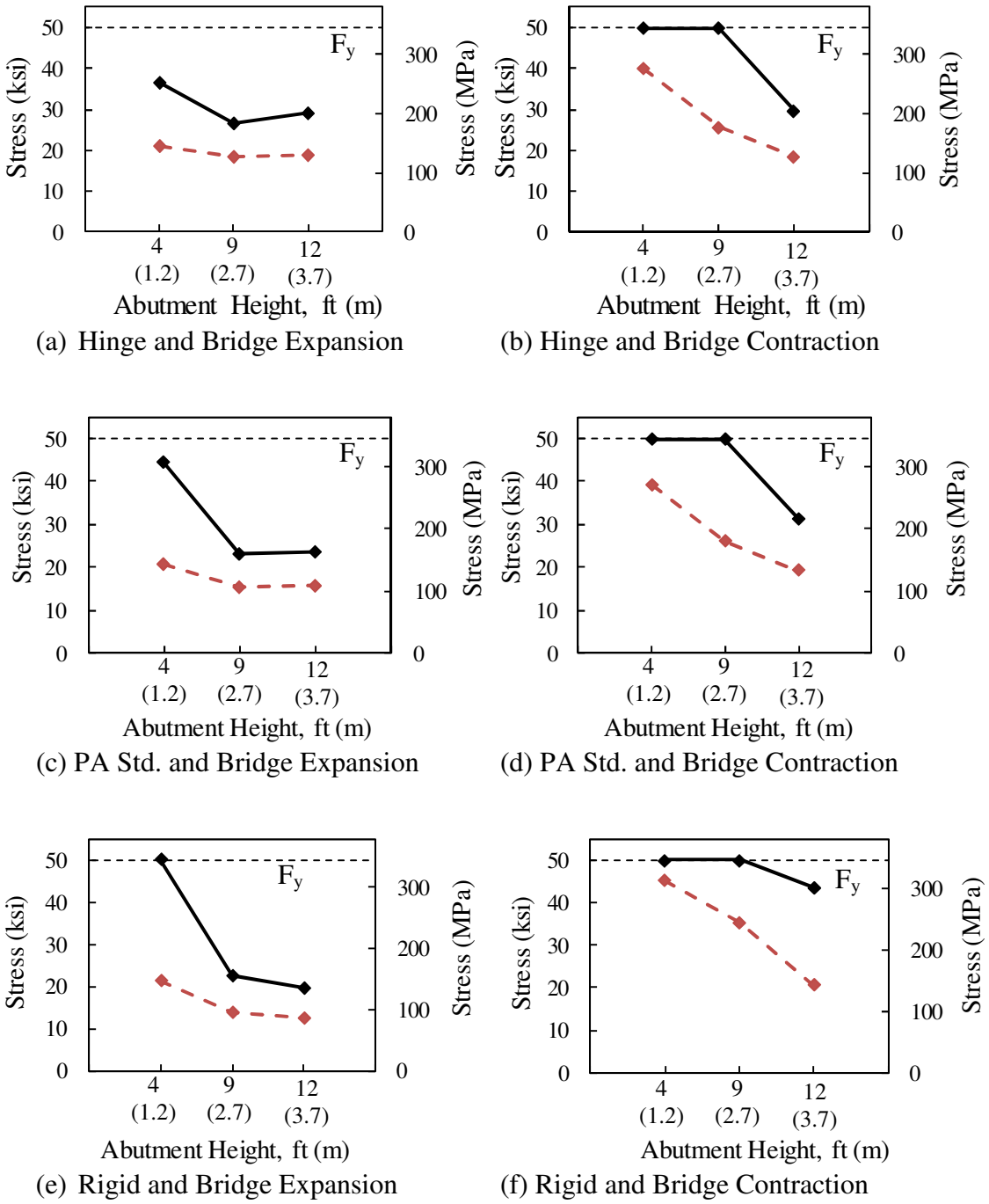

Soil Type: Stiff Clay

(– –◆– – :Strong Axis; ——◆—— :Weak Axis)

Figure 4.5 Abutment Height Influence on Maximum Pile Stress

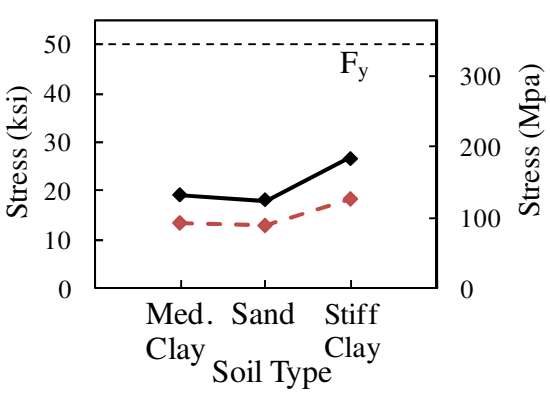

(a) Hinge and Bridge Expansion

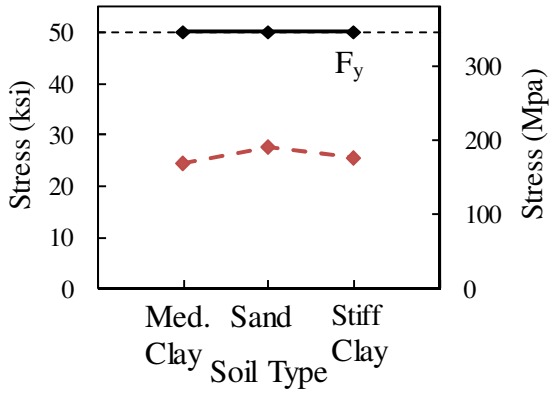

(b) Hinge and Bridge Contraction

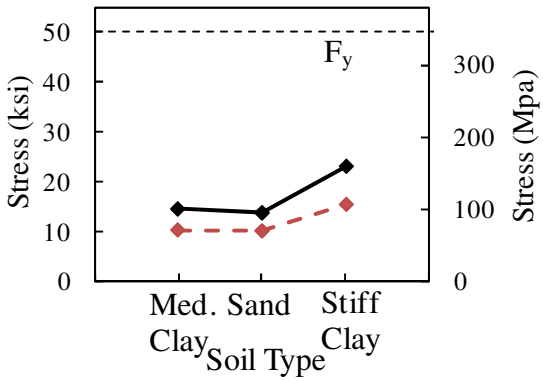

(c) PA Std. and Bridge Expansion

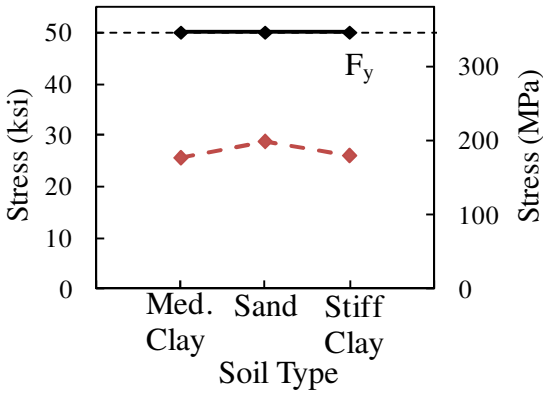

(d) PA Std. and Bridge Contraction

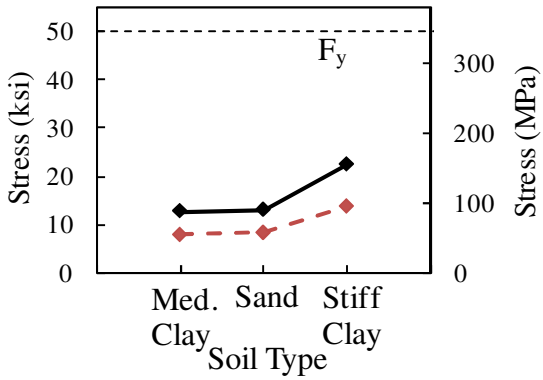

(e) Rigid and Bridge Expansion

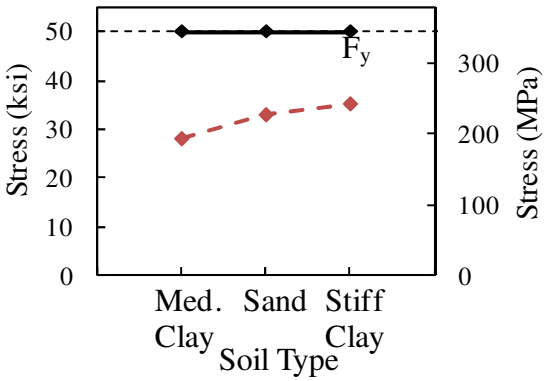

(f) Rigid and Bridge Contraction

Abutment Height: 9′-0″ (2.7 m)

(– – ◆ – – : Strong Axis; —◆—: Weak Axis)

Figure 4.6 Soil Type Influence on Maximum Pile Stress

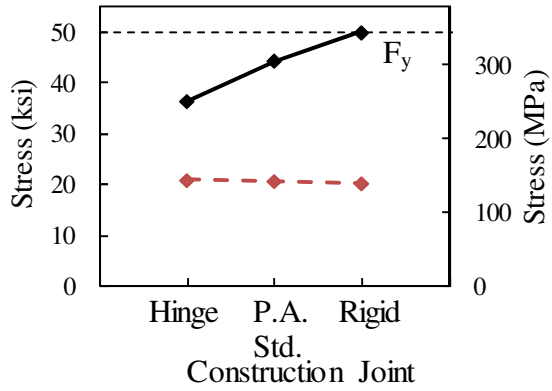

(a) H = 4 ft (1.2 m) Bridge Expansion

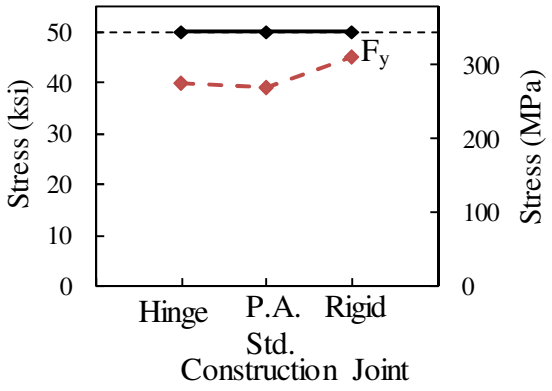

(b) H = 4 ft (1.2 m) Bridge Contraction

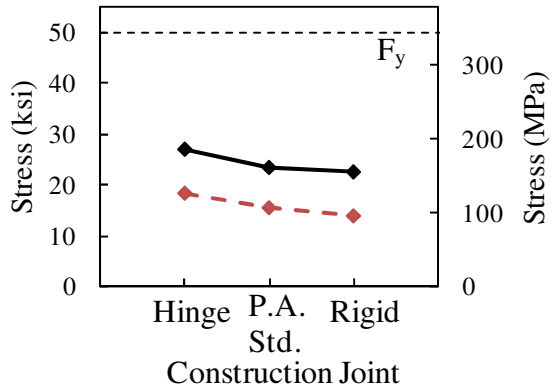

(c) H = 9 ft (2.7 m) Bridge Expansion

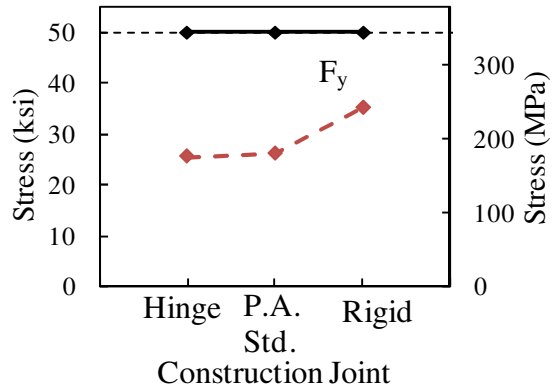

(d) H = 9 ft (2.7 m) Bridge Contraction

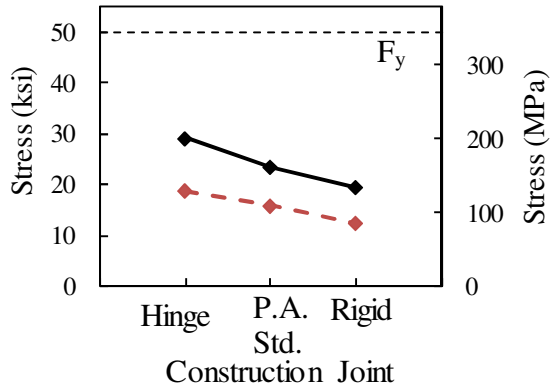

(e) H = 12 ft (3.7 m) Bridge Expansion

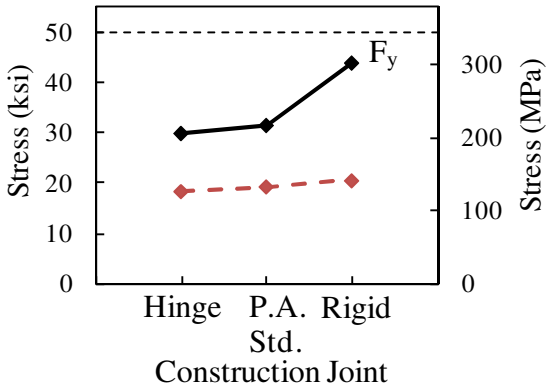

(f) H = 12 ft (3.7 m) Bridge Contraction

Soil Type: Stiff Clay

(- - ◆ - - : Strong Axis; ——◆—— :Weak Axis)

Figure 4.7 Construction Joint Influence on Maximum Pile Stress

4.4 Pile Moment

Figures 4.8 through 4.10 present the maximum pile bending moment, with respect to: (1) abutment height; (2) soil stiffness; (3) construction joint stiffness; and (4) pile orientation for both expansion and contraction cases. The HP12x74 (HP310x110) piles used in this study have a bending capacity of $M_{yielding}$ = 127 k-ft (93.4 kN-m) and $M_{plastic}$ = 194 k-ft (142.6 kN-m) based on a yield stress of 50 ksi (345 MPa). $M_{plastic}$ is represented by the dotted lines in the figures.

Abutment height has a significant influence on pile moment as observed from Figure 4.8. There is up to a 62% decrease in pile moment when the abutment height is increased for expansion cases and up to a 59% decrease is observed in contraction cases. The magnitudes of pile moments for the contraction cases are up to 98% larger than those of expansion cases. This trend indicates that bridge contraction is the more critical state for pile moment and initiated yielding in most of the piles.

The soil stiffness significantly influences pile moment as observed from Figure 4.9. An increase in soil stiffness shows up to a 73% increase pile bending moment for expansion and a 23% increase in contraction cases. Construction joint flexibility influences the maximum pile bending moment such that an increase in construction joint stiffness shows up to a 33% decrease pile bending moment for expansion but shows up to a 47% increase in pile bending moment for contraction cases. However, cases with an abutment height of 4′ (1.2 m) did not follow a similar trend.

Overall, weak axis pile orientation results in higher pile bending moment than strong axis orientation. Contraction cases shows up to a 107% increase in pile bending moment magnitudes from weak to strong axis pile orientation.

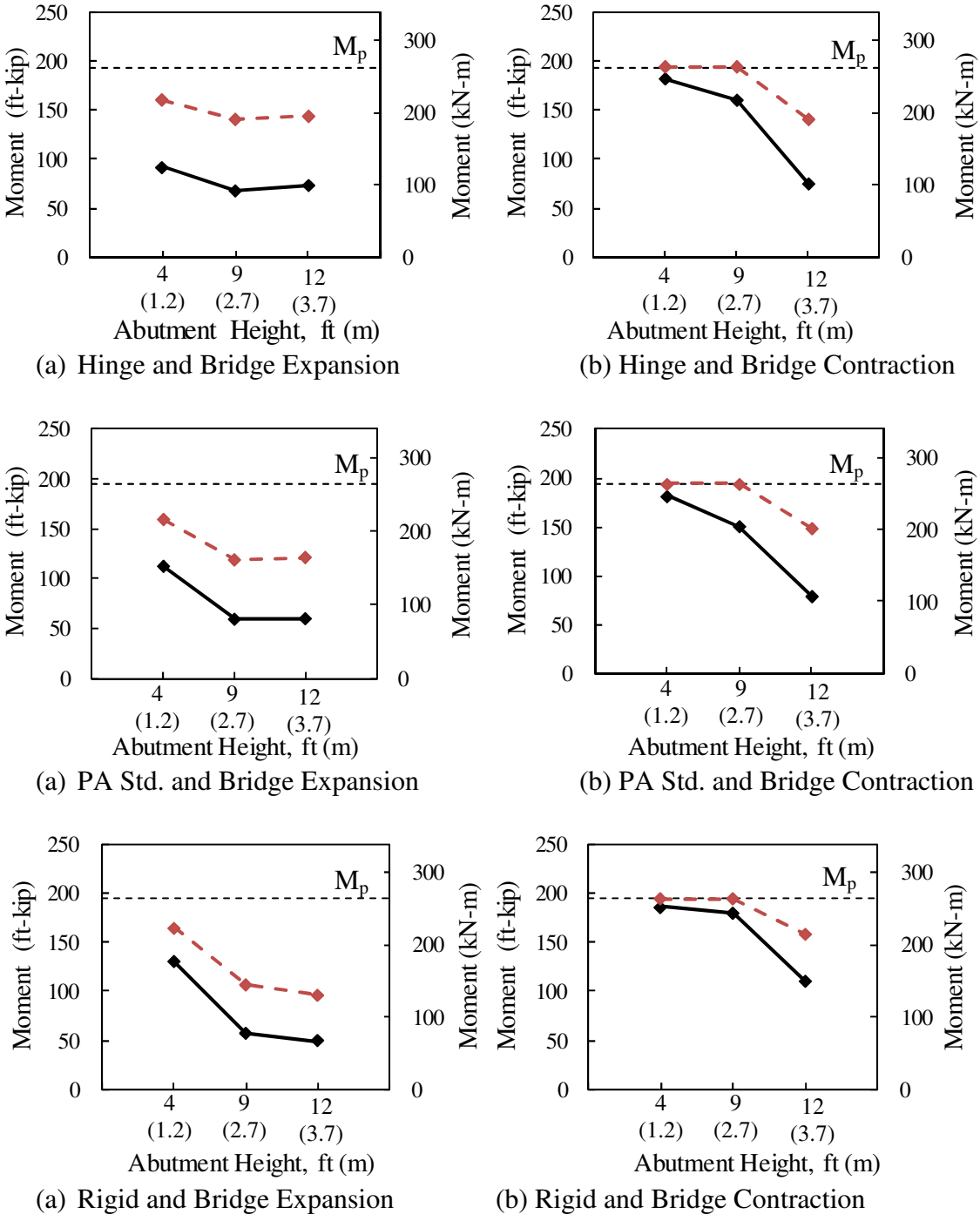

Figure 4.8 Abutment Height Influence on Maximum Pile Moment

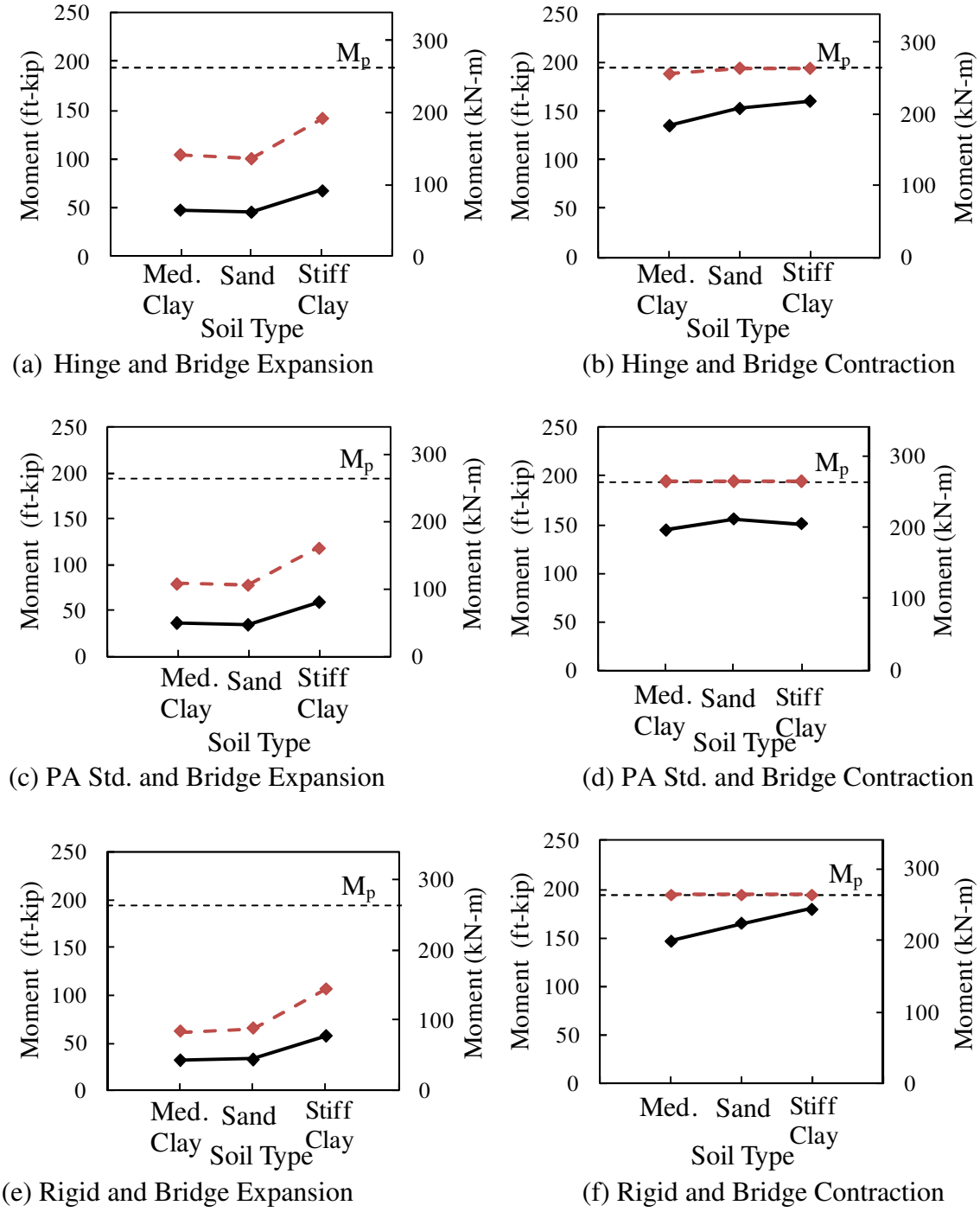

Abutment Height: 9′-0″ (2.7 m)

(– –◆– – : Strong Axis; ——◆—— : Weak Axis)

Figure 4.9 Soil Type Influence on Maximum Pile Moment

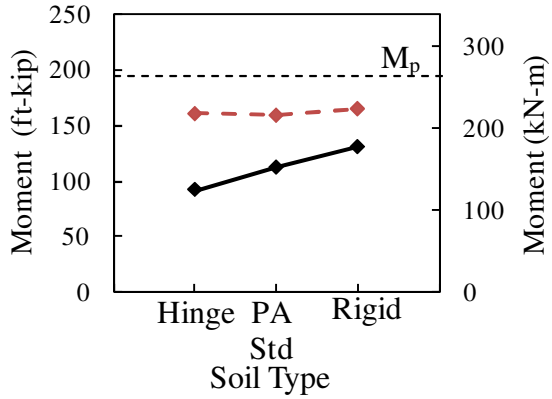

(a) H = 4 ft (1.2 m) Bridge Expansion

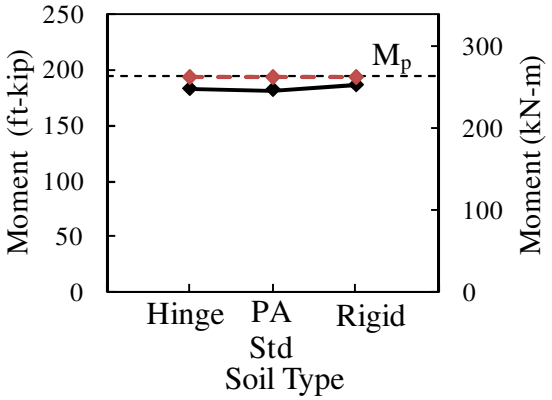

(b) H = 4 ft (1.2 m) Bridge Contraction

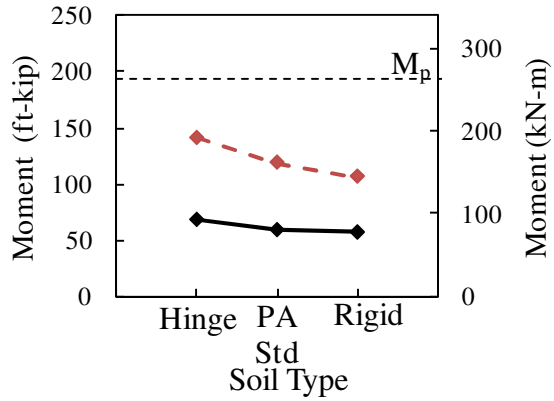

(c) H = 9 ft (2.7 m) Bridge Expansion

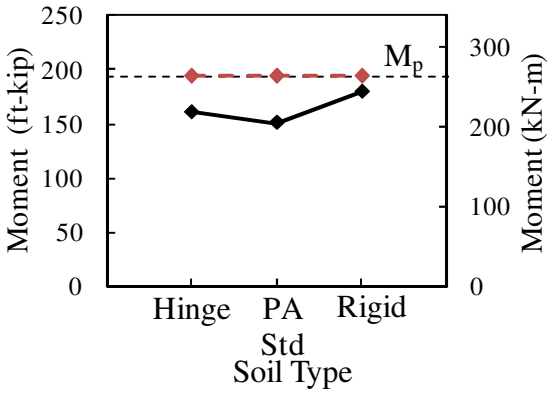

(d) H = 9 ft (2.7 m) Bridge Contraction

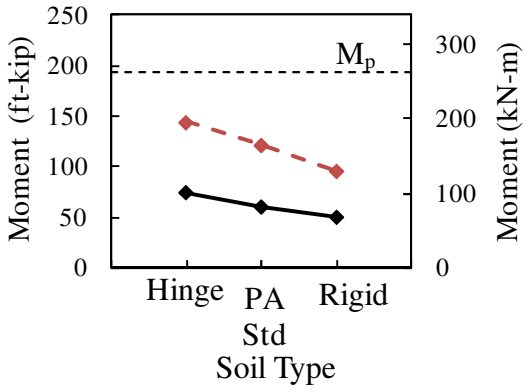

(e) H = 12 ft (2.7 m) Bridge Expansion

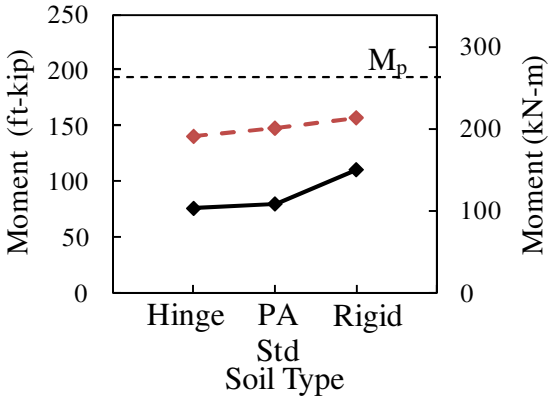

(f) H = 12 ft (2.7 m) Bridge Contraction

Soil Type: Stiff Clay

(– – ◆ – – : Strong Axis; ——◆—— : Weak Axis)

Figure 4.10 Construction Joint Influence on Maximum Pile Moment

4.5 Concrete Stress at Abutment-Pile Connection

Figures 4.12 through 4.14 present the concrete stress at the abutment-pile connection with respect to: (1) abutment height; (2) soil stiffness; (3) construction joint stiffness; and (4) pile orientation, for both expansion and contraction cases. Steel H-piles are embedded 2′-0″ (0.61 m) into the abutment and the pile tips are modeled as roller supports. The present study evaluated Von Mises 3D stresses in the concrete region shown in Figure 4.11.

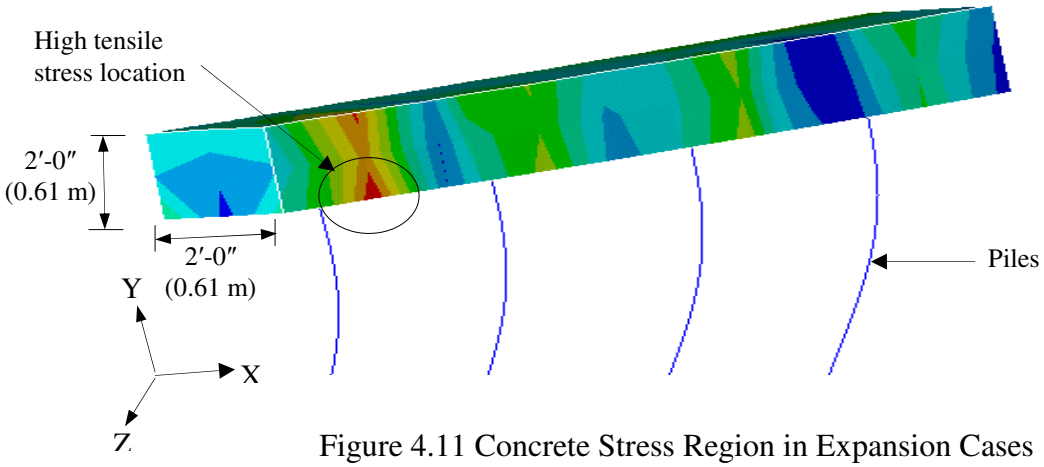

Figure 4.11 Concrete Stress Region in Expansion Cases

An increase in abutment height influences concrete stress, as observed from Figure 4.12. As the abutment height increases, there is up to a 61% decrease in the concrete stress for both expansion and contraction. An increase in soil stiffness resulted in a 41% increase in stress for contraction cases, as observed from Figure 4.13, but only had up to a 7% increase in concrete stress for expansion cases. The influence of the construction joint stiffness did not follow a distinct trend for abutment height equal to 4′ (1.2 m); however a 29% reduction in stress for abutment heights 9′ (2.7 m) and 12′ (3.7 m) during expansion, is observed in Figure 4.14. Generally, strong axis bending produced higher concrete stresses than weak axis bending with up to a 38% increase observed.

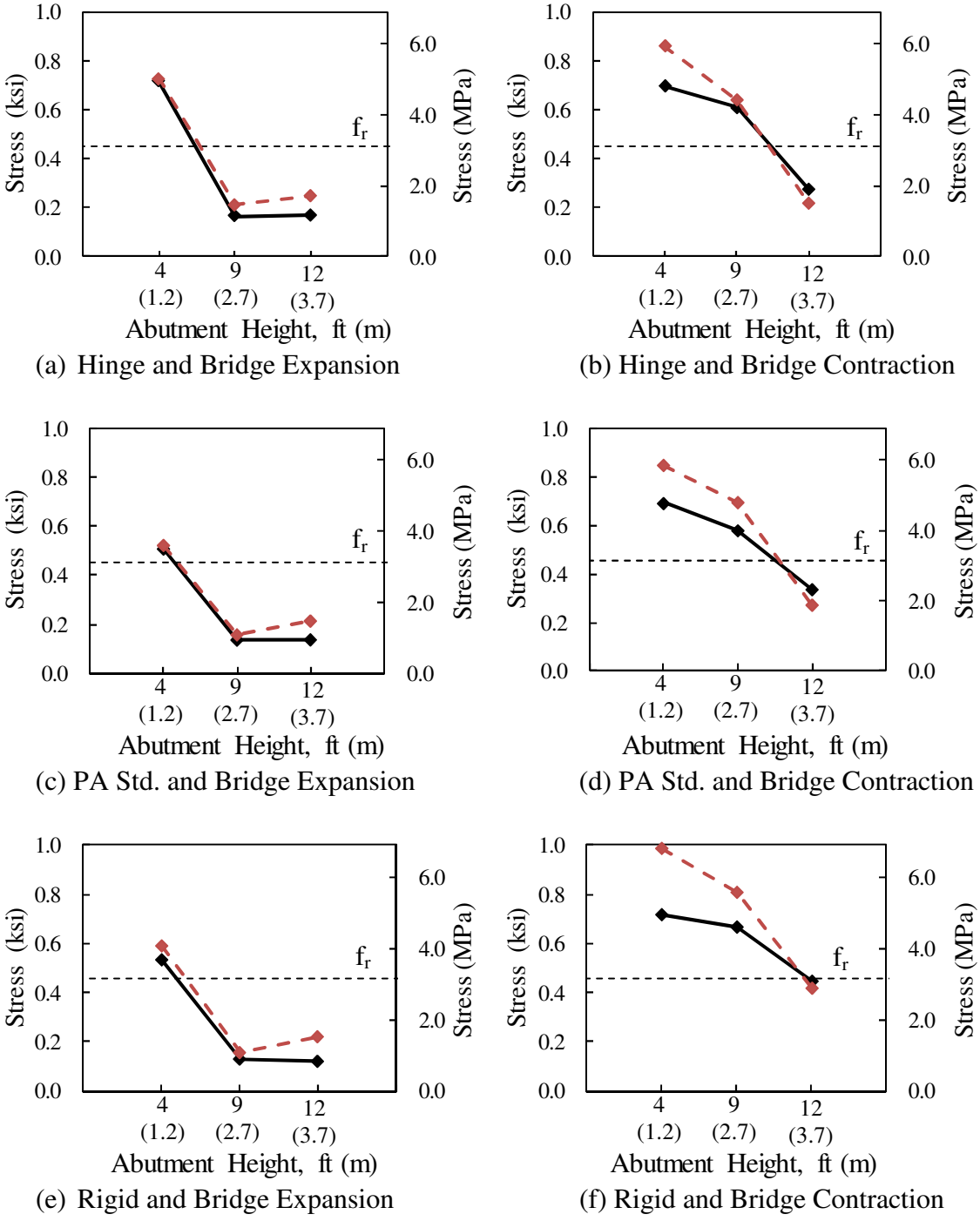

Figure 4.12 Abutment Height Influence on Concrete Stress at Abutment-Pile Location

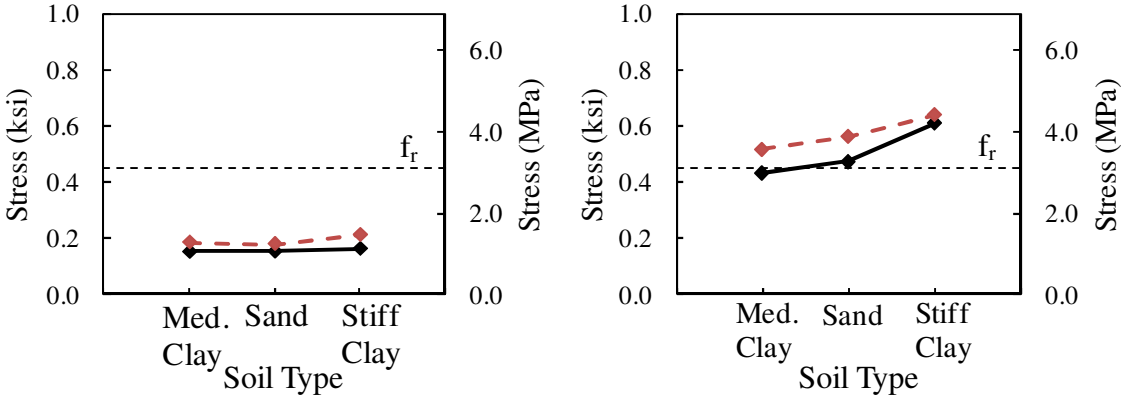

(a) Hinge and Bridge Expansion

(b) Hinge and Bridge Contraction

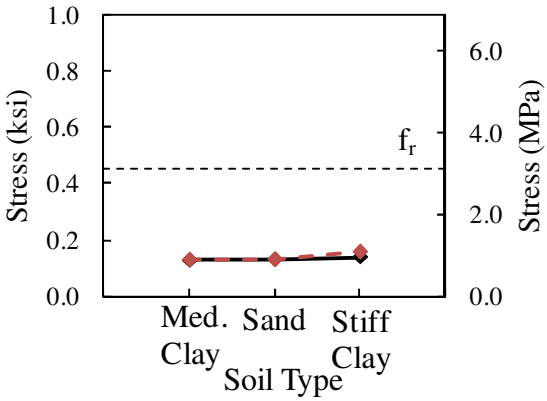

(c) PA Std. and Bridge Expansion

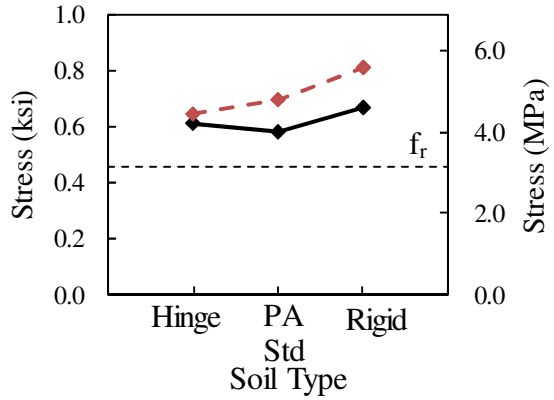

(d) PA Std. and Bridge Contraction

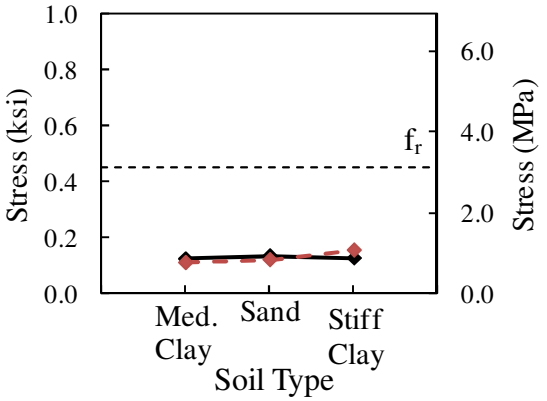

(e) Rigid and Bridge Expansion

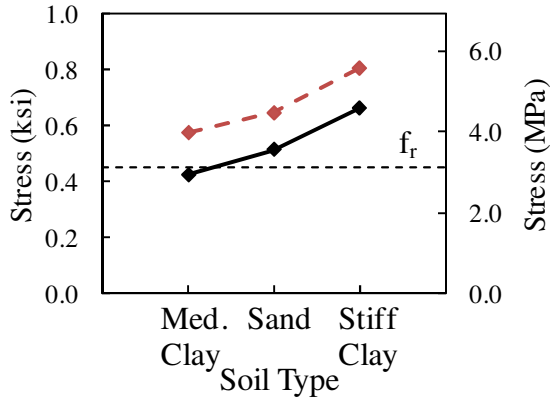

(f) Rigid and Bridge Contraction

Abutment Height: 9′-0″ (2.7 m)

(– – ◆ – – : Strong Axis; ——◆—— : Weak Axis)

Figure 4.13 Soil Type Influence on Concrete Stress at Abutment-Pile Location

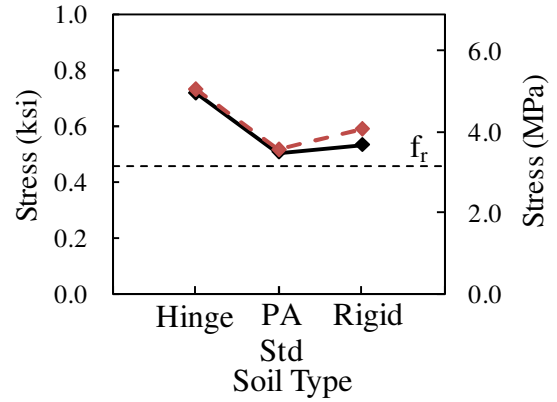

(a) H = 4 ft (1.2 m) Bridge Expansion

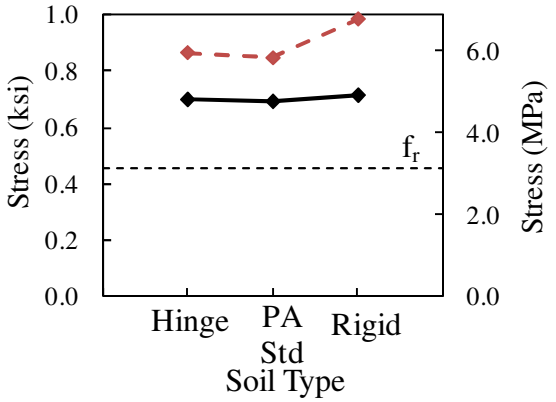

(b) H = 4 ft (1.2 m) Bridge Contraction

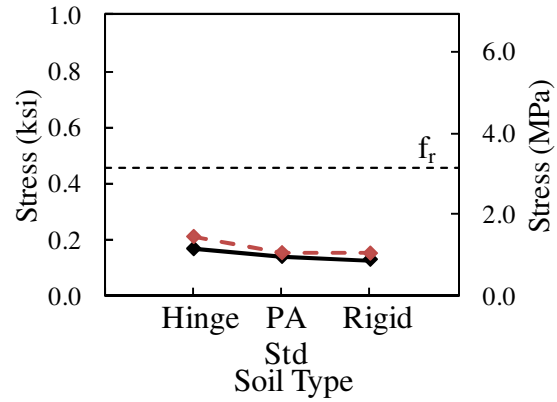

(c) H = 9 ft (2.7 m) Bridge Expansion

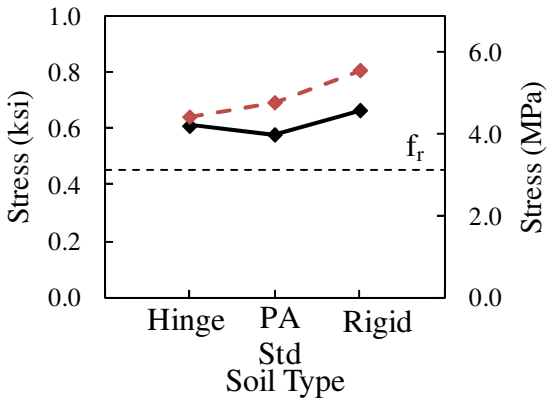

(d) H = 9 ft (2.7 m) Bridge Contraction

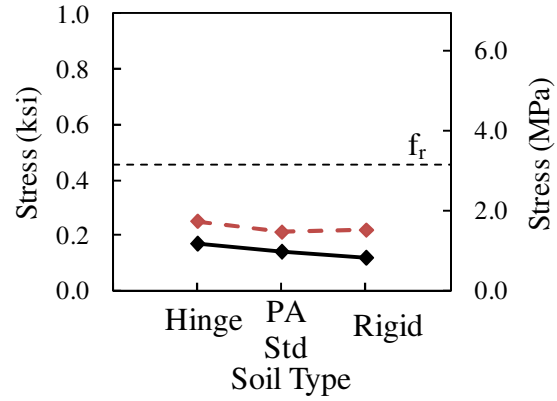

(e) H = 12 ft (3.7 m) Bridge Expansion

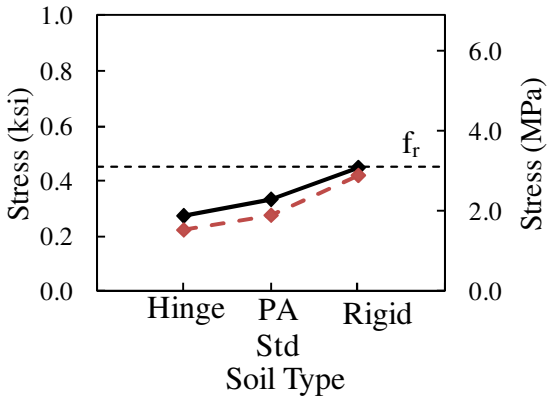

(f) H = 12 ft (3.7 m) Bridge Contraction

Soil Type: Stiff Clay

(- - ◆ - - : Strong Axis; ——◆—— : Weak Axis)

Figure 4.14 Construction Joint Influence on Concrete Stress at Abutment-Pile Location

4.6 Girder Bottom Stress

Figures 4.15 through 4.17 present the girder bottom stress with respect to: (1) abutment height; (2) soil stiffness; (3) construction joint stiffness; and (4) pile orientation, for both expansion and contraction. The largest girder bending moment occurs at the mid-span of the external girder and is used to calculate bottom girder stress presented. Expansion cases induce compressive (-) stresses at the bottom of the girder, while contraction induces tensile (+) stress on the bottom of the girder. AASHTO specifies a tensile limit of $0.19\sqrt{f'_c}$ (AASHTO 5.9.4.4.2) which translates to 0.537 ksi (3.7 MPa) and a compression limit of $0.45\ f'_c$ (AASHTO 5.9.4.2.2) which translates to 3.6 ksi (24.8 MPa) for the bottom girder stress, using a girder f'_c of 8 ksi.

The abutment height has a significant influence on girder bottom stress, as observed from Figure 4.15. As the abutment height increases there is up to a 40% decrease in the bottom girder stress in expansion cases. However, girder bottom stress does not show a distinct trend for an increase in abutment height in contraction cases. Girder bottom stress, for expansion cases, is not significantly influenced by soil stiffness as observed from Figure 4.16. Contraction cases exhibit up to an 11% increase in girder bottom stress with an increase in soil stiffness. A 29% increase is observed in girder bottom stress for the expansion and contraction cases when the construction joint flexibility is increased (Figure 4.17).

Overall, pile orientation did not influence girder bottom stress with only a 3% decrease observed from weak and strong axis bending.

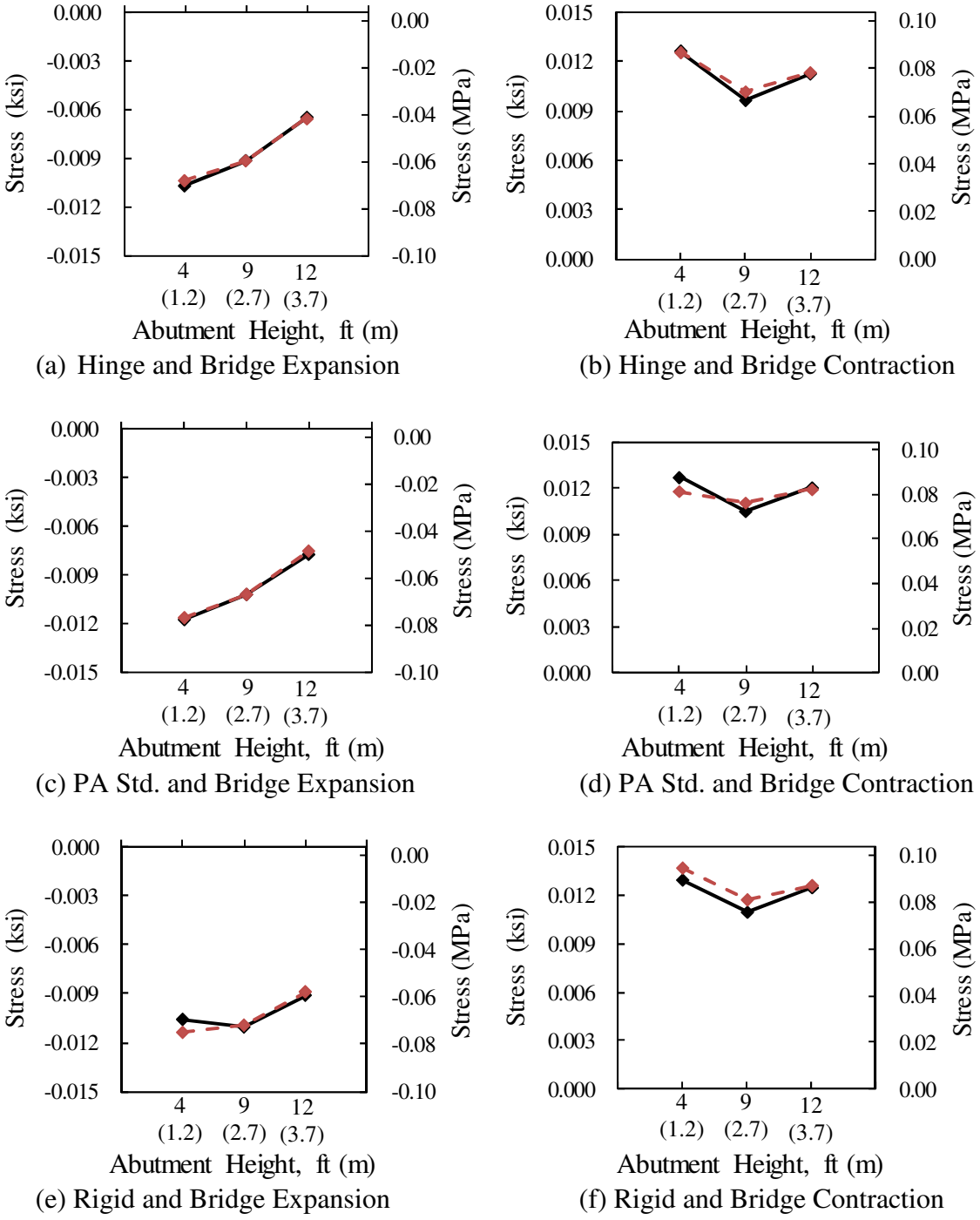

Soil Type: Stiff Clay

(– –◆– – : Strong Axis; ——◆—— : Weak Axis)

Figure 4.15 Abutment Height Influence on Bottom Girder Stress

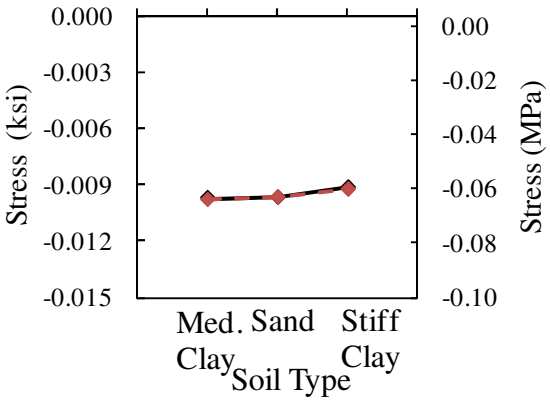

(a) Hinge and Bridge Expansion

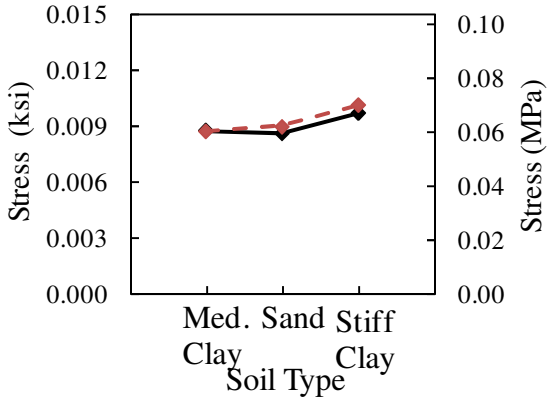

(b) Hinge and Bridge Contraction

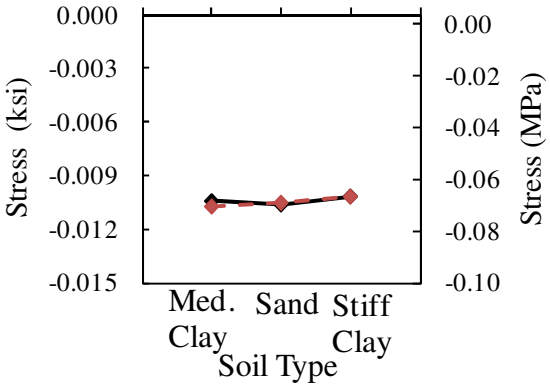

(c) PA Std. and Bridge Expansion

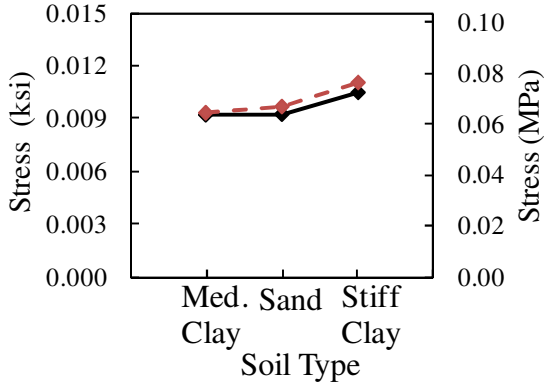

(d) PA Std. and Bridge Contraction

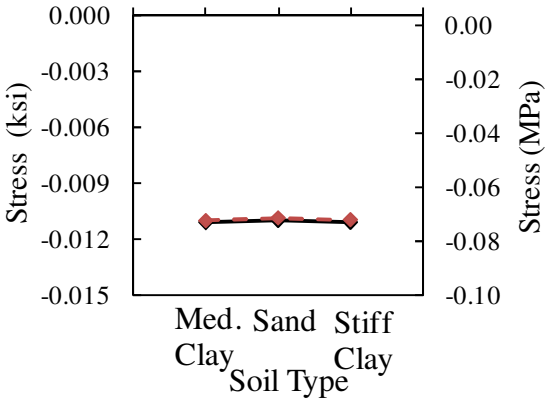

(e) Rigid and Bridge Expansion

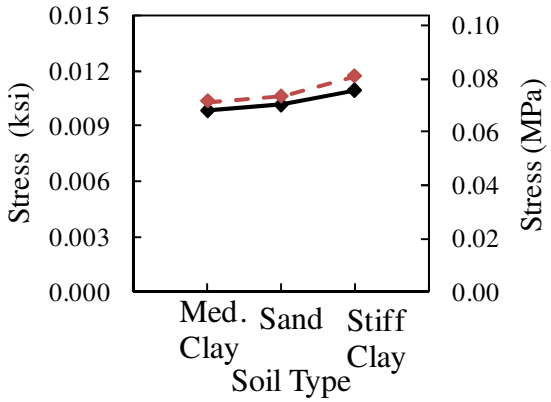

(f) Rigid and Bridge Contraction

Abutment Height: 9′-0″ (2.7 m)

(– – ◆ – – : Strong Axis; —◆— : Weak Axis)

Figure 4.16 Soil Type Influence on Bottom Girder Stress

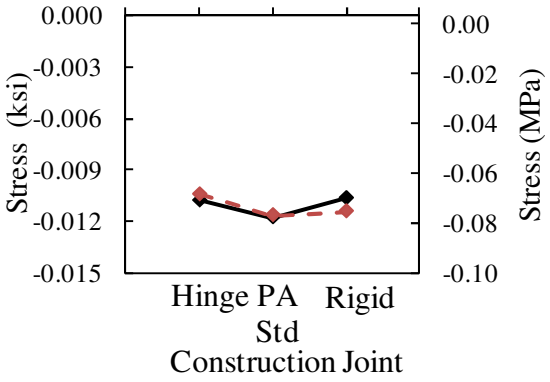

(a) H = 4 ft (1.2 m) Bridge Expansion

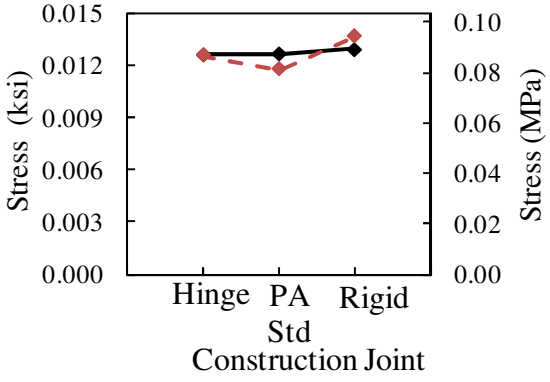

(b) H = 4 ft (1.2 m) Bridge Contraction

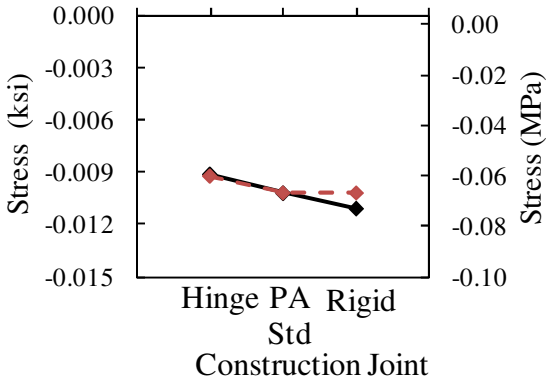

(c) H = 9 ft (2.7 m) Bridge Expansion

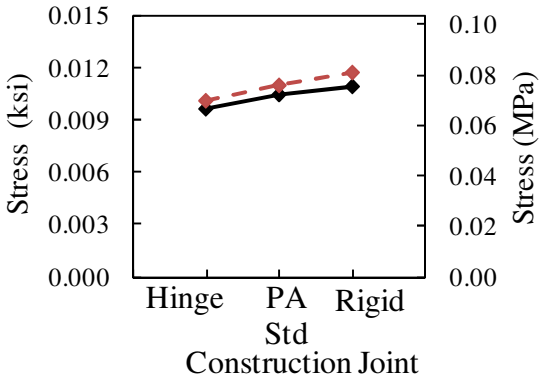

(d) H = 9 ft (2.7 m) Bridge Contraction

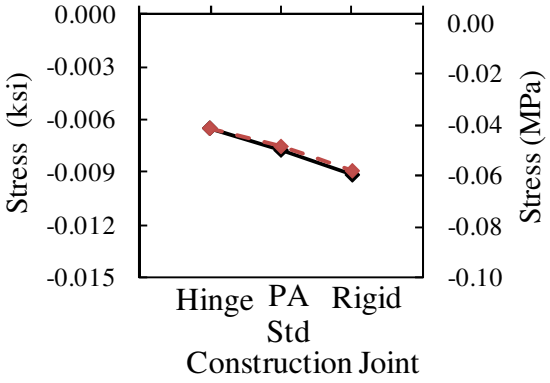

(e) H = 12 ft (3.7 m) Bridge Expansion

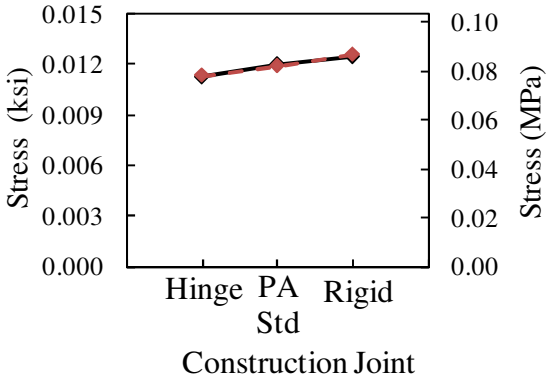

(f) H = 12 ft (3.7 m) Bridge Contraction

Soil Type: Stiff Clay

(– – ◆ – – : Strong Axis; ——◆—— : Weak Axis)

Figure 4.17 Construction Joint Influence on Bottom Girder Stress

4.7 Other Bridge Components

4.7.1 Reinforcing Bars at Construction Joint

The reinforcement used in the PennDOT construction joint is investigated to determine the magnitude of stress in the bars and if yielding occurs. Table 4.1 presents the range of stress values and the corresponding percentage of yield stress, f_y, of the rebars used in the construction joint. The yield stress of the steel used in the construction joint is 60 ksi (414 MPa). The abutment heights 4′ (1.2 m), 9′ (2.7 m), and 12′ (3.7 m) are investigated because abutment height is observed to have the largest effect on bridge response in this study. All other bridge parameters are held constant utilizing medium clay soil with weak axis pile orientation. This configuration is chosen based on the results from the parametric study to obtain a bridge configuration with increased rotation in the construction joint.

Table 4.1 Stress in Reinforcing Bars at Construction Joint

Abutment Height, ft (m)	Stress in bars, ksi (MPa)					
	Expansion			*Contraction*		
	Value	Yield	% f_y	Value	Yield	% f_y
4 (1.2)	24 (163)	60 (414)	40	10 (69)	60 (414)	17
9 (2.7)	40 (276)	60 (414)	67	16 (110)	60 (414)	27
12 (3.7)	44 (306)	60 (414)	73	36 (251)	60 (414)	60

The maximum stress of 44 ksi (306 MPa) is obtained from the case model with abutment height 12′ (3.7 m) because of the larger rotation experienced with a taller abutment. The contraction cases experience lower stress in the rebar than the expansion

cases because the bearing is connected to the directly abutment, though shared ANSYS keypoints, which couples rotation and displacement. These coupled connections reduce the rotation of the backwall during contraction and results in lower stress in the reinforcement.

4.7.2 Abutment Concrete Stress at Construction Joint

The tensile stress in the abutment at the construction joint is also examined in this study. During bridge expansion, tensile stresses develop in the concrete as a result of the tensile forces from the reinforcement at the construction joint, as observed in Figure 4.18. Abutment rotation during expansion is larger because the bearing is connected directly to the abutment and girder, through shared ANSYS keypoints, restricting some of its rotation. Figure 4.18 shows the Von Mises stress distribution of the concrete abutment during bridge expansion for a case with PennDOT Standard construction joint, using medium clay and weak axis oriented piles. Relatively large compressive forces are observed below the girder seat, while tensile stresses are induced at the other end of the abutment due to tension in the construction joint reinforcing bars.

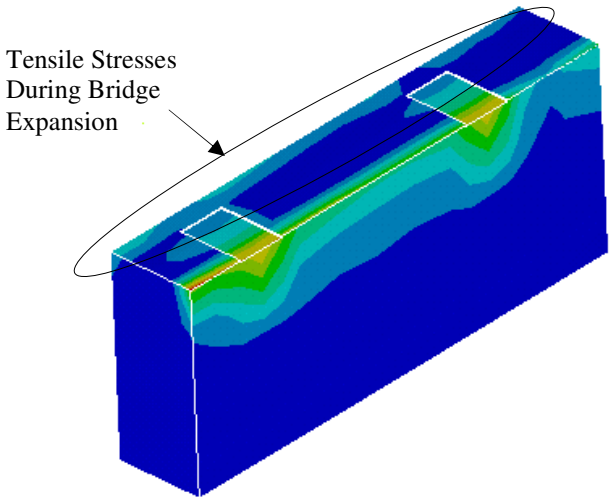

Figure 4.18 Von Mises Stresses at Abutment During Expansion

Table 4.2 shows the magnitude of the Von Mises tensile stresses observed in the concrete abutment. The magnitudes of the stress all exceed the modulus of rupture of the concrete used in this study indicating a cracked section. The abutment reinforcement is engaged and accommodates some of the tensile stress.

Table 4.2 Von Mises Stresses in Abutment During Expansion

Abutment Height, ft (m)	Abutment Tensile Stress, ksi (MPa)		Modulus of Rupture ksi (MPa)
	Expansion	*Contraction*	
4 (1.2)	0.470 (3.24)	0.861 (5.94)	0.455 (3.14)
9 (2.7)	0.501 (3.46)	1.033 (7.13)	0.455 (3.14)
12 (3.7)	0.586 (4.05)	1.86 (12.84)	0.455 (3.14)

4.7.3 Girder-Backwall Connection

During bridge expansion, large compressive forces are transferred from the girders to the backwall. The girder-backwall connection, simulated in the numerical model as a contact surface, is investigated to determine the magnitude of compressive stress at this location. Figure 4.19 shows the location of the maximum compressive stress at the girder-backwall connection. The values shown Table 4.3 utilized models with abutment height equal to 9′ (2.7 m) and 12′ (3.7 m) with stiff clay soil, rigid construction joint, and strong axis pile orientation. The magnitudes of the compressive stress at the backwall-girder connection are compared against AASHTO LRFD (2008) limit for concrete in compression using the compressive strength of the backwall since the backwall has a lower compressive strength, 4 ksi (27.6 MPa), than the girder.

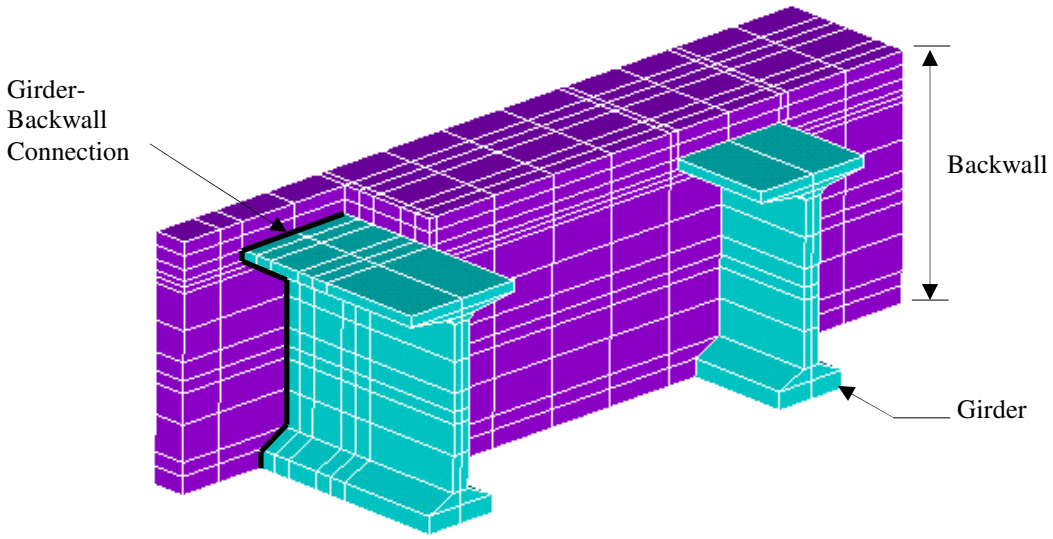

Figure 4.19 Girder-Backwall Connection

Table 4.3 Stress at Girder-Backwall Connection

Abutment Height, ft (m)	Girder Stress, ksi (MPa)	Backwall Compressive Stress, ksi (MPa)	% Limit
9 (2.7)	-1.56 (-10.76)	-1.8 (-27.6)	87%
12 (3.7)	-1.46 (-10.07)	-1.8 (-27.6)	81%

4.7.4 Transverse Threading

The transverse rebars between the girders in the backwall, shown in Figure 3.4 are investigated to determine the shear stress in the rebars due to large contraction forces from the girder. During bridge contraction, the girders are pulled away from the backwall and induce a large shear force on the transverse threading. Table 4.4 shows the magnitudes of the shear stress in the transverse rebars for cases with abutment height equal to 9′ (2.7 m) and 12′ (3.7 m), utilizing medium clay soil, a rigid construction joint and strong axis oriented piles. Table 4.4 shows the shear stress is significantly lower than

the shear yield stress, τ_y, of the steel bars used and abutment height does not influence transverse threading stress.

$$\tau_y = 0.58 f_y \tag{4.2}$$

where f_y is the tension-compression yield stress. From Equation 4.2 the shear yield stress used in this study is 34.8 ksi (240 MPa). No yielding of the transverse threading is expected at the 1000' (305 m) bridge length investigated. The girder stress at the location of the transverse threading is also investigated. Figure 4.20 shows the XY shear stress of the concrete girder. The darker contours show the region of relatively higher shear stresses adjacent to the transverse rebar. The shear stress in the concrete girder adjacent to the transverse rebar is compared to a shear capacity of:

$$\tau = 4\sqrt{f'_c} \tag{4.3}$$

where f'_c is the compressive strength of concrete in psi. Using Equation 4.3, shear stress of 0.358 ksi (2.5 MPa) is determined. The shear stress obtained from the numerical analysis exceeds the girder shear capacity observed from Table 4.4.

Table 4.4 Transverse Rebar Stress, Concrete Stress and Percent Yield

Abutment Height, ft (m)	Shear Stress in Transverse Rebar ksi (MPa)		Shear Yield Stress of Rebar ksi (MPa)	Girder Stress at Transverse Rebar Location ksi (MPa)		Girder Shear Strength ksi (MPa)
	Magnitude	% Limit		Magnitude	% Limit	
9 (2.7)	14 (97)	40	34.8 (240)	0.331 (2.28)	92	0.358 (2.5)
12 (3.7)	14 (97)	40	34.8 (240)	0.369 (2.55)	103	0.358 (2.5)

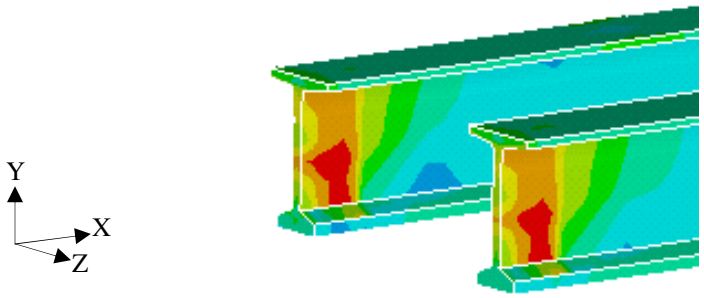

Figure 4.20 Girder XY Shear Stress at Transverse Rebar

4.7.5 Elastomeric Bearing

The abutment elastomeric bearings are investigated to determine if damage to the bearings can be expected in IABs at extreme lengths. AASHTO LRFD (2008) specifies that the maximum shear deformation of bearings must satisfy (AASHTO S14.7.5.3.4-1):

$$h_{rt} \geq 2\Delta_s \tag{4.1}$$

where h_{rt} is the total elastomer thickness and Δ_s is the maximum shear deformation of the elastomer at the service limit state.

Three bridge models are used to compare the magnitudes of the bearing displacement utilizing abutment heights equal to 4′ (1.2 m), 9′ (2.7 m) and 12′ (3.7 m) with a rigid construction joint, stiff clay soil and strong axis oriented piles.

Table 4.5 shows in all cases the shear deformation of the bearings is less than the maximum allowable value of 0.375 in (9.5 mm) indicating no distress in the elastomeric bearings for IABs at extreme lengths.

Table 4.5 Elastomeric Bearing Displacement and Capacity

Abutment Height, ft (m)	Displacement in bearings, in (mm)	Max. Allowable Displacement, in (mm)	% Capacity
4 (1.2)	0.012 (0.302)	0.375 (9.5)	3.2
9 (2.7)	0.013 (0.338)	0.375 (9.5)	3.5
12 (3.7)	0.019 (0.450)	0.375 (9.5)	5.1

4.7.6 Deck

The stress on the deck connection is examined to identify potential distress at this location. This rigid connection between the backwall and the deck is susceptible to high tensile stress developing as a result of bending of the deck and girders during expansion. During expansion, the deck and girders form a convex curve at the abutment, developing tensile stress at the top of the deck.

This study investigates the tensile stresses that develop on the deck during bridge expansion. Table 4.6 shows the maximum stress in the deck during expansion for abutment height equal to 9′ (2.7 m) and 12′ (3.7 m). All other parameters are held constant using stiff clay soil, rigid construction joint and strong axis oriented piles. An increase in the abutment height results in a 2% increase in deck stress for expansion cases. From Table 4.6 it is observed that the maximum tensile stress in the deck is more than twice the modulus of rupture of the 4 ksi concrete used for the deck. These values indicate a cracked section and the rebar in the deck is engaged during expansion. Figure 4.12 shows the Von Mises tensile stresses on the deck and the location of the largest tensile stress.

Table 4.6 Stress at the Backwall-Deck Connection and Limit

Abutment Height, ft (m)	Stress in Deck, ksi (MPa)	Modulus of Rupture ksi (MPa)	% Limit
9 (2.7)	1.136(7.84)	-0.525 (-3.62)	216%
12 (3.7)	1.110 (7.66)	-0.525 (-3.62)	211%

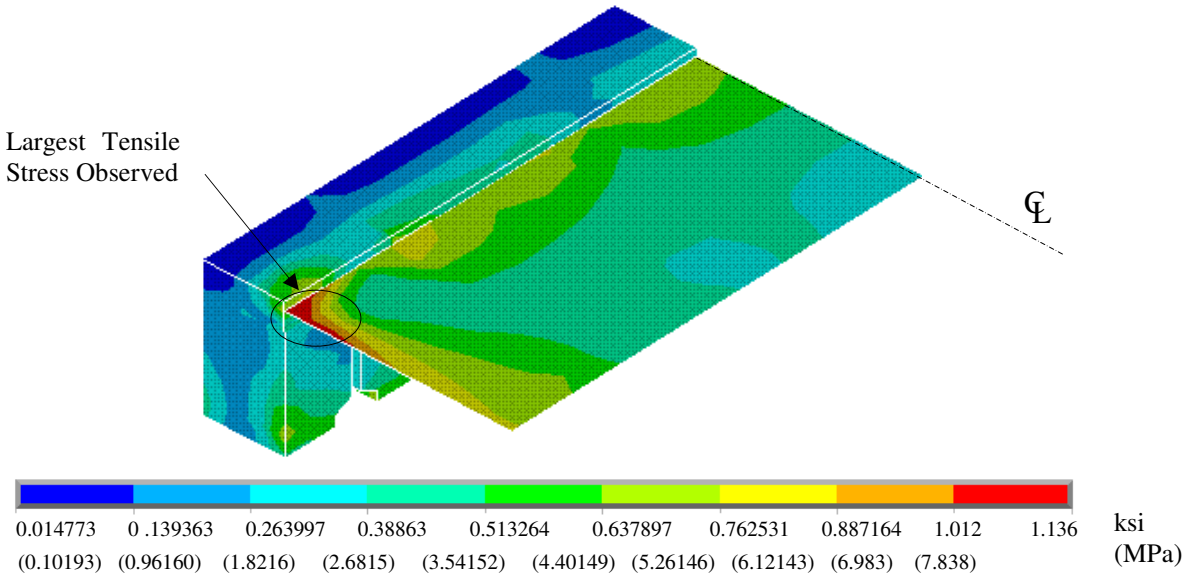

Figure 4.21 Von Mises Tensile Stress in the Deck- Backwall Connection

4.8 Discussion of Results

This section discusses the parametric study results. The influence of: (1) abutment height; (2) soil stiffness; (3) construction joint stiffness; and (5) pile orientation, on the bridge behavior is discussed. From the results of the parametric study, the bridge configuration used to determine the maximum length is determined.

4.8.1 Abutment Height

4.8.1.1 Pile Head Displacement

An increase in abutment height has an influence on pile head displacement. Figure 4.2 shows a decrease in pile head displacement, in both expansion and contraction cases, when the abutment height is increased. This trend is shown in the study case with hinged construction joint, stiff clay soil type and weak axis pile orientation for expansion where a decrease in pile head displacement from 0.826 in (20.98 mm) for abutment height equal to 4′ (1.2 m) to 0.256 in (6.5 mm) for abutment height 12′ (3.7 m) is observed. This corresponds to a 69% decrease in pile head displacement. The decrease in pile head displacement with an increase in abutment height is due to the fact that the taller abutment has an increased soil passive pressure, because of its larger surface area. This makes the abutment more difficult to move laterally and as a result decreases the lateral pile displacement.

Generally, contraction cases produce pile head displacements larger than those of expansion cases. For case studies with abutment height equal to 4′ (1.2 m), rigid construction joint, stiff clay soil type and weak axis oriented piles, the pile head displacement increased from 0.85 in (21.5 mm) for expansion to 1.99 in (50.6 mm) representing a 136% increase in pile head displacement.

4.8.1.2 Pile Bending Stress and Moment

Maximum pile bending stress and pile bending moment followed a similar trend to pile head displacement showing a decrease in pile bending stress and moment with an increase in abutment height. Figure 4.5 and Figure 4.8 show a decrease in pile bending

stress and moment, in both expansion and contraction cases, when the abutment height is increased. This decrease in pile bending stress and moment, in expansion cases, is most evident in study case with rigid construction joint, stiff clay soil type and weak axis pile orientation. The pile bending stress decreases from 50 ksi (345 MPa) for abutment height equal to 4′ (1.2 m) to 19.5 ksi (134.84 MPa) for abutment height equal to 12′ (3.7 m) and pile bending moment decreases from 131 k-ft (178 kN-m) for abutment height equal to 4′ (1.2 m) to 49 k-ft (67 kN-m) for abutment height 12′ (3.7 m) both corresponding to 61% decrease in pile bending stress and moment.

The pile bending stress and moment for contraction cases were larger than for expansion cases. Case studies with abutment height equal to 12′ (3.7 m), PennDOT Std. construction joint, stiff clay soil and weak axis orientation piles shows an increase in pile bending stress from 22.5 ksi (155 MPa) to 50 ksi (345 MPa) corresponding to a 122% increase and an increase in pile bending moment from 56.81 k-ft (77 kN-m) to 180 k-ft (244 kN-m) corresponding to a 217% increase. This increase in both pile bending stress and bending moment is due to the addition of the time dependant for contraction cases. This shows that bridge contraction is more critical state for pile stress and resulted in most piles reaching yield stress.

4.8.1.3 Concrete Stress at Abutment-Pile Connection

Figure 4.12 shows a decrease in the concrete stress at the abutment-pile connection, in both expansion and contraction cases. The stress in the concrete at the pile-abutment location is likely to be influenced by the lateral movement of the abutment as opposed to rotation. Therefore, the concrete stress is highest in the cases with abutment height equal to 4′ (1.2 m), where more lateral displacement is observed.

During expansion, the concrete stress at the abutment-pile location for study case with a hinged construction joint, stiff clay soil type and weak axis oriented piles decreased from 0.721 ksi (4.97 MPa) for abutment height equal to 4′ (1.2 m) to 0.16 ksi (1.15 MPa) for abutment height equal to 12′ (3.7 m). This corresponds to a 77% reduction in concrete stress at the abutment-pile connection. For contraction, study cases with a hinged construction joint, stiff clay soil type and weak axis oriented piles, the concrete stress at the abutment-pile location decreased from 0.699 ksi (4.83 MPa) for abutment height 4′ (1.2 m) to 0.275 ksi (1.90 MPa) for abutment height equal to 12′ (3.7 m) corresponding to a 61% reduction in concrete stress at the abutment-pile location.

The concrete stress at the abutment-pile connection, for contraction cases, is significantly larger than for expansion cases. Case studies with abutment height equal to 12′ (3.7 m), PA. Std. construction joint, stiff clay soil and weak axis orientation piles shows an increase in pile bending stress from 0.14 ksi (0.96 MPa) for expansion to 0.33 ksi (2.3 MPa) for contraction, corresponding to a 139% increase in concrete stress at the abutment-pile connection.

4.8.1.4 Girder Bottom Stress

For the expansion cases, the girder bottom stress shows a general decrease as the abutment height increased (Figure 4.15). This trend is evident in case study with a hinged construction joint, stiff clay soil type and weak axis oriented piles. The girder bottom stress decreased from 0.011 ksi (0.074 MPa) for abutment height equal to 4′ (1.2 m) to 0.006 ksi (0.045 MPa) for abutment height equal to 12′-0″ (3.7 m) corresponding to a 40% reduction in girder bottom stress. However, no distinct trend for girder bottom stress is observed for contraction cases.

Generally, the girder bottom stress for expansion cases is lower than for contraction cases. Case studies with abutment height equal to 12′ (3.7 m), PennDOT Std. construction joint, stiff clay soil and weak axis orientation piles shows an increase in pile bending stress from 0.008 ksi (0.053 MPa) to 0.012 ksi (0.083 MPa) corresponding to a 56% increase in concrete stress at the abutment-pile connection.

4.8.2 Soil Stiffness

4.8.2.1 Pile Head Displacement

Soil stiffness does not have a significant effect on the pile head displacement for the expansion cases, however a larger effect is observed for contraction cases, as observed from Figure 4.3. For expansion, the study case with abutment height equal to 9′ (2.7 m), hinged construction joint, and weak axis pile orientation shows a decrease in pile head displacement from 0.39 in (9.93 mm) for medium clay to 0.34 in (8.6 mm) for stiff clay corresponding to a 13% decrease in pile head displacement. For contraction, the study case with abutment height equal to 9′-0″ (2.7 m), hinged construction joint, and weak axis pile orientation shows a decrease in pile head displacement from 1.9 in (49 mm) for medium clay to 1.6 in (40 mm) for stiff clay corresponding to a 19% decrease in pile head displacement.

Contraction cases produced pile head displacements larger than for expansion cases. For case studies with abutment height equal to 4′-0″ (1.2 m), rigid construction joint, stiff clay soil type and weak axis oriented piles, the pile head displacement

increased from 0.5 in (12.8 mm) for expansion to 2.0 in (50.8 mm) representing a 297% increase in pile head displacement.

4.8.2.2 Pile Bending Stress and Moment

Maximum pile bending stress and moment show a general increase, with an increase in soil stiffness, in both expansion and contraction cases (Figure 4.6 and Figure 4.9). This trend is most evident in case study with rigid construction joint, abutment height equal to 9′-0″ (2.7 m) and weak axis pile orientation during expansion. The pile bending stress increased from 12.8 ksi (88 MPa) medium clay to 22.5 ksi (155 MPa) for stiff clay and pile bending moment increased from 32 k-ft (44 kN-m) for medium clay to 56.8 k-ft (77 kN-m) for stiff clay, both corresponding to 76% increase in pile bending stress and moment.

The pile bending stress and moment for contraction cases are larger than for expansion cases. Case studies with abutment height equal to 9′-0″ (2.7 m), PennDOT Std. construction joint, medium clay soil type and strong axis orientation piles shows an increase in pile bending stress from 10.4 ksi (71.6 MPa) for expansion to 25.7 ksi (177.4 MPa) for contraction, corresponding to a 148% increase. Pile bending moment increased from 79.6 k-ft (108 kN-m) to 194 k-ft (263 kN-m) corresponding to a 144% increase. This is because bridge expansion considers the effect of overburden pressure from the backfill material above in the generation of soil springs. For bridge contraction, the soil is assumed to have a 24° angle with the vertical with a height of 4′-0″ (1.2 m). The expansion soil is therefore relatively stiffer that contraction soil as observed in Figure 4.22.

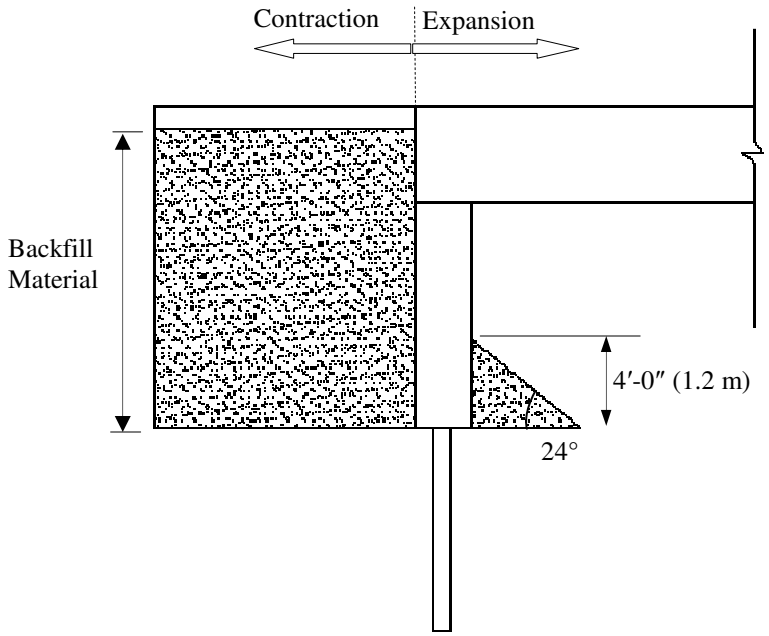

Figure 4.22 Overburden Pressure

4.8.2.3 Concrete Stress at Abutment-Pile Connection

Soil stiffness has little effect on the concrete stress at the abutment pile location for expansion cases, however, an increase for the contraction cases is observed. This trend can also be attributed to the decrease in stiffness of the contraction soil (Figure 4.22). For expansion, the study case with a hinged construction joint, stiff clay soil type and weak axis oriented piles, the concrete stress at the abutment-pile location increased from 0.155 ksi (1.07 MPa) for medium clay to 0.166 ksi (1.15 MPa) for stiff clay corresponding to a 7% increase in concrete stress at the abutment-pile connection. For contraction cases with a hinged construction joint, stiff clay soil type and weak axis oriented piles, the concrete stress at the abutment-pile location increased from 0.44 ksi

(4.83 MPa) for medium clay to 0.61 ksi (4.21 MPa) for stiff clay corresponding to a 40% increase in concrete stress at the abutment-pile location.

The concrete stress at the abutment-pile connection, for contraction cases, is larger than for expansion cases. Case studies with abutment height equal to 9′-0″ (3.7 m), PennDOT Std. construction joint, stiff clay soil and weak axis orientation piles shows an increase in pile bending stress from 0.14 ksi (0.96 MPa) for expansion to 0.58 ksi (4.0 MPa) for contraction, corresponding to a 317% increase in concrete stress at the abutment-pile connection.

4.8.2.4 Girder Bottom Stress

Girder bottom stress is not influenced by soil stiffness. The girder bottom stress remains relatively unchanged as the soil stiffness increases for expansion cases and a slight increase in bottom girder stress is observed in contraction cases (Figure 4.16). For expansion case with abutment height equal to 9′-0″ (1.2 m), hinged construction joint and weak axis oriented piles, the girder bottom stress decreased from 0.01 ksi (0.067 MPa) for medium clay to 0.009 ksi (0.063 MPa) for stiff clay corresponding to a 6% reduction in girder bottom stress.

Generally the girder bottom stress, for expansion cases, is slightly lower than for contraction cases. Case studies with abutment height equal to 9′-0″ (2.7 m), PennDOT Std. construction joint, stiff clay soil and weak axis orientation piles shows an increase in pile bending stress from 0.010 ksi (0.070 MPa) for expansion to 0.0105 ksi (0.072 MPa) for contraction corresponding to a 2.7% increase in concrete stress at the abutment-pile connection

4.8.3 Construction Joint Stiffness

4.8.3.1 Pile Head Displacement

Construction joint stiffness does not have a significant effect on the pile head displacement for both expansion and contraction cases. Figure 4.4 shows a slight increase in pile head displacement, in both expansion and contraction cases, when the construction joint stiffness increases. The study case with abutment height equal to 4′-0″ (1.2 m), stiff clay soil type and weak axis pile orientation for expansion shows an increase in pile head displacement from 0.826 in (20.98 mm) for hinge construction joint to 0.846 in (21.5 mm) for rigid construction joint corresponding to a 2.4% increase in pile head displacement.

Generally, contraction cases produced pile head displacements larger than expansion cases. For case study with abutment height equal to 4′-0″ (1.2 m), PennDOT Std. construction joint, stiff clay soil type and weak axis oriented piles, the pile head displacement increased from 0.83 in (21.1 mm) for expansion to 1.98 in (50.3 mm) for contraction representing a 139% increase in pile head displacement.

4.8.3.2 Pile Bending Stress and Moment

Construction joint flexibility has an influence on maximum pile bending stress and moments. Pile bending stress and moments show a general decrease with an increase in the construction joint stiffness in expansion cases, as observed from Figure 4.7 and Figure 4.8. In contraction cases, however, there is an increase in pile bending stress and moments with an increase in construction joint stiffness. For expansion cases the largest reduction in pile bending stress and moment occurs in case study with abutment height

equal to 12′-0″ (3.7 m), stiff clay soil type and weak axis pile orientation. The pile bending stress decreased from 29.2 ksi (201 MPa) for hinged construction joint to 19.5 ksi (135 MPa) for rigid construction joint and pile bending moment decreased from 73.6 k-ft (100 kN-m) for hinged construction joint to 49.3 k-ft (67 kN-m) for rigid construction joint both corresponding to 33% increase for bending stress and pile bending moment.

Contraction cases show a decrease in pile bending stress and moment with an increase in construction joint stiffness. Case study with abutment height equal to 12′-0″ (3.7 m), stiff clay soil type and weak axis pile orientation produced an increase in pile bending stress from 29.7 ksi (205 MPa) for hinged construction joint to 43.6 ksi (301 MPa) for rigid construction joint and pile bending moment increased from 75.1 k-ft (102 kN-m) for hinged construction joint to 110 k-ft (149 kN-m) for rigid construction joint both corresponding to 47% increase for bending stress and pile bending moment

4.8.3.3 Concrete Stress at Abutment-Pile Connection

The concrete stress at the abutment-pile connection does not exhibit a distinct trend with respect to the construction joint stiffness, shown in Figure 4.14. Cases with abutment height equal to 9′-0″ (2.7 m) and 12′-0″ (2.7 m), however, showed a small decrease in concrete stress as the construction joint stiffness increases for expansion cases, while contraction cases show an increase in concrete stress. Cases with abutment height equal to 4′-0″ (1.2 m), however, do not show a distinct trend.

For expansion cases, study case with abutment height equal to 12′-0″ (3.7 m), stiff clay soil type and weak axis pile orientation, the concrete stress at the abutment-pile connection decreased from 0.17 ksi (1.16 MPa) for hinged construction joint to 0.12 ksi

(0.82 MPa) for rigid construction joint. This corresponds to 29% decrease concrete stress at the abutment-pile connection. For contraction cases, study case with abutment height equal to 12′-0″ (3.7 m), stiff clay soil type and weak axis pile orientation, the concrete stress at the abutment-pile connection increased from 0.28 ksi (1.9 MPa) for hinged construction joint to 0.45 ksi (3.1 MPa) for rigid construction joint corresponding to 29% increase for concrete stress at the abutment-pile connection.

Generally, contraction cases exhibit concrete stress at the abutment-pile connection larger than expansion cases. For case studies with abutment height equal to 4′ (1.2 m), PennDOT Std. construction joint, stiff clay soil type and weak axis oriented piles the concrete stress increased from 0.507 ksi (3.5 MPa) for expansion to 0.69 ksi (4.8 MPa) representing a 37% increase in pile head displacement.

4.8.3.4 Girder Bottom Stress

An increase in girder bottom stress is observed, with an increase in construction joint stiffness for both expansion and contraction cases, shown in Figure 4.17. The increase in construction joint stiffness decreases the rotation in the backwall. There is therefore a larger resistance at the bottom of the girder from the decreased rotation in the backwall, as a result increasing the girder bottom stress. For expansion cases, with an abutment height equal to 12′-0″ (3.7 m), stiff clay soil type and weak axis oriented piles, the girder bottom stress increases from 0.006 ksi (0.045 MPa) for hinged construction joint stiffness to 0.009 ksi (0.064 MPa) for rigid construction joint corresponding to a 41% increase in girder bottom stress.

Generally, girder bottom stress for expansion cases is lower than for contraction cases. Case studies with abutment height equal to 12′-0″ (3.7 m), PennDOT Std.

construction joint, stiff clay soil and weak axis orientation piles shows a increase in girder bottom stress from 0.008 ksi (0.053 MPa) to 0.012 ksi (0.083 MPa) corresponding to a 56% increase in girder bottom stress.

4.8.4 Pile Orientation

4.8.4.1 Pile Head Displacement

Pile head displacement is not significantly influenced by pile orientation in both expansion and contraction cases with respect to abutment height, soil stiffness and construction joint stiffness, shown in Figure 4.2 through Figure 4.4. The magnitudes of the pile head displacement are, however, larger for weak axis oriented pile cases than strong axis bending cases because of a lower moment of inertia in weak axis oriented piles. For study case with abutment height equal to 12′-0″ (3.7 m), rigid construction joint and stiff clay soil type produce a pile displacement of 0.318 in (8.07 mm) for weak axis pile orientation and 0.313 in (7.95 mm) for strong axis pile orientation representing a 1.4% decrease.

4.8.4.2 Pile Bending Stress and Moment

Pile orientation has an effect on the pile bending stress and moments as observed from Figure 4.5 through Figure 4.10. In case study with abutment height equal to 4′-0″ (1.2 m), rigid construction joint, stiff clay soil type has a stress of 50 ksi (345 MPa) for weak axis pile orientation and a stress of 21.5 ksi (148 MPa) for strong axis pile orientation corresponding to a 57% decrease from weak to strong axis pile orientation. For pile bending moment, however, strong axis pile orientation experience higher bending moments that weak axis pile orientation. In case study with abutment height

equal to 4′-0″ (1.2 m), rigid construction joint, stiff clay soil type and weak axis pile orientation produced a bending moment of 131 k-ft (178 kN-m) for weak axis pile orientation and a bending moment of 165 k-ft (224 kN-m) for strong axis pile orientation corresponding to a 26% increase from weak to strong axis pile orientation.

4.8.4.3 Concrete Stress at Abutment-Pile Connection

Concrete pile stress at the abutment-pile connection, in most cases, is not influenced by pile orientation. The largest difference is observed in contraction study case with abutment height equal to 4′-0″ (1.2 m), rigid construction joint, and stiff clay soil type. A concrete stress at the abutment-pile location of 0.714 ksi (4.93 MPa) for weak axis pile orientation and 0.985 ksi (6.80 MPa) for strong axis pile orientation is observed representing a 38% increase for weak to strong pile orientation.

4.8.4.4 Girder Bottom Stress

Pile orientation has little effect on girder bottom stress, as observed from Figure 4.15 through Figure 4.17. The most significant change is observed in study case with abutment height equal to 4′-0″ (1.2 m), rigid construction joint, and stiff clay soil type for contraction. A girder bottom stress of 0.0109 ksi (0.0752 MPa) for weak axis pile orientation and 0.0117 ksi (0.0809 MPa) for strong axis pile orientation is observed, representing a 7% increase for weak to strong pile orientation.

4.8.5 Summary

The results of the parametric study show that substructure moments and stresses are significantly influenced by abutment height, soil stiffness, construction joint stiffness

and pile orientation. A decrease in the bottom girder stress is also observed in with an increase abutment height.

Soil stiffness had a significant effect on pile behavior, showing an increase in pile bending moment and stress with an increase in soil stiffness. Pile displacement, concrete stress and bottom girder moment were not significantly influenced by soil stiffness. The construction joint stiffness had the greatest influence on the maximum pile bending stress and pile moment. These results, in some cases, caused the pile to reach yield moments 194 k-ft (142.6 kN-m) and stress 50 ksi (345 MPa) in contraction cases and rigid construction joint connections. Therefore, to reduce pile stress for contraction cases, a construction joint allowing some rotation should be used. Pile orientation also had a large effect on maximum pile stress and moment. The maximum pile bending stress is considerable larger for cases with weak axis pile orientation.

Chapter 5

LENGTH LIMITS

5.1 Introduction

This chapter investigates the distress at critical bridge locations when the IAB length is increased. The total pile stress (bending and axial), maximum bending moment, concrete stress at abutment-pile connection, and girder bottom stress are compared with respect to bridge length. Distress at other bridge locations is also investigated, including:

- construction joint;
- compressive stress at girder-backwall location;
- girder stress at transverse threading; and
- deck stress

The magnitudes of forces, stresses and displacements are compared with the limiting value of each case to determine the distress that occurs at each location. Four models are generated for each bridge length both considering expansion and contraction as well as strong and weak pile orientation.

5.2 Bridge Configuration

From these results, it was determined that a taller abutment and low soil stiffness are best suited for IABs at extreme lengths to reduce pile stress and moments. Construction joint stiffness should allow some rotation, and strong axis pile orientation is best suited to minimize pile bending stress and moments. The bridge configuration using

abutment height equal to 12′ (3.7 m), medium clay soil, PennDOT standard construction joint with strong axis pile orientation is used to establish length limits.

Table 5.1 Geometric Properties of Bridge Used to Establish Length Limits.

Properties	Bridge
No. of girders	4
Deck Thickness, in (mm)	9 (229)
Girder Type	BT-72
No. of Piles	8
Abutment Height, ft (m)	12 (3.7)
Pile Type	HP12x74 (HP310x110)
Construction Joint (PA Std)	#5 "U" @ 9″ (#16mm bars @ 229 mm)
Pile Length, ft (m)	30 (9.1)
Soil Type	Medium Clay
Pile Orientation	Strong and Weak

Table 5.2 Critical Response of Bridge Used to Establish Length Limits

Property	Bridge			
	Expansion		Contraction	
	Value	% Limit	Value	% Limit
Pile Displacement, in (mm)	-0.323 (-8.25)	-	1.24 (31.7)	-
Pile Stress, ksi (MPa)	11.84 (81.7)	24%	12.40 (85.5)	25%
Pile Moment, k-ft (kN-m)	90.75 (123.1)	47%	95.1(129)	49%
Concrete Stress, ksi (MPa)	0.179 (1.24)	39%	0.26 (1.76)	51%
Girder Bottom, ksi (MPa)	-0.0081 (-0.06)	0.23%	0.011 (0.077)	2.0%

Table 5.3 Displacement and Stresses of Other Bridge Components.

Component	Bridge			
	Expansion		Contraction	
	Value	% Limit	Value	% Limit
Construction Joint				
Reinforcement, ksi (MPa)	43 (296)	72%	38 (264.2)	63%
Abutment, ksi (MPa)	0.53 (3.7)	116%	1.95 (13.5)	429%
Girder-Backwall Stress, ksi (MPa)	-1.3 (9.0)	72%	-	-
Elastomeric Bearing, in (mm)	-	-	0.006(0.16)	1.7%
Transverse Rebar Stress, ksi (MPa)	-	-	15.2 (105)	44%
Concrete Stress at Transverse Rebar, ksi (MPa)	-	-	1.33	371%
Deck Stress, ksi (MPa)	0.97 (6.7)	212%	-	-

5.3 Length Models

The second bridge length investigated is 1250′-0″ (381 m) with 10 spans each 125′ (38.1 m) long, as shown in Figure 5.1 (a). This length is chosen to maintain a symmetrical structure with a constant span length. Figure 5.1 (b) shows the elevation view of third bridge length investigated in this study a 1500′-0″ (457 m) long bridge with 12 spans each 125′ (38.1 m) long.

The geometric configuration selected in Chapter 4 (refer to Table 5.1) are kept constant for these models.

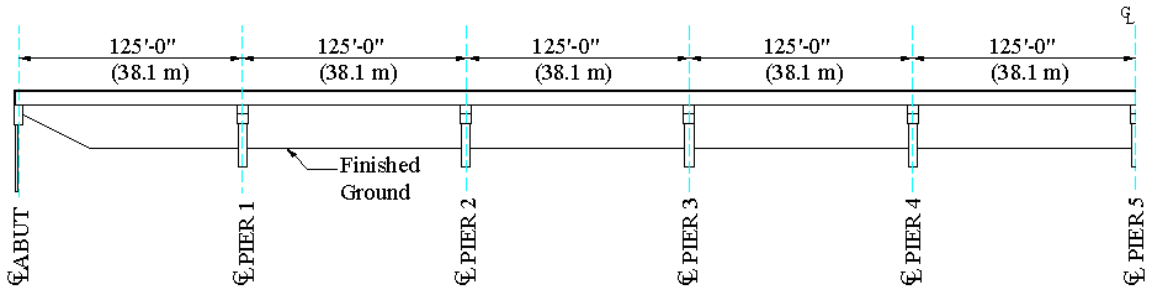

(a) Bridge Length 1250′-0″ (381 m)

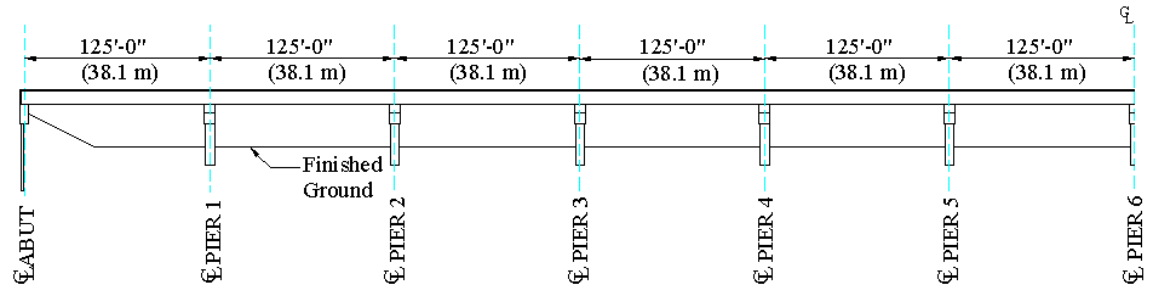

(b) Bridge Length 1500′-0″ (457 m)

Figure 5.1 Elevation View of Length Models (a) 1250′ (381 m), (b) 1500′ (457 m)

5.4 Maximum Pile Stress

Expansion

The maximum pile stress for bridge lengths 1000′ (305 m), 1250′ (381 m) and 1500′ (457 m) during expansion are shown in Figure 5.2. The axial stress due to dead load, i.e. self weight, of the bridge, is included in this section to provide a more realistic representation of pile stress at extreme lengths when establishing IAB length limits. An axial stress of 14.0 ksi (101 MPa) from the dead loads was calculated and added to the bending stress from the ANSYS models.

A general increase in maximum pile stress is observed with an increase in bridge length. For weak pile orientation, bridge length 1500′ (457 m) showed the highest pile stress of 35.5 ksi (245 MPa) corresponding to 71% of the pile capacity. Strong axis pile orientation produced the highest pile stress of 29.4 ksi (203 MPa) corresponding to 59% of the pile capacity. Weak axis pile orientation showed higher stress values than strong axis pile orientation. The magnitudes of pile stress are, however, less than the yield stress F_y and no pile yielding is anticipated at 1500′ (457 m).

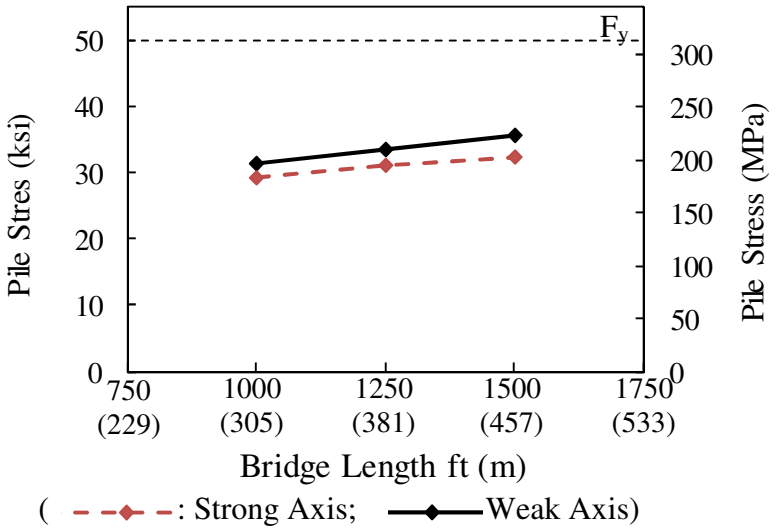

Figure 5.2 Maximum Pile Stress for Bridge Expansion

Contraction

The maximum pile stress for bridge lengths 1000′ (305 m), 1250′ (381 m) and 1500′ (457 m) during contraction are shown in Figure 5.3. A 25% increase in maximum pile stress is observed with an increase in bridge length for weak axis pile orientation and a 30% increase is observed for strong axis pile orientation. Pile orientation shows up to a

44% decrease in stress values from weak to strong axis pile orientation and contraction magnitudes are also greater than those in expansion cases.

The study case with bridge length 1500′ (457 m) and weak axis orientation produced a maximum pile stress of 50 ksi (345 MPa) which translates to 100% of the pile stress capacity. Strong axis pile orientation produced the highest pile stress of 35 ksi (242 MPa) corresponding to 70% of the pile capacity. At the maximum bridge length investigated, 1500′ (457 m), no distress is expected for cases with strong axis oriented piles, however, weak axis oriented piles reached yield strength.

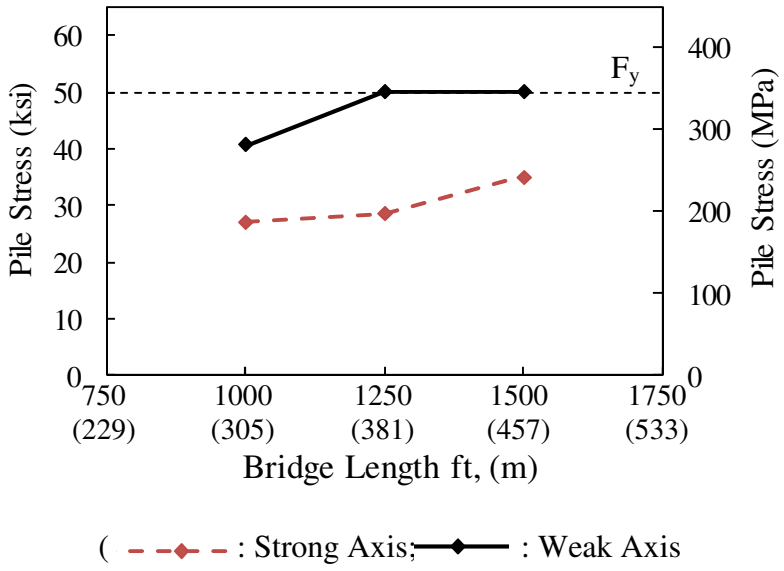

Figure 5.3 Bridge Length Influence on Maximum Pile Stress (Contraction)

5.5 Concrete Stress at Abutment-Pile Connection

Contraction

The tensile concrete stress at the abutment-pile location for bridge lengths 1000′ (305 m), 1250′ (381 m) and 1500′ (457 m) during contraction are shown in Figure 5.4. A 64% increase in concrete tensile stress is observed with an increase in bridge length. The magnitude of concrete tensile stress for study cases with strong axis orientation is up to 9% greater than of weak axis pile orientation and contraction magnitudes are generally greater than expansion cases.

The study case with bridge length 1500′ (457 m) and weak axis orientation produce a maximum pile stress of 0.422 ksi (2.9 MPa) which is 93% of the modulus of rupture. At the maximum bridge length investigated, 1500′ (457 m), tensile cracks can potentially develop at this location for both strong and weak axis oriented piles.

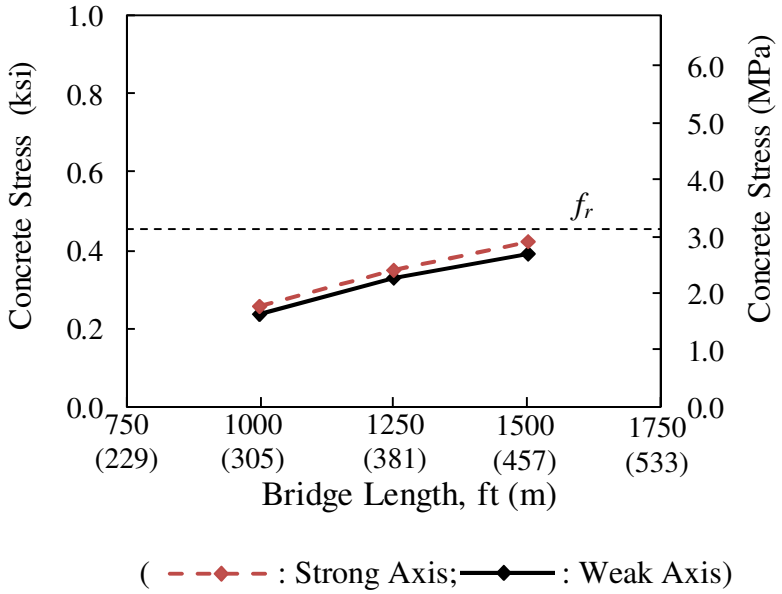

Figure 5.4 Bridge Length Influence on Concrete Stress

Figure 5.5 shows the displaced shape of the abutment during bridge contraction and the predicted crack progression as a result of the thermal movement of the bridge. Tensile cracks are most likely to start at the abutment-pile interface and propagate further into the abutment. It is recommended that additional "U" shaped bars should be placed around the pile head to minimize the cracking at this location.

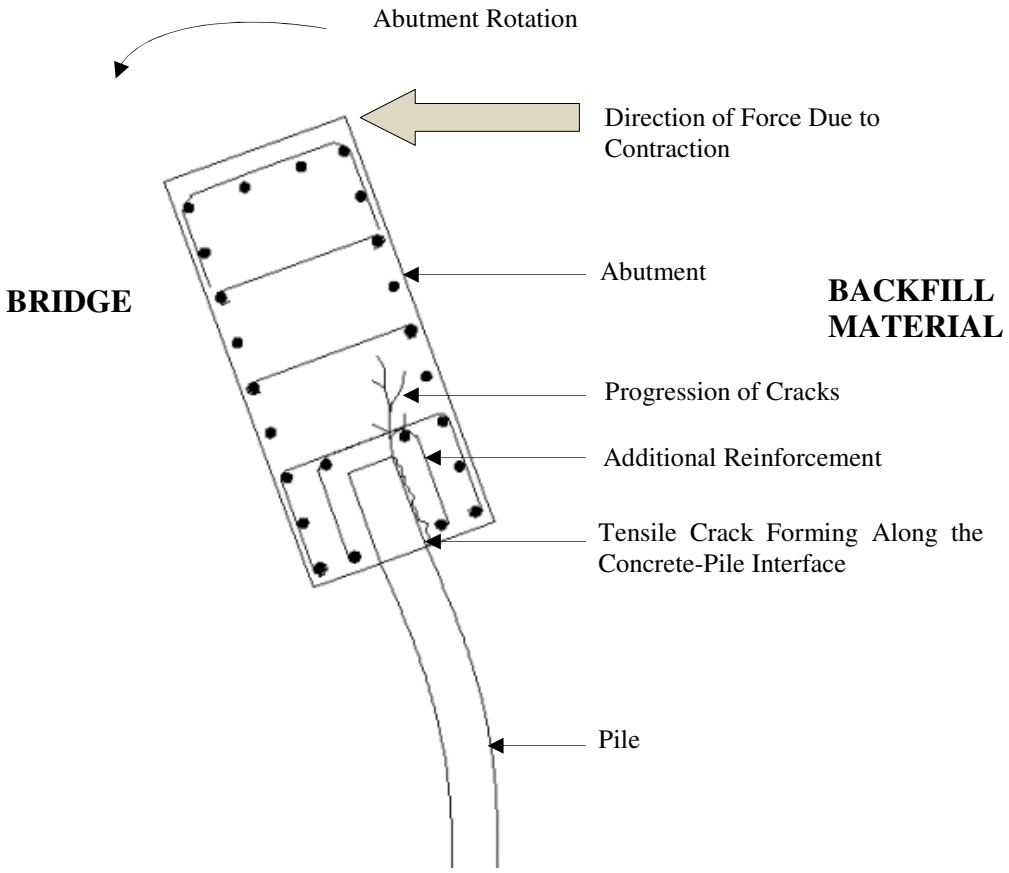

Figure 5.5 Crack Formation at the Abutment-Pile Connection

Expansion

The tensile concrete stress at the abutment-pile location for bridge lengths 1000′ (305 m), 1250′ (381 m) and 1500′ (457 m) during expansion are shown in Figure 5.6. A 31% increase in tensile concrete stress is observed with an increase in bridge length and strong axis orientation shows up to 40% higher stress values than weak axis orientation.

The largest concrete stress obtained from the three bridge lengths investigated is 0.23 ksi (1.6 MPa) which translates to 51% of the modulus of rupture of 0.455 ksi (3.1 MPa) for concrete used for the abutment. For expansion, no cracking is anticipated in the concrete at 1500′ (457 m) for both strong and weak axis pile orientation.

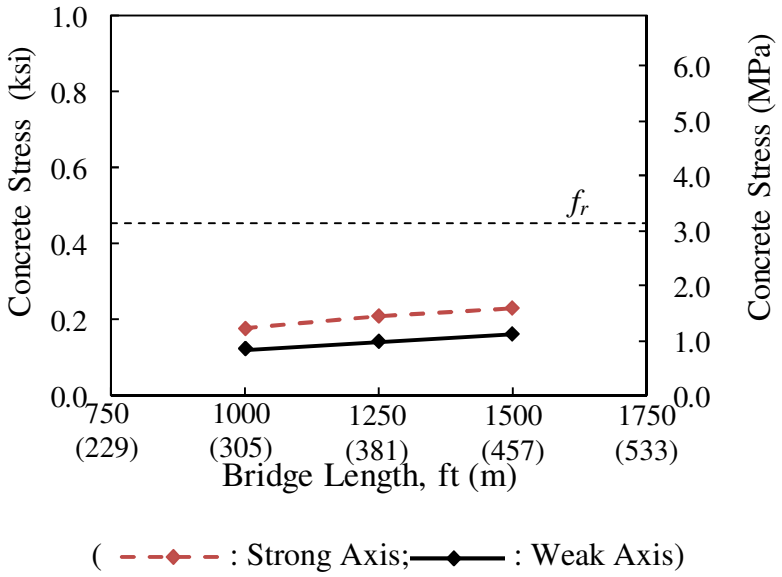

Figure 5.6 Concrete Stress at Abutment-Pile Location

5.6 Construction Joint

5.6.1 Reinforcing Bars

Expansion

The stress in the reinforcing bars at the construction joint for bridge lengths 1000′ (305 m), 1250′ (381 m) and 1500′ (457 m) during contraction are shown in Figure 5.7. The stress in the reinforcing bars is a result of thermal loads only and compared to the full yield of the steel reinforcing bar used, i.e. 60 ksi (414 MPa). A 13% increase in stress is observed in the rebar stress with an increase in bridge length. Pile orientation did not have an effect on the stress in the reinforcing bars. Pile orientation showed a 3% decrease from weak to strong axis for expansion cases.

The expansion study case with bridge length 1500′ (457 m) and strong axis orientation, there is a stress of 50.2 ksi (346.5 MPa) which corresponds to 84% of the yield stress of the reinforcing bars. From the trend observed, some distress in the form of yielding in the reinforcing bars is likely to occur in bridge length beyond 1500′ (457 m).

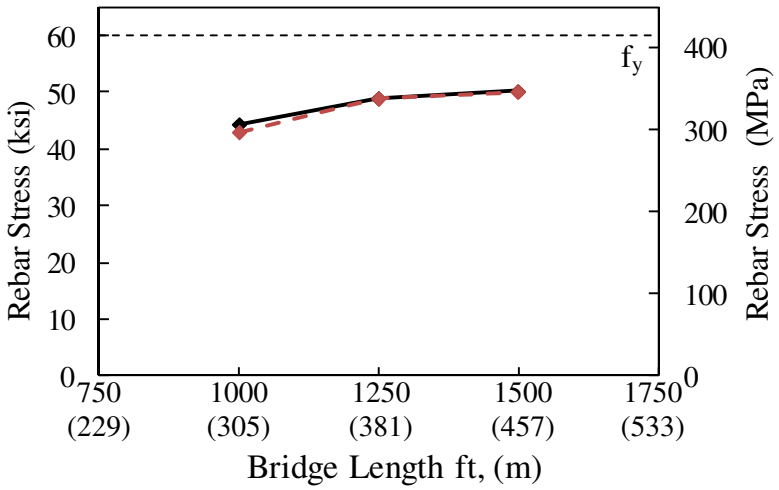

(– –◆– – : Strong Axis;—◆— : Weak Axis)

Figure 5.7 Reinforcement Stress for Bridge Expansion

Contraction

The stress in the reinforcing bars at the construction joint for bridge lengths 1000′ (305 m), 1250′ (381 m) and 1500′ (457 m) during expansion are shown in Figure 5.8. The stress in the reinforcing bars is a result of thermal loads only and compared to the full yield of the steel reinforcing bar used, i.e. 60 ksi (414 MPa). A 21% increase in stress is observed with an increase in bridge length. The magnitudes for strong axis pile orientation are up to 9% greater than that of weak axis orientation and expansion cases are up to 18% greater than contraction magnitudes.

The expansion study case with bridge length 1500′ (457 m) and strong axis orientation resulted in a stress of 48 ksi (331.9 MPa) which corresponds to 80% of the yield stress of the reinforcing bars. From the trend observed, some distress in the form of yielding in the reinforcing bars is likely to occur in bridge length beyond 1500′ (457 m).

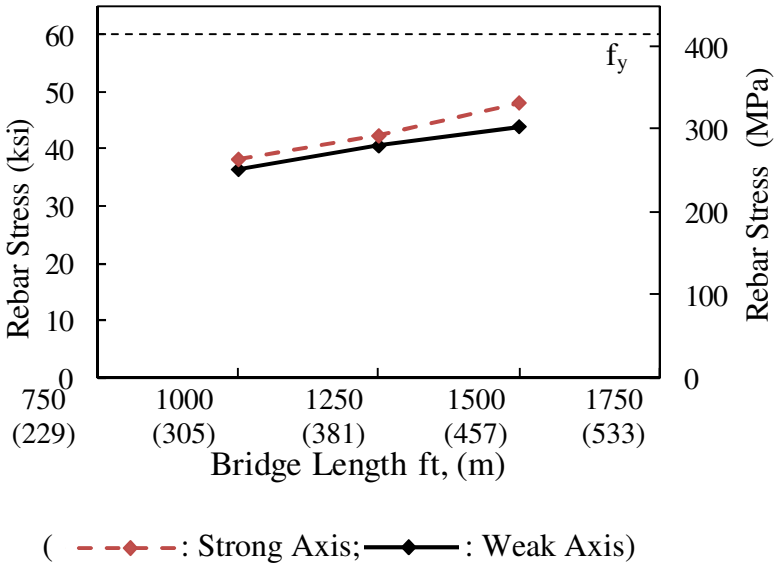

Figure 5.8 Bridge Length Influence on Construction Joint Rebars

5.6.2 Abutment

Expansion

The concrete stress on the abutment at construction joint is investigated for expansion cases shown in Figure 5.9. The tensile stress in the concrete at the construction joint for bridge lengths 1000′ (305 m), 1250′ (381 m) and 1500′ (457 m) during expansion are shown in Figure 5.10.

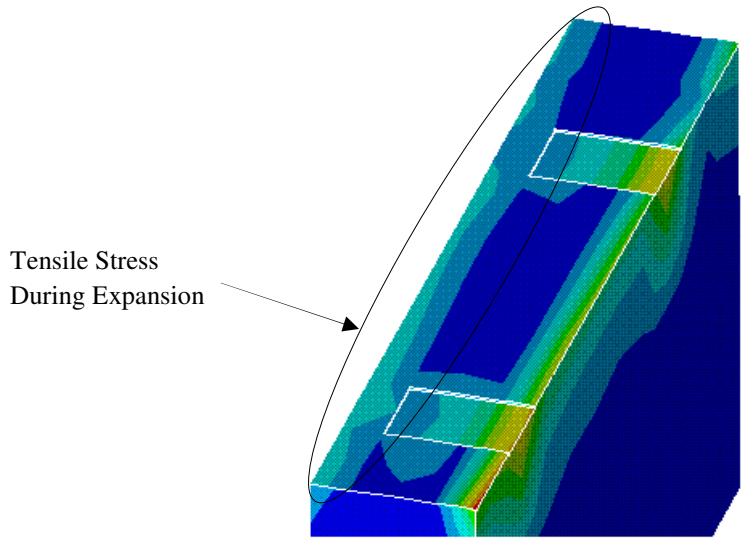

Figure 5.9 Tensile Stress at Construction Joint

A 93% increase in tensile concrete stress is observed with an increase in bridge length. Tensile concrete stresses for strong axis pile orientation is 7% greater than for weak axis pile orientation.

The tensile concrete stress in the abutment is a result of the rebar tensile pull of the rebars during expansion. All bridge lengths investigated resulted in tensile stresses exceeding the calculated modulus of rupture of 0.455 ksi (3.1 MPa) for both strong and weak axis pile orientation. For bridge length 1500′ (437 m) and weak axis pile

orientation, a concrete stress of 1.13 ksi (7.81 MPa) at the abutment is observed, corresponding to 238% of the modulus of rupture. Despite the presence of reinforcement bars at this location, the magnitude of stress can result in significant cracking in the abutment.

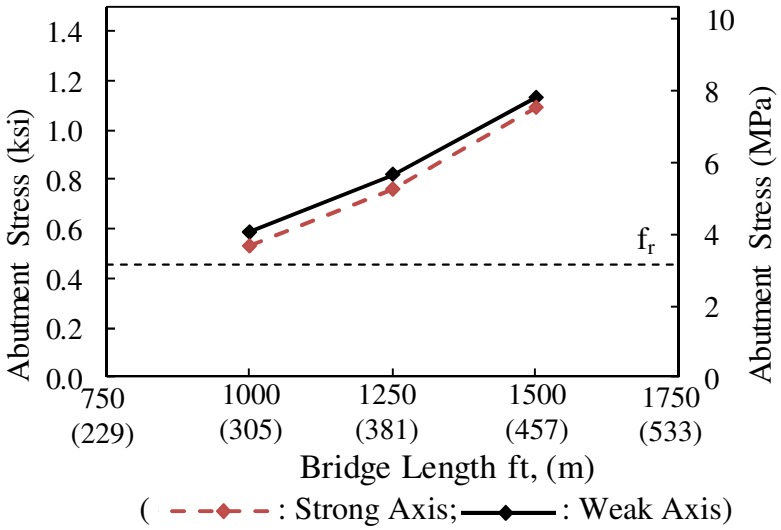

Figure 5.10 Abutment Stress for Bridge Expansion

Contraction

The concrete stress on the abutment at construction joint is also investigated for contraction cases shown in Figure 5.9. The abutment tensile concrete stress, at the construction joint, for bridge lengths 1000′ (305 m), 1250′ (381 m) and 1500′ (457 m) during contraction are shown in Figure 5.11. A 21% increase in tensile concrete stress is observed with an increase in bridge length. Tensile concrete stress for strong axis pile orientation is 11% greater than for weak axis pile orientation.

All bridge lengths investigated, produced concrete stress exceeding the modulus of rupture of 0.455 ksi (3.1 MPa) for both strong and weak axis pile orientation. For bridge length 1500′ (437 m) and strong axis pile orientation, a concrete stress of 2.5 ksi (17.1

MPa) at the abutment is observed, corresponding to 545% of the modulus of rupture. At these stress levels the reinforcement is engaged but can result in significant cracking.

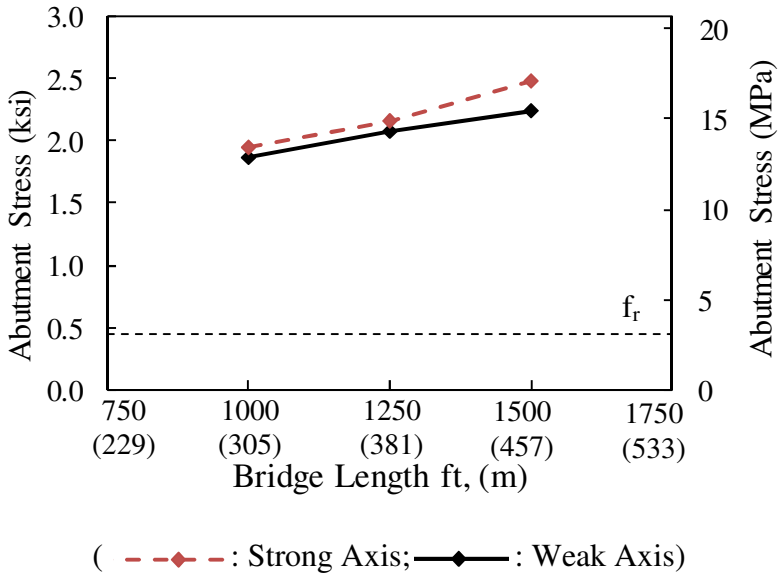

Figure 5.11 Abutment Stress for Bridge Contraction

5.7 Deck

The tensile concrete stress in bridge deck for bridge lengths 1000′ (305 m), 1250′ (381 m) and 1500′ (457 m) during expansion are shown in Figure 5.12. A 4% decrease in deck tensile stress is observed with an increase in bridge length. Tensile deck stress for strong axis pile orientation is 11% greater than for weak axis pile orientation. The concrete stress in the deck slab for all bridge lengths investigated exceeds the modulus of rupture of, 0.525 ksi (3.6 MPa) for the concrete used in this study as observed in Figure 5.12. For bridge length 1500′ (437 m) and strong axis pile orientation, a concrete stress of 0.93 ksi (6.4 MPa) at the abutment is observed, corresponding to 174% of the modulus of rupture.

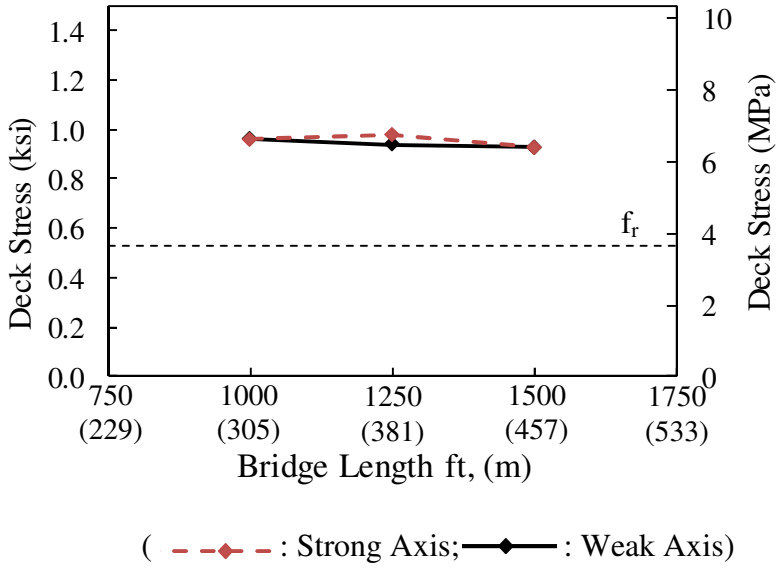

Figure 5.12 Bridge Length Influence on Reinforced Concrete Deck

Despite the presence of reinforcement at this location, the magnitude of stress can result in significant cracking. The concrete stress on the deck investigated for expansion cases is shown in Figure 5.13. Additional reinforcement should be considered in the bridge deck for bridge lengths equal to and exceeding 1500′ (437 m). Figure 5.13 shows the suggested reinforcement layout for the additional reinforcement.

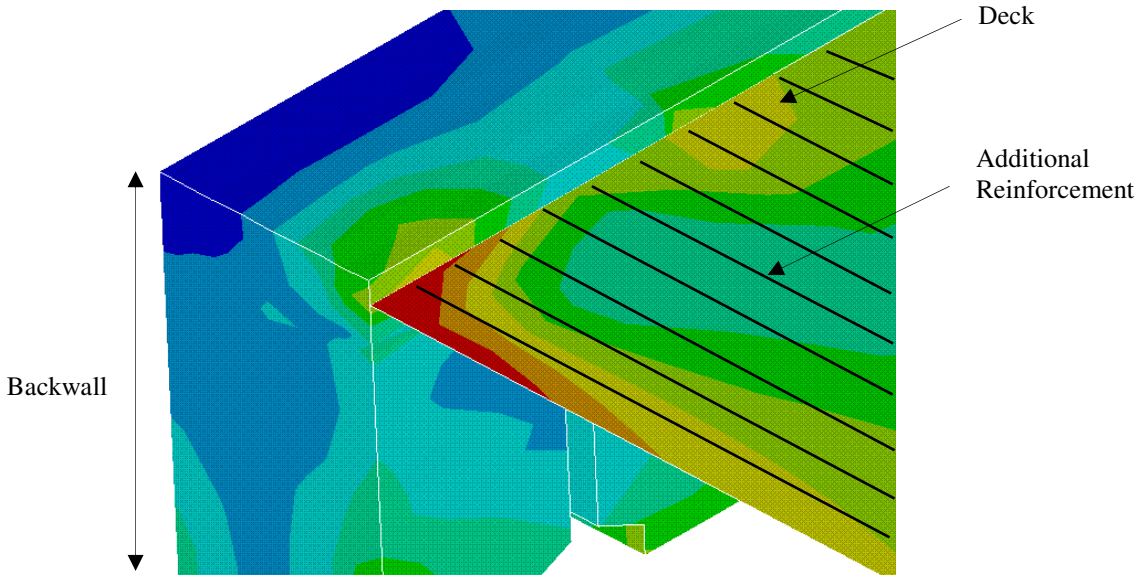

Figure 5.13 Tensile Stress On Bridge Deck

5.8 Girder Stress

The girder stress at the backwall-girder connection for 1000′ (305 m), 1250′ (381 m) and 1500′ (457 m) during expansion, are shown in Figure 5.14. A 30% increase in the girder compressive stress is observed with an increase in bridge length from 1000′ (305 m) to 1500′ (457 m). Pile orientation does not have a significant effect on the girder stress for expansion cases with only a 1% decrease in compressive stress from weak to strong axis pile orientation.

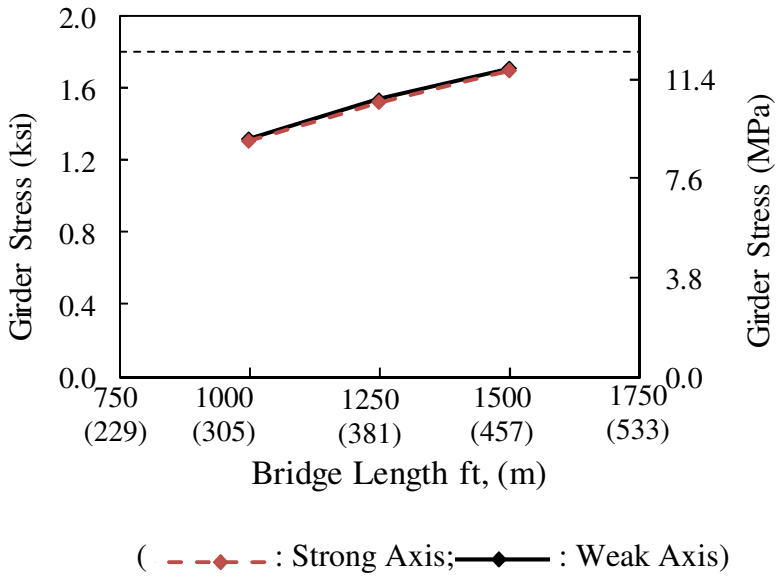

Figure 5.14 Bridge Length Influence on Girder Stress

The largest compressive stress obtained at the girder backwall connection, in the investigation of the three bridge lengths is 1.7 ksi (-11.7 MPa) which is 94% of the allowable compressive stress of the concrete used for the backwall in this study. Consequently, for the lengths investigated, the backwall will experience distress in the form of concrete crushing in the region shown in Figure 5.15 during bridge expansion.

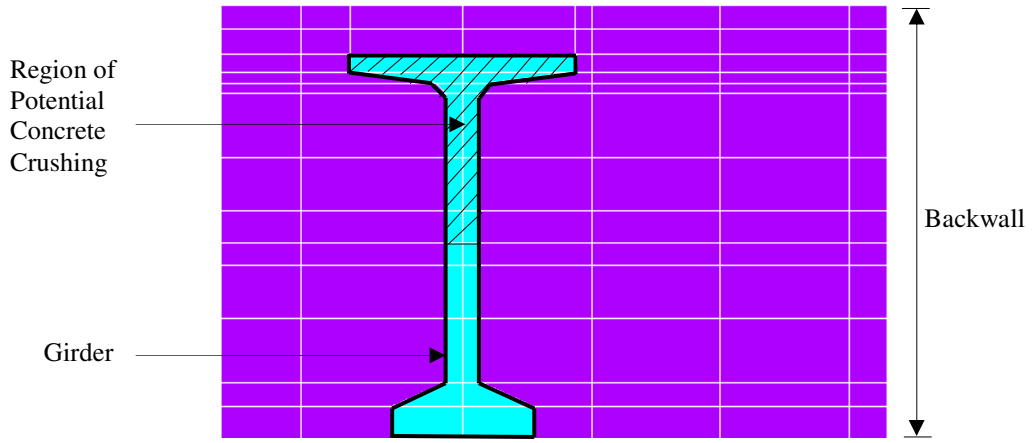

Figure 5.15 Region of Distress at Backwall-Girder Connection

5.9 Stress in Girder at Transverse Threading Location

The shear stress in the girder at the transverse threading location, shown in Figure 5.16 is investigated for potential distress. Girder shear stress for bridge lengths 1000′ (305 m), 1250′ (381 m) and 1500′ (457 m) during contraction are shown in Figure 5.17. The graph shows a 23% increase in girder concrete shear stress at the transverse threading location with an increase in bridge length. Pile orientation showed up to an 11% decrease in girder shear stress from weak axis orientation to strong axis orientation at bridge length equal to 1500 ' (457 m).

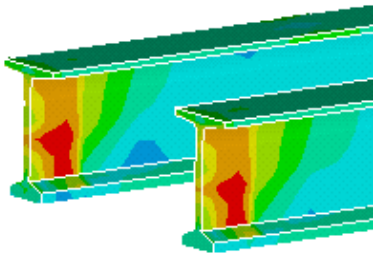

Figure 5.16 Shear Stress in Girder at Transverse Threading Location

The largest concrete shear stress obtained in the investigation of the three bridge lengths is 1.73 ksi (12.0 MPa) which is significantly larger than the 0.358 ksi (2.47 MPa) shear strength of the shear strength of concrete girder used in this study. As a result, the girder at the transverse threading connection will experience significant distress in the form shear failure during bridge contraction at the lengths investigated.

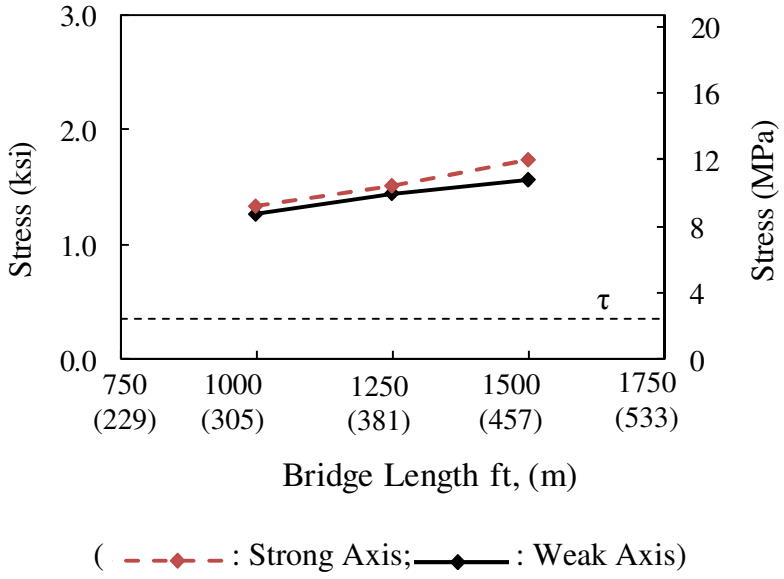

Figure 5.17 Bridge Length Influence on Girder at Transverse Threading

Chapter 6

SUMMARY, CONCLUSIONS AND RECOMMENDATIONS

6.1 Summary

The present study developed numerical models that simulate IAB behavior to investigate the critical response and identify potential distress of IABs at extreme lengths, and to ultimately establish a practical IAB length. The models incorporated key components to IAB behavior such as: (1) soil-pile interaction; (2) abutment pile interaction; and (3) construction joint detail. The loads on the numerical models include: (1) ambient temperature; (2) temperature gradient; (3) time-dependant loads, and (4) backfill pressure.

A parametric study was performed to investigate the response of: (1) pile head displacement; (2) maximum pile stress; (3) maximum pile bending moment; (4) concrete stress at the abutment-pile connection; and (4) bottom girder stress, to both temperature and time dependant loads. The parametric study utilized 108 numerical models varying:

- abutment height;
- soil stiffness;
- construction joint stiffness; and
- pile orientation.

Other bridge locations were also examined to determine if distress occurs, these locations include: (1) construction joint; (2) elastomeric bearing pads; (3) transverse threading; (4) girder stress at abutment-girder connection; and (5) girder stress at

transverse threading. The bridge configuration that yielded comparatively lower stresses was chosen to investigate the critical response at increased lengths. Two additional lengths were investigated until a practical limit, based on bridge response, was established. This chapter presents the conclusions of this study and design recommendations based on the results of this study. Recommendations of future research are also presented.

6.2 Conclusions

From the results of the parametric study and the length limit investigation this study has found that:

- At 1000′ (305 m) IABs developed high stress and moments in the piles, high stress in the abutment-pile connection, deck, backwall-girder connection and high stress in the girder at the transverse threading location making these the limiting factors for IABs at extreme lengths in this study.
- A practical maximum IAB length of 1500′ (457 m) was established based on the limiting factors.
- IABs beyond 1500′ (457 m) are most likely to develop cracking deck, cracking in the abutment at the construction joint location, concrete crushing at the abutment-girder connection, and yielding of piles during contraction.
- Bridge contraction produced up to 526% higher forces, stresses and displacements than expansion due to time dependant effects.
- Contrary to common practice, weak axis pile orientation produced up to 60% larger thermally induced pile stress than strong axis orientation.

- The abutment height has the largest influence on pile head displacement, maximum pile stress, maximum pile moment, concrete stress and girder bottom stress.
- A decrease in maximum pile stress, maximum pile moment, concrete stress and girder bottom stress were observed with a taller abutment.
- Soil stiffness did not have a significant effect on the pile head displacement for both expansion and contraction cases with only a 20% decrease observed. An increase in soil stiffness, however, showed up to a 60% increase in maximum pile stress, maximum pile moment, concrete stress and girder bottom stress.
- Construction joint stiffness showed a significant effect on pile bending stress, pile moment, concrete stress and girder bottom stress. For expansion cases there was up to a 37% decrease in pile bending stress, pile moment, concrete stress and girder bottom stress with an increase in construction joint stiffness. During contraction there was up to a 61% increase pile bending stress, pile moment, concrete stress and girder bottom stress with an increase in construction joint stiffness.
- The abutment experienced high tensile stresses at the construction joint location. This tensile stress increased by 27% with an increase in bridge length.
- The reinforcing bars used in the PennDOT Std. construction joint experienced stresses close to the yield stress of 60 ksi (414 MPa) for the #5 bars used.

- High shear stress in the girder at the transverse location was observed. This shear stress increased by 23% with an increase in bridge length. The largest stress value represented 484% of the shear capacity of the girder.
- The backwall experienced high compressive stress during expansion at the backwall-girder connection. This compressive stress increased by 30% with an increase in bridge length. The largest stress value represented 94% of the allowable compressive stress.
- High tensile stresses developed in the top of the deck during expansion in IABs at extreme lengths. This tensile stress decreased by 3% with an increase in bridge length. The largest stress values represented 182% of the modulus of rupture of the concrete used in this study.
- Taller abutments, moderate construction joint stiffness, low soil stiffness and strong axis pile orientation are best suited for IABs at extreme lengths.

6.3 Design Recommendations

For IABs with extreme lengths it is recommended that:

- An increase in deck reinforcement in the deck connection or a higher concrete compressive strength used for the deck, i.e. greater than 4 ksi (27.6 MPa) used in this study.
- An increase in abutment reinforcement or increase in compressive strength used for the abutment, i.e. greater than 3 ksi (20.7 MPa) used in this study.
- A higher strength concrete should be used for the backwall to prevent concrete crushing at the backwall-girder connection during expansion.

- The size of reinforcement used in the construction joint should be increased and/or spacing should be decreased to avoid yielding of the reinforcement bars.
- Strong axis orientation pile should be considered to avoid high stress developing in piles.
- An increase in pile size can be considered to decrease the stress in the piles.

6.4 Recommendations for future research

Based on the scope and the results obtained in this study, the following recommendations are made:

- Investigation of the effects of superimposed live load and its effect on the superstructure and substructure stresses in IABs at extreme lengths.
- Future studies investigating the effect of skew angle and span length on IABs at extreme lengths.
- Effect of approach slab and wingwalls on overall IAB response.

REFERENCES

1. Alampalli, S. and Yannotti, A., (1998). In-Service Performance of Integral Bridges and Jointless Decks. Transportation Research Board *1624*, TRB, National Research Council, Washington, D.C., 1998, pp. 1-7.

2. American Association of State Highway and Transportation Officials. (2005). AASHTO LRFD Bridge Design Specifications, Washington, D.C.

3. American Association of State Highway and Transportation Officials (AASHTO Guide). *AASHTO Guide Specifications Thermal Effects in Concrete Bridge Superstructures.* (1989). Washington, D.C.

4. American Concrete Institute Committee 209 (ACI 209). (2004). "Prediction of Creep, Shrinkage, and Temperature Effects in Concrete Structures," *ACI Manual of Concrete Practice Part I*, American Concrete Institute, Farmington Hills, MI.

5. ANSYS Release 11.0, ANSYS University Advanced, ANSYS Inc.

6. ANSYS Inc. Release 9.0, (2004). ANSYS Contact Technology Guide

7. Arockiasamy, M., Butrieng, N., Sivakumar, M., (2004). State-of-the-Art of Integral Abutment Bridges: Design and Practice. *Journal of Bridge Engineering*, Vol. 9, No. 5, pp 497-506.

8. Arsoy, S., Barker, R.M. and Duncan, J.M., (2002). Experimental and Analytical Investigations of Piles and Abutments of Integral Bridges, Report VTRC02-CR6, 2002 (Virginia Transportation Research Council: Charlottesville, VA).

9. Burdette, E.G., et.al. (2005). Behavior of Pile Supported Integral Abutments, *Proceedings of the 2005-FHWA Conference on Integral Abutment and Jointless Bridges (IAJB 2005).*

10. Burdette, E.G., et.al. (2003). A Half-Mile of Bridge Without a Joint, Concrete International, 2003, February, 47-51.

11. Burke, M. P., Jr. Integral Bridges. *Transportation Research Record 1275*, TRB, National Research Council, Washington, D.C., 1990, pp. 53-61.

12. Burke, M. P., Jr., (1993). "Integral Bridges: Attributes and Limitations." *Transportation Research Record 1393*, TRB, National Research Council, Washington, D.C., 1993, pp. 1-8

13. Burke, M. P., Jr. Cracking of Concrete Decks and Other Problems with Integral-Type Bridges. In *Transportation Research Record 1688*, TRB, National Research Council, Washington, D.C., 1999, pp. 131-138.

14. Cobb, Fiona (2004), Structural Engineer's Pocket Book, Elsevier Butterworth-Heinemann

15. Dicleli, M., (2000). A rational design approach for prestressed-concrete-girder integral bridges. *Engineering Structures,* 22, pp. 230-245.

16. Dicleli, M., and Albhaisi, S., (2003). Maximum length of integral bridges supported on steel H- piles driven in sand. *Engineering Structures*, 25, pp. 1491-1504.

17. Dunker, K.F., and Lui, D., (2007). Foundations for Integral Abutments. *Practice Periodical on Structural Design and Construction,* Vol. 12, No. 1, pp. 22-30.

18. Emmanuel, J.H., and Hulsey, J.L., (1997). Prediction of the thermal coefficient of concrete. *ACI Journal*, Vol 74, No. 4, pp. 149-155.

19. Fennema, J, Laman, J.A., Linzell, D., (2003). Predicted and Measured Response of an Integral Abutment Bridge. Master of Science Thesis. The Pennsylvania State University, University Park, PA.

20. Ghali, A., Favre, R., and Elbadry, M. (2002). *Concrete Structures: Stresses and Deformation*, 3th Ed., Spon Press, London.

21. Girton, D.D., and Hawkinson, T.R., and Greimann, L.F., (1991). Validation of Design Recommendations for Integral-Abutment Piles. *Journal of Structural Engineering,* ASCE, Vol. 117, No. 7, July 1991, pp. 2117-2134.

22. Greimann, L.F., and Wolde-Tinsae, A.M., (1988). Design Model for Piles in Jointless Bridges. *Journal of Structural Engineering,* ASCE, Vol. 114, No. 6, June 1988, pp 1354-1371.

23. Hambly, E., (1976). Bridge Deck Behavior. John Wiley & Sons, Inc., New York.

24. Hassiotis, S. and Roman, E.K., (2005). A survey of the current issues on the use of integral abutment bridges. *Bridge Structures*, Vol. 1, No. 2, June 2005, pp 81-101.

25. Huang, J., Shield, C., French, C., (2008). Parametric Study of Concrete Integral Abutment Bridges. *Journal of Bridge Engineering*, Vol. 13, No. 5, September 2008, pp 511-526.

26. Huckabee, P. (2005). Plastic Design of Steel HP-Piles for Integral Abutment Bridges, *Proceedings of the 2005-FHWA Conference on Integral Abutment and Jointless Bridges (IAJB 2005).*

27. Kim, W. (2008). Simplified Nonlinear Numerical Analysis Method for Integral Abutment Bridges, *Proceedings of the 2008 International Bridge Conference,* Pittsburgh, PA, IBC-08-43, June 2-4.

28. Kim, W., J.A. Laman (2008). Integral Abutment Bridge Response under Thermal Loading. *Transportation Research Record,* Transportation Research Board of the National Academies (in review).

29. Kim, W. and J.A. Laman (2009). Load and Resistance Factor Design for Integral Abutment Bridges. Ph.D. Dissertation. The Pennsylvania State University, PA.

30. Knickerbocker, D., Basu, P., and Wasserman, E., (2005). Behavior of Two-Span Integral Bridges Unsymmetrical about the Pier Line. *Proceedings of the 2005-FHWA Conference on Integral Abutment and Jointless Bridges (IAJB 2005).*

31. Kunin, Jonathan and Alampalli, Sreenivas, (2000). Integral Abutment Bridges: Current Practice in United States and Canada

32. Laman, J.A., Pugasap, K., and Kim, W., (2006). Field Monitoring of Integral Abutment Bridges, Report No. FHWA-PA-2006-006-510401-01, Pennsylvania Transportation Research Council.

33. Lawver, A., French, C., and Shield, C.K. Field Performance of an Integral Abutment Bridge. *Transportation Research Record 1740,* TRB, National Research Council, Washington, D.C., 2000, pp. 108-117.

34. Lawver, A., and French, C., and Shield, C.K (1998). Field Performance of an integral abutment bridge

35. Loveall, C. L. Jointless Bridge Decks. *Civil Engineering*, Vol. 55, No. 11, November 1985, pp. 64-67.

36. MacGregor, J. C. (1997). *Reinforced concrete mechanics and design*, 3rd Ed., Prentice-Hall, Upper Saddle River, N.J.

37. Maruri, R., and Petro, S., Intgral Abutments and Jointless Bridges (IAJB) 2004 Survey Summary. *FHWA Conference on Integral Abutment and Jointless Bridges (IAJB 2005).*

38. Mistry, V. (2005). Integral Abutment and Jointless Bridges. *Proceedings of the 2005-FHWA Conference on Integral Abutment and Jointless Bridges (IAJB 2005).*

39. Moorty, S. and C. W. Roeder. Temperature-Dependent Bridge Movements. *Journal of Structural Engineering*, Vol. 118, no. 4, April 1992, pp. 1090-1105.

40. Mourad, S., Tabsh, S., (1999). Deck Slab Stresses in Integral Abutment Bridges. *Journal of Bridge Engineering*. , May 1999, pp. 125-130.

41. Ndon, U.J., and K.L. Bergeson., (1995). Thermal Expansion of Concretes: Case Study in Iowa. *Journal of Materials in Civil Engineering,* ASCE, Vol. 7, No. 4, November 1995, pp. 246-251.

42. Oesterle, R. G, Refai, T. M., Volz, J. S., Scanlon, A., and Weiss, W. J. (1998). "Jointless and Integral Abutment Bridges Analytical Research and Proposed

Design Procedures", Construction Technology Laboratories, Inc., Draft Final Report to Federal Highway Administration, Washington, D.C.

43. Paul, M., Laman, J.A., Linzell, D., (2003). Thermally Induced Superstructure Stresses in Prestressed Girder Integral Abutment Bridges. Master of Science Thesis, The Pennsylvania State University, University Park, PA.

44. PCI (2005). *PCI Bridge Manual*, Precast/Prestressed Concrete Institute, Chicago, IL.

45. Pugasap, K., Kim W., and Laman, J.A., (2009). Long-Term Response Prediction of Integral Abutment Bridges. *Journal of Bridge Engineering*, March 2009, pp 129-139.

46. Pugasap, K. (2006). Hysteresis Model Based Prediction of Integral Abutment Bridge Behavior. Ph.D. Dissertation. The Pennsylvania State University, University Park, PA.

47. Rajagopalan, N. (2006). Bridge Superstructure. Alpha Science International Ltd. Oxford, U.K.

48. Reese, L.C., and Van Impe, W.F., (). Single Piles and Pile Groups under Lateral Loading.

49. Reese, Lymon C. and Wang, S. T. (1997). LPILE Plus 3.0 for Windows, Technical Manual, Ensoft Inc., Austin, TX.

50. Thippeswamy, H. K., GangaRao, H. V. S. and Franco, J. M. (2002). "Performance Evaluation of Jointless Bridges," *Journal of Bridge Engineering*, ASCE, Vol. 7, No. 5.

51. Vesić, A. S. 1977. "Design of Pile Foundations," NCHRP Synthesis of Highway Practice., 42,Transporation Research Board, pp40.

52. Wang, S., and L.C. Reece. COM624P- Laterally Loaded Pile Analysis Program for the Microcomputer, Version 2.0. Report Number FHWA-SA-91-048. FHWA, Office of Technology Applications, Washington, D.C., August 1993.

53. Wasserman, E.P. (1987). Jointless Bridge Decks. Engineering Journal, AISC, Vol. 24, No.3, pp 93-100.

54. Wasserman, E.P. (2007). Integral Abutment Design. *Proceedings from the 1st U.S-Italy Seismic Bridge Workshop (2007).*